NONLINEAR PLASMA WAVES AND THEIR APPLICATIONS

Mohamed Ruhul Amin

A Thesis Submitted for the Degree of PhD
at the
University of St Andrews

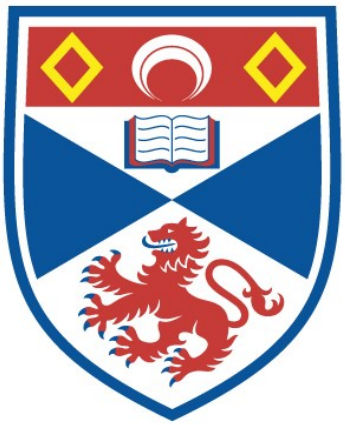

1999

NONLINEAR PLASMA WAVES AND THEIR APPLICATIONS

by

MOHAMED RUHUL AMIN

THESIS SUBMITTED IN JUNE 1990 TO THE FACULTY OF SCIENCE OF ST ANDREWS UNIVERSITY FOR THE DEGREE OF DOCTOR OF PHILOSOPHY

NONLINEAR PLASMA WAVES AND THEIR APPLICATIONS

Abstract

The possibility of beat wave current drive in tokamaks is considered in this thesis in steady state 2D geometry. The problem is considered by including in the analysis the 2D toroidal inhomogeneity effect and the effect of finite spatial width of the pump microwave pulses on the beat wave excitation. Both a Langmuir beat wave as well as an obliquely propagating upper-hybrid cyclotron beat wave are considered in this study. The three wave coupled system of equations in a magnetized plasma has been derived and solved numerically for this purpose. It has been found that Langmuir type beat wave excited by two almost antiparallel pump microwaves is more efficient for action transfer than a cyclotron beat wave. It has also been found that for the same input parameters, right hand polarized pumps are more efficient than left hand polarized pump microwaves for depositing power in the beat wave.

The second part of the thesis considers the relativistic excitation mechanism of a large amplitude plasma wake field by a single ultra-short laser pulse. This type of large amplitude wake field has been proposed for particle acceleration to very high energies for future generation of accelerators. The problem has been modelled self consistently in 1D geometry and the relevant

coupled system of equations have been solved numerically. It has been found that the shape of the laser pulse profile and the ratio of the ambient plasma frequency to the incident laser frequency play an important role for the excitation of the wake-field and the stability of the laser pulse profile.

To my parents

ACKNOWLEDGEMENTS

I wish to thank my supervisor Dr. Alan Cairns for his helpful advice, encouragement and unending patience throughout my three years in the Department of Mathematical and Computational Sciences. His insight has been a constant source of inspiration.

My thanks also go to the other members of the Plasma Physics Group of the Department, namely, Professor Jeffrey Sanderson, Dr. Brian Harvey, Alastair McGowan, Andrew Miller, Ashley Buckner and Helen Forrester for their helpful support.

I would also like to thank Professor U. de Angelis, Mr. Brendan McNamara and Dr. Robert Bingham. The second part of the thesis is really a result of our joint work. I owe an especial debt of gratitude to Dr. Robert Bingham, for his constant encouragement. His enthusiasm for Plasma Physics has been an inspiration to me.

I am grateful to Professor M. A. Quader for his encouragement in my higher studies and to Professor M. Salimullah who first introduced me to the subject of Plasma Physics and who encouraged me in the study of it.

I would like to thank Dr. John Henderson for assistance and help. I gratefully acknowledge the financial support of the Commonwealth Scholarship Commission in the United Kingdom in the form of a research studentship during this project. Finally I would like to thank all my friends for their nice company and constant inspiration during my stay in St Andrews.

M R Amin

Certificate

I certify that M. Ruhul Amin has satisfied the conditions of the Ordinance and Regulations and is thus qualified to submit the accompanying application for the Degree of Doctor of Philosophy.

Postgraduate career

I was admitted into the University of St Andrews as a research student under Ordinance General No. 12 in October 1987 to work on Nonlinear Plasma Waves under the supervision of Dr. R. Alan Cairns. I was admitted under the above resolution as a candidate for the Degree of Doctor of Philosophy in October 1988.

Declaration

I declare that the following thesis is a record of research work carried out by me, that the thesis is my own composition, and that it has not previously been submitted in application for a higher degree.

In submitting this thesis to the University of St Andrews I understand that I am giving permission for it to be made available for use in accordance with the regulations of the University Library for the time being in force, subject to any copyright vested in the work not being affected thereby. I also understand that the title and abstract will be published, and that a copy of the work may be made and supplied to any bona fide library or research worker.

CONTENTS

PART 1

Excitation of a Large Amplitude Plasma Wave by Two Intense Free-Electron Laser Pulses for Current Drive in Tokamaks

PART 2

Excitation of a Large Amplitude Plasma Wave by a Single Ultra-Short Laser Pulse for Particle Accelerators

PART 1

Excitation of a Large Amplitude Plasma Wave by Two Intense Free-Electron Laser Pulses for Current Drive in Tokamaks

chapter 1

INTRODUCTION

The Tokamak

The tokamak, a toroidal machine has emerged today as an exciting prospect to controlling nuclear fusion for the purpose of electrical power generation. To confine the charged constituents of the fusile fuel it has been recognized that two types of magnetic field are necessary, the toroidal field and the poloidal field. The effects of these two fields is to twist the magnetic lines of force while they are being bent into the toroidal shape. The toroidal field encircling the torus hole and the poloidal field encircling the centre of the minor cross section of the torus (Fig.1.1). In a tokamak, the toroidal field component is large compared to the poloidal field component.

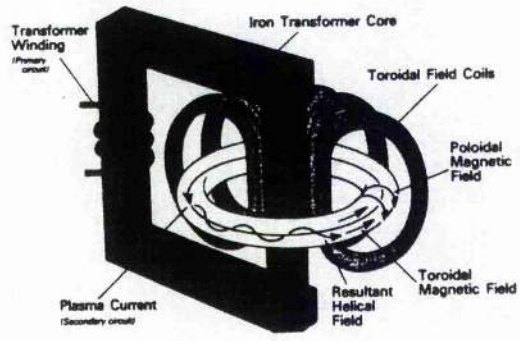

Figure 1.1: Schematic diagram of a tokamak.

Current Drive in Tokamaks

The toroidal magnetic field can easily be produced by poloidal electric currents flowing in coils outside the plasma that encircle the minor cross section and thread the torus hole. The poloidal magnetic field is more difficult to produce. It may be produced by a toroidal current, but this current must flow inside the plasma. The natural way to produce this current is by inducing a constant toroidal electric field inside the plasma. The toroidal electric field is induced by treating the plasma as a secondary in a transformer circuit. Placed outside the plasma is a primary coil whose axis threads the hole of the plasma torus. So, in the present form the tokamak is a pulsed reactor due to the inductive mechanism used for driving the plasma current. It has severe engineering problems associated with thermal cycling of the walls and the pulsing of the poloidal magnetic circuit. There is a considerable technological advantage in building a tokamak that could operate in a continuous rather than pulsed mode. The desirability of maintaining a steady current has long been recognized, and various methods have been proposed for doing this (Fisch, 1987).

Method 1 (Neutral Beam Current Drive)

Ohkawa (1970) suggested that neutral beam injection could be used for driving steady currents. The neutral injection methods produce a beam current of fast charged particles circulating around the torus. The slowing down of these fast ions by collisions with the plasma electrons causes the electron to drift toroidally, producing a plasma current. This electron current is in the reverse direction to the ion current and so tends to reduce the net current. The degree of cancellation depends on the effective ion charge Z_{eff} and the number of trapped electrons. Currents driven by the neutral beams were first observed by Start et al (1978) on Culham Levitron. The first measurement of a beam driven current in a tokamak was made by Clark et al (1980) in experiments on the Culham DITE tokamak. In these experiments, about half of the toroidal current (total toroidal current was 250 kA) appears to be beam driven.

Method 2 (Alfven Wave Current Drive)

Wort (1971) proposed the use of travelling Alfven waves to impart momentum to resonant electrons. The idea is to impart momentum with as little as possible energy expenditure to the resonant electrons and hence, by

collisions, to produce a drift of the electron fluid. A current drive effect using the fast Alfven wave has been reported by Goree et al (1985) and by McWilliams and Platt (1985). In a toroidal device, Osovets and Popov (1972, 1976) detected currents as large as 3 kA in the presence of a toroidal magnetic field with compressional Alfven waves.

Method 3 (Lower Hybrid Current Drive)

Fisch (1978) suggested that lower hybrid waves could be used to drive toroidal current in a tokamak. High energy electrons are preferentially driven one way by Landau damping. A series of experiments (Bernabei et al, 1982; Hooke et al, 1983) on the PLT tokamak in Princeton have been done to drive current using lower hybrid waves. In a very encouraging experiment reported by Jobes et al (1984), both the plasma and the current were initiated without the aid of the Ohmic transformer coils. A current of over 100 kA was generated by the lower hybrid waves alone. But all these PLT experiments were carried out with relatively low density ($n<10^{13}$ cm^{-3}) plasmas. Higher density experiments, more relevant to the reactor regime, were performed on the Alcator C tokamak at MIT, and in particular, the theoretical efficiency scaling was confirmed by Porkolab et

al (1984). The high density operation of the current drive experiments on the Alcator C tokamak was possible because of the relatively high frequency (4.6 GHz), the high magnetic field (11T), and the relatively high power (1.1MW) employed. In general, it has been observed that efficient current drive is obtained only when $\omega/\omega_{LH} > 2$, where ω_{LH} is the lower hybrid frequency and ω is the wave frequency. A systematic experimental study of this observation (Mayberry et al, 1985) suggests that there is no absolute density limit for the current drive effect when $\omega/\omega_{LH} > 2$, but that when $\omega/\omega_{LH} \leq 2$, there is a density limit and the lower hybrid wave power tends to be deposited in ions rather than in electrons.

The **common feature** of the three methods outline above is that

- to drive current one species of charged particle must be given a net velocity relative to the other,

- any wave (or beam) with net momentum can, in principle generate a current by transferring its momentum via the appropriate damping mechanisms to the charged particles,

- desirable to minimize power dissipation, better to drive electrons (momentum dissipation rate is the same for electrons and ions but

ratio of current/momentum is greater for electrons by ratio m_i/m_e),

- an asymmetry must be introduced into the toroidal geometry so that one toroidal direction is favoured over the other.

The first two methods were both motivated by the **two principles** that guided early current drive research.

a) An external source that deposits toroidal momentum into electrons is necessary for current generation.

b) It is most efficient to push slow electrons.

The first principle is exemplified by each of the two early suggestions, neutral beams and Alfven waves. Neutral beams enter the plasma, ionize, and then collide primarily with the electrons, resulting in a drift of electrons relative to ions. Alfven waves similarly push the electrons. Exemplifying the second principle, in both cases, is the fact that thermal electrons are pushed. In the case of neutral beams, this occurs because, while all electrons contribute to slowing down the beams, most electrons are thermal. In the case of Alfven waves, this occurs because the wave phase velocity is picked so that only slow electrons are pushed by the wave. For

wave-particle interaction, momentum and energy can be exchanged between waves and particles obeying a resonance condition: either the so-called Landau resonance

$$\omega - \vec{k} \cdot \vec{v} = 0, \tag{1.1}$$

or in the case of a strong magnetic field, the cyclotron resonance

$$\omega - k_{\parallel} v_{\parallel} - n\Omega_e = 0, \tag{1.2}$$

where ω and $\vec{k}$ are the wave frequency and wave number, Ω_e is the particle cyclotron frequency, $\vec{v}$ is the particle velocity, and n is an integer. Vector quantities may be decomposed into projections parallel and perpendicular to the magnetic field, thus

$$\vec{v} = v_{\parallel} \hat{e}_z + \vec{v}_{\perp}, \tag{1.3}$$

where $\hat{e}_z$ is the unit vector in the parallel direction. The problem, of course, is to generate current in the parallel, which is roughly the toroidal direction. The sense of the wave-particle interaction is dictated by the sense of a diffusion process: particles near equilibrium generally occupy lower-energy states rather than high-energy states; hence it is the wave that

transfers its energy (a positive quantity) and momentum to the resonant particles. In the case of Alfven waves, the Landau resonance condition Eq.(1.1) pertains, and the wave frequency and wave number are picked so that v is subthermal, i, e., $v<v_{th}$, where v_{th} is the electron thermal velocity, while the perpendicular velocity of resonant electrons is, on average, $v_{\perp}\approx v_{th}$. The first early principle is merely an intuition; the second principle rests on the notion that it is easier to push a slow electron than a fast electron (slow and fast refer here to motion in the direction parallel to the push).

Now we shall see why it is favourable to accelerate a slower, rather than a faster, electron. Let us suppose an electron with mass m and charge q ($q\equiv -1$), in interacting with a wave or other source of momentum, is accelerated from velocity

$$\vec{v}_i = v_{\parallel}\hat{e}_z + \vec{v}_{\perp} \tag{1.4}$$

to velocity

$$\vec{v}_f = \vec{v}_i + \Delta v_{\parallel}\hat{e}_z . \tag{1.5}$$

The parallel momentum absorbed by this electron is

$$\Delta p = m_e \Delta v_{\parallel} ; \tag{1.6}$$

the incremental current carried by this electron is

$$\Delta j = q \Delta v_{\parallel} ; \tag{1.7}$$

and the incremental increase in the electron kinetic energy is

$$\Delta \varepsilon = \Delta \left(\frac{m_e v_{\parallel}^2}{2} \right) = m_e v_{\parallel} \Delta v_{\parallel} . \tag{1.8}$$

The ratio

$$\frac{\Delta j}{\Delta \varepsilon} = \left(\frac{q \Delta v_{\parallel}}{m_e v_{\parallel} \Delta v_{\parallel}} \right) = \left(\frac{q}{m_e v_{\parallel}} \right) \tag{1.9}$$

of the incremental current to absorbed energy is inversely proportional to the velocity projection $v_{\parallel}$ indicates that it is energetically favourable to accelerate a slower, rather than faster, electron. Thus, Ohkawa's neutral beams push thermal electrons, and Wort's Alfven waves are designed to push low-$v_{\parallel}$ electrons.

Although it may be easier to push slow-electrons, it may actually be more effective to push fast electrons. In practice, this would be done by injecting waves with faster parallel phase velocities to deposit momentum in faster resonant electrons. The Coulomb collision cross-section becomes smaller with increasing relative speed between the colliding particles. Thus fast, superthermal $v>v_{th}$, electrons collide less often than slower, thermal electrons, since the average relative speed between superthermal electrons and most other electrons and ions is far greater than the relative speed between thermal electrons and most other electrons and ions. In fact, the ratio of these speeds is roughly v/v_{th}, where v is the superthermal electron velocity.

Although it may be energetically expensive to accelerate fast electrons in the first place, this energy deposition need occur less often. Current lasts longer when carried by relatively less collisional electrons, so the power requirements to sustain a given current against collisions can be small. To see this, let us assume that the velocity v of an electron is randomized by collisions in a momentum destruction time of $1/\nu(v)$. An incremental energy input $\Delta\varepsilon$ then produces an incremental current Δj that persist for

time $1/\nu(v)$. From Eq.(1.9), we have the relationship

$$\Delta j = \left(\frac{q \Delta \varepsilon}{m_e v_{\parallel}} \right). \tag{1.10}$$

The power requirement to refresh this current at time interval of $1/\nu(v)$ is

$$P_d = \nu \, \Delta \varepsilon . \tag{1.11}$$

Combining Eqs.(1.10) and (1.11) and adapting the notation $J=\Delta j$ (the only current is the driven current), we have the steady state efficiency

$$\frac{J}{P_d} = \left(\frac{q}{m_e v_{\parallel} \nu} \right). \tag{1.12}$$

We see from this equation (1.12) that the efficiency (or current per power dissipated) is maximized when $v_{\parallel}\nu(v)$ is minimized. There are two important limits:

(1) for $v_{\parallel} \rightarrow 0$, but $v_{\perp} \approx v_{th}$,

we have $\nu(v) \Rightarrow$ constant; (1.13)

(2) for $v_{||} >> v_{th}$,

however, we have

$$\nu(v) \sim \left(\frac{1}{v_{||}^3}\right). \tag{1.14}$$

The first limit , which characterizes the case of Alfven waves, results in a high efficiency, since

$$\frac{J}{P_d} \sim \left(\frac{1}{v_{||}}\right), \tag{1.15}$$

and $v_{||}$ is small. The second limit, which characterizes the case waves with high parallel phase velocity, also results in a high efficiency, since

$$\frac{J}{P_d} \sim v_{||}^2, \tag{1.16}$$

with $v_{||}$ large. The second case, identified by Fisch (1978), argues for the utilization of the so called lower-hybrid wave, which can be excited in a plasma with high parallel phase velocity. Although, in principle, high current drive efficiency can be realized in either of these limits, the low

phase velocity approach suffers from a serious drawback. In tokamaks, it is just the low $v_{\parallel}$, average $v_{\perp}$ electrons that are trapped in magnetic wells and prevented from flowing freely along the field lines. As pointed out by Bickerton (1972), these electrons cannot carry current as required for Alfven wave current drive. This objection is both fundamental and serious. Luckily, the problem of trapped electrons does not touch on the opposite high efficiency limit, i. e., that of lower hybrid waves. Electrons with high $v_{\parallel}$ and average $v_{\perp}$ would be just those electrons that are not trapped. The most intense effort in current drive research has in fact, been directed at this limit, and lower hybrid current drive experiments have now been performed at major tokamaks all over the world. However, current drive by lower hybrid waves has been achieved in relatively low density tokamak discharges with slide-away electrons. When the plasma density increases, the current drive efficiency drops abruptly. This is called density limit and may be due to the slide-away electrons not being able to couple to the wave, the power flow to ions and so on. The physical mechanism responsible for the density limit has yet to be explained.

Method 4 (Electron Cyclotron Current Drive)

A basically different method was proposed by Fisch and Boozer (1980), in which no net toroidal momentum is injected. Instead, the collisionality of the plasma is altered so that, for example, electrons moving to the left collide more frequently with the ions than do electrons moving to the right. There is then a net current with ions moving to the left and electrons moving to the right. A feature of this scheme is that collisions are an integral part and without them there would be no current, whereas in the earlier methods, collisions between electrons and ions will reduce the current. The means of achieving this collisionality of the plasma is to preferentially heat electrons travelling to the right, for example, so that, being hotter, they collide less. An electron cyclotron wave can do this. It is suggested that, despite their low parallel momentum content, electron cyclotron waves can drive currents with a similar efficiency to other methods, this efficiency being measured in terms of the total current driven per unit power dissipated in the plasma. Fisch and Boozer argued as follows: imagine a wave capable of pushing particles in velocity space. Consider the displacement of a small number, δn, of electrons from region 1 to region 2. The energy required is

$$\Delta\varepsilon = (\varepsilon_2 - \varepsilon_1)\,\delta n, \tag{1.17}$$

where ε_i is the kinetic energy associated with region i. Now, since electrons in different regions of velocity space scatter at different rates, the z-directed current density generated is given by

$$j(t) = e\,\delta n\left(v_{z1}\exp(-\nu_1 t) - v_{z2}\exp(-\nu_2 t)\right), \tag{1.18}$$

where ν_i is the scattering rate associated with region i. The time average of j(t) over an interval Δt long compared to ν_i^{-1} is

$$J = \frac{1}{\Delta t}\int_0^{\Delta t} j(t)\,dt = \frac{e\,\delta n}{\Delta t}\left(\frac{v_{z1}}{\nu_1} - \frac{v_{z2}}{\nu_2}\right). \tag{1.19}$$

Substituting for δn from Eq.(1.19) and identifying $\Delta\varepsilon/\Delta t$ as the dissipated power, Eq.(1.17) gives

$$\frac{J}{P_d} = -\left(\frac{e}{\varepsilon_2 - \varepsilon_1}\right)\left(\frac{v_{z2}}{\nu_2} - \frac{v_{z1}}{\nu_1}\right). \tag{1.20}$$

In the limit as $\nu_1 \Rightarrow \nu_2$

$$\frac{J}{P_d} \Rightarrow -\left\{ \frac{e\hat{\vec{s}} \cdot \nabla_v \left(\frac{v_z}{v} \right)}{\left(\hat{\vec{s}} \cdot \nabla_v \right) \varepsilon} \right\}, \tag{1.21}$$

where $\hat{\vec{s}}$ is a unit vector in the direction in velocity space in which the radio-frequency field is increasing the electrons' velocity. This expression now enables an important conclusion to be drawn. Assuming only that $v \propto 1/v^3$, where v is the velocity of the resonant electrons, the form of J/P_d can be easily obtained. For lower hybrid waves, $\hat{\vec{s}} \| \hat{\vec{e}}_{\|}$ and the Fisch-Boozer expression yields

$$\frac{J}{P_d} \propto \left\{ \frac{1}{v_{\|}} \left(v_{\|}^2 + v_{\perp}^2 \right)^{3/2} + 3 v_{\|} \left(v_{\|}^2 + v_{\perp}^2 \right)^{1/2} \right\}. \tag{1.22}$$

Now the most effective current drive is obtained with superthermal electrons for which $v_{\|} >> v_{\perp}$. The above result then shows that the term arising from energy input is three times greater than the term due to momentum input. This remarkable result suggests that even waves which carry very little momentum, e. g., electron cyclotron waves, are capable of driving currents with comparable efficiency to lower hybrid waves. Start et al (1982) first observed the electron cyclotron wave current drive effect on

the Culham Levitron device. They observed the current to depend linearly on injected power, and inversely with density, as would be predicted by theory. In addition, the current per power dissipated was observed to depend linearly on electron temperature. The net plasma current generated had an efficiency of about 30 mA/W. It should be remarked, however, that the plasma parameters attained here are very far from what is required for practical reactor.

Method 5 (Beat Wave Current Drive)

Another interesting current drive scheme, one that relies on nonlinear wave interactions such as are possible only with free-electron lasers (Orzechowski et al, 1986), was first suggested by Cohen (1984) and Galvao et al (1984). This beat wave scheme would launch two intense pulsed sources into the plasma and produce a beat wave. This beat wave is a longitudinal plasma wave, e. g., a Langmuir wave propagating along the toroidal magnetic field or an obliquely propagating upper-hybrid wave. The resonant electrons will damp the generated plasma beat waves as they propagate around the torus and absorb wave momentum, and thus drive a current. Momentum deposition into plasma beat waves by the pump

electromagnetic waves and from the plasma beat waves into the electrons continues until a balance is established with momentum loss process, like scattering of electrons by ions and neutrals, or until nonlinear effects on the plasma beat wave terminate the beat wave scattering process.

The dissipation of the electron plasma oscillation introduces irreversibility into the three wave interaction process, and is the mechanism for the eventual thermalization of part of the energy provided by the electromagnetic waves. The dissipation may be due to collisional, Landau damping, cyclotron damping, convective loss, or nonlinear mode coupling processes.

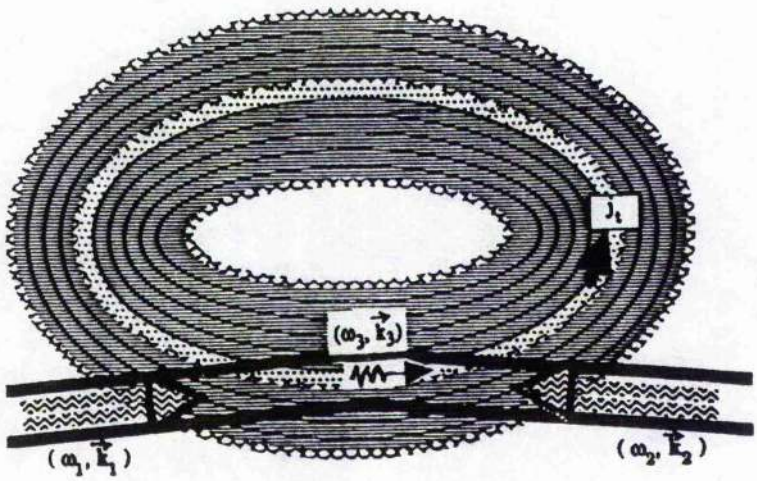

Figure 1.2: Schematic diagram of beat wave current drive.

One realization of this new idea of current generation by a Langmuir type beat wave, shown in Fig.1.2 is being examined in detail for the MTX at Livermore (Thomassen, 1988). The second source differs in frequency from the first by the plasma frequency, and its intensity is perhaps as low as a few percent of the first source. This scheme is an example of a resonant three-wave interaction with frequency and wavenumber matching conditions:

$$\omega_1 = \omega_2 + \omega_3, \tag{1.23}$$

$$\vec{k}_1 = \vec{k}_2 + \vec{k}_3, \tag{1.24}$$

where $(\omega_1,\vec{k}_1)$ and $(\omega_2,\vec{k}_2)$ are the pump microwaves and $(\omega_3,\vec{k}_3)$ is the excited beat wave. To understand the physics of the problem, we consider the action flux density $\vec{J}_t$ of the transverse waves, which is defined (Cohen et al, 1988) in natural units as

$$\vec{J}_t = \frac{\vec{k}_t}{2\pi}\left|\frac{v_t}{c}\right|^2, \tag{1.25}$$

where v_t is the electron quiver velocity in the wave field $(\omega_t,\vec{k}_t)$ and c is the speed of light. In terms of action flux density $\vec{J}_t$, the energy and momentum

flux densities are defined respectively as $\vec{J}_t\omega_t$ and $\vec{J}_t\vec{k}_t$. Let us consider $\vec{\Delta J}$ to be the action flux density transferred from the higher frequency pump $(\omega_1,\vec{k}_1)$ to the lower frequency pump $(\omega_2,\vec{k}_2)$ due to the beat wave scattering process. Multiplying Eqs.(1.23) and (1.24) from the left by $\vec{\Delta J}$ and rearranging the terms, we get

$$\left(\vec{\Delta J}\right)\omega_1=\left(\vec{\Delta J}\right)\omega_2+\left(\vec{\Delta J}\right)\omega_3, \tag{1.26}$$

$$\left(\vec{\Delta J}\right)\vec{k}_1=\left(\vec{\Delta J}\right)\vec{k}_2+\left(\vec{\Delta J}\right)\vec{k}_3, \tag{1.27}$$

From these equations we see that the energy loss $(\vec{\Delta J})\omega_1$ of pump $(\omega_1,\vec{k}_1)$ is partitioned, with $(\vec{\Delta J})\omega_2$ going to pump $(\omega_2,\vec{k}_2)$ and $(\vec{\Delta J})\omega_3$ being deposited in the excited beat wave. Similarly, the momentum loss $(\vec{\Delta J})\vec{k}_1$ of the higher frequency pump is partitioned and the corresponding momentum flux density deposited in the beat wave is $(\vec{\Delta J})\vec{k}_3$. This energy $(\vec{\Delta J})\omega_3$ and momentum $(\vec{\Delta J})\vec{k}_3$ of the excited beat wave is available for accelerating electrons and thus driving current. We notice from Eq.(1.27) that for antiparallel pump propagation (where $\vec{k}_3$ is largest), the

momentum flux deposited in the beat wave is the largest compared to the other configurations of pump propagation. Beat wave current drive in a tokamak offers some advantages over other radio-frequency (RF) current drive methods.

(i) The high frequency pump microwaves can easily propagate any region of a tokamak plasma, which provides excellent possibilities to localize the generation region and to control the current profile.
(ii) An intense beat wave with a large phase velocity is able to generate very energetic, nearly collisionless electrons.
(iii) Since the beat wave current drive does not suffer from density limitations due to pump wave propagation, the method is also suitable for high density tokamaks.

However, there are a number of requirements to be met for the achievement of high efficiency in beat wave current drive.

(i) The difference frequency of the two pump microwave beams must match the electron plasma frequency where the current is to be excited.

(ii) The difference wave number must have a substantial component along the toroidal magnetic field line.

(iii) The beat wave phase velocity must not fall too far out on the tail of the electron distribution function so that there are insufficient electrons to damp the plasma beat wave and carry all the current.

(iv) The two pump transverse waves should be similarly polarized.

(v) Finally, the product of the two microwave beam powers must exceed a threshold condition in order to deposit much momentum in the plasma.

The research on beat wave current drive has not advanced much. It is now at a preliminary stage only. No experiment on beat wave current drive has yet been performed. So far, Cohen (1984) and Cohen et al (1988) have studied the possibility of beat wave current drive in tokamak plasmas. They considered parallel and antiparallel pump wave propagation in their analytic as well as numerical studies. They found quite strong coupling of the beat wave momentum to the electron distribution for $1.5 \leq v_{ph}/v_{th} \leq 7.5$ for both the parallel and antiparallel cases in Microwave Tokamak Experiment (MTX) and Engineering Test Reactor (ETR) plasmas (where v_{ph} is the phase velocity of the beat wave and v_{th} is the thermal velocity of

the electrons). Recently, Heikkinen et al (1988) also investigated the basic properties of a beat wave current drive scheme in which parallel pump wave propagation was considered. Both of the earlier considerations of beat wave current drive are restricted to 1D geometry. To model a realistic experiment on beat wave current drive, however, we must take into account the actual toroidal geometry of the tokamak and the finite spatial extent of the pump microwave pulses.

The purpose of the first part of the present thesis is to study the possibility of beat wave current drive by including in our analysis the 2D toroidal inhomogeneity effect and the effect of finite spatial width of the pump microwave pulses on beat wave excitation for current drive application. The toroidal inhomogeneity effect on the beat wave excitation comes through the wavevector mismatch in the exponential factors in the coupled mode equations of beat wave plasma interaction, which is described in chapter 2.

The plan of the first part of the thesis is as follows. First of all, the beat wave coupling formalism and the derivation of the coupled mode equations

associated with current drive in tokamaks is described in Chapter 2. The expression for beat wave current drive efficiency for a Langmuir type beat wave has been derived in Chapter 3, where a simple fluid theory is employed in the same line of view of Cohen et al (1988). Chapter 4 describes the numerical solutions of the coupled mode equations for a Langmuir beat mode whereas Chapter 5 describes the numerical solutions for a cyclotron type beat mode. Finally, a general discussion has been given in Chapter 6.

chapter 2

MODEL EQUATIONS FOR BEAT WAVE CURRENT DRIVE

Derivation of the Coupled Mode Equations

For the derivation of the coupled mode equations of beat wave plasma interaction we employ fluid theory with Maxwell's equations and assume the effects of a weak spatial inhomogeneity on the 2D geometry. The wave modes we consider are high frequency waves. In this case we assume that the plasma ions are immobile.

Maxwell's Equations:

$$\nabla \times \vec{E} = -\frac{1}{c}\frac{\partial \vec{B}}{\partial t}, \tag{2.1}$$

$$\nabla \times \vec{B} = \frac{4\pi}{c}\vec{J} + \frac{1}{c}\frac{\partial \vec{E}}{\partial t}, \tag{2.2}$$

$$\vec{J} = -en\vec{v}, \tag{2.3}$$

where $\vec{E}$ and $\vec{B}$ are the electric and magnetic field vectors, respectively, $\vec{J}$ is the electron current density, n is the electron plasma density, $\vec{v}$ is the electron fluid velocity, e is the absolute value of the electron charge and c is the speed of light.

Poisson's Equation:

$$\nabla \cdot \vec{E} = -4\pi en. \tag{2.4}$$

Momentum Balance Equation:

$$m_e\left(\frac{\partial}{\partial t} + \vec{v}\cdot\nabla\right)\vec{v} = -e\left(\vec{E} + \frac{1}{c}\vec{v}\times\vec{B}\right) + \frac{\nabla P}{n}, \tag{2.5}$$

where P is the plasma pressure and m_e is the electron mass. It can be shown that for the electromagnetic pump fields $(\omega_1,\vec{k}_1)$ and $(\omega_2,\vec{k}_2)$, the electron quiver velocities are given by

$$\vec{v}_j = \left(\frac{-ie}{m_e\omega_j}\right)\vec{\vec{K}}_j\cdot\vec{E}_j, \tag{2.6}$$

where j=1,2 for the electromagnetic pump waves. The dyadics $\vec{\vec{K}}_j$ are related to the mobility tensor $\vec{\vec{M}}_j$ by the relation

$$\vec{\vec{K}}_j = \left(\frac{i\omega_j}{\Omega_e}\right)\vec{\vec{M}}_j, \tag{2.7}$$

where $\Omega_e = eB_0/m_e c$ is the electron cyclotron frequency, B_0 is the toroidal

magnetic field. The current densities oscillating at $(\omega_1,\vec{k}_1)$ and $(\omega_2,\vec{k}_2)$ are given respectively by

$$\vec{J}_1 = -en_0\vec{v}_1 - \frac{1}{2}en_3\vec{v}_2, \tag{2.8}$$

and

$$\vec{J}_2 = -en_0\vec{v}_2 - \frac{1}{2}en_3^*\vec{v}_1, \tag{2.9}$$

where n_0 is the equilibrium electron density and n_3 is the density fluctuation at $(\omega_3,\vec{k}_3)$ due to the nonlinear interaction of the two pump waves with the plasma. The current density $\vec{J}_3$ due to this density fluctuation n_3 is given by

$$\vec{J}_3 = -en_0\vec{v}_3, \tag{2.10}$$

where $\vec{v}_3$ is the electron quiver velocity in the excited beat mode. Using Maxwell's equations, it can be shown that

$$\frac{1}{c^2}\frac{\partial^2\vec{E}_i}{\partial t^2} - \nabla^2\vec{E}_j + \nabla\left(\nabla\cdot\vec{E}_j\right) = \left(\frac{-4\pi}{c^2}\right)\frac{\partial\vec{J}_j}{\partial t}. \tag{2.11}$$

Now substituting the expression for $\vec{J}_1$ and $\vec{J}_2$ from Eqs.(2.8) and (2.9) into Eq.(2.11) and using Poisson's equation

$$n_3 = \left(\frac{-ik_3}{4\pi e}\right) E_3, \tag{2.12}$$

we obtain

$$\frac{1}{c^2}\frac{\partial^2 \vec{E}_1}{\partial t^2} - \nabla^2 \vec{E}_1 + \nabla\left(\nabla \cdot \vec{E}_1\right) + \left(\frac{\omega_p^2}{c^2}\right) \vec{\vec{K}}_1 \cdot \vec{E}_1$$

$$= \left(\frac{-ek_3}{2m_e c^2 \omega_2}\right) \vec{\vec{K}}_2 \cdot \frac{\partial}{\partial t}\left(\vec{E}_2 E_3\right), \tag{2.13}$$

and

$$\frac{1}{c^2}\frac{\partial^2 \vec{E}_2}{\partial t^2} - \nabla^2 \vec{E}_2 + \nabla\left(\nabla \cdot \vec{E}_2\right) + \left(\frac{\omega_p^2}{c^2}\right) \vec{\vec{K}}_2 \cdot \vec{E}_2$$

$$= \left(\frac{ek_3}{2m_e c^2 \omega_1}\right) \vec{\vec{K}}_1 \cdot \frac{\partial}{\partial t}\left(\vec{E}_1 E_3^*\right). \tag{2.14}$$

We assume the rapidly varying part of the wave fields is of the form:

$$\sim \exp\left(i\int \vec{k}\cdot\vec{dx} - i\omega t\right), \tag{2.15}$$

and therefore

$$\frac{\partial}{\partial t} \equiv -i\omega, \tag{2.16a}$$

$$\nabla \equiv i\vec{k}. \tag{2.16b}$$

Eqs (2.13) and (2.14) then take the following form:

$$\vec{\vec{D}}_1\cdot\vec{E}_1 = \left(\frac{iek_3\omega_1}{2m_e\omega_2}\right)\left(\vec{\vec{K}}_2\cdot\vec{E}_2\right)E_3, \tag{2.17}$$

$$\vec{\vec{D}}_2\cdot\vec{E}_2 = \left(\frac{-iek_3\omega_2}{2m_e\omega_1}\right)\left(\vec{\vec{K}}_1\cdot\vec{E}_1\right)E_3^*, \tag{2.18}$$

where

$$\vec{\vec{D}}_j = \left(c^2k_j^2 - \omega_j^2\right)\vec{\vec{I}} - c^2\vec{k}_j\vec{k}_j + \omega_p^2\vec{\vec{K}}_j. \tag{2.19}$$

From the momentum balance equation (2.5):

$$\frac{\partial \vec{v}_3}{\partial t}+\left(\frac{e}{m_e c}\right)\vec{v}_3\times\vec{B}_0=\left(\frac{-e}{m_e}\right)\vec{E}_3-\left(\frac{3v_{th}^2}{n_0}\right)\nabla n_3+\frac{\vec{f}_{NL}}{m_e}, \qquad (2.20)$$

from which it can be shown that

$$\vec{v}_3=\left(\frac{\vec{\vec{iK}}_3}{\omega_3}\right)\cdot\left(-\frac{e\vec{E}_3}{m_e}-\frac{3v_{th}^2\vec{k}_3^2\vec{E}_3}{4\pi n_0 e}+\frac{\vec{f}_{NL}}{m_e}\right), \qquad (2.21)$$

where $\vec{\vec{K}}_3$ is related to the mobility tensor $\vec{\vec{M}}_3$ by the relation similar to Eq.(2.7), $\vec{v}_3$ is the electron quiver velocity in the excited beat mode and $\vec{f}_{NL}$ is the component of the ponderomotive force oscillating at $(\omega_3=\omega_1-\omega_2, \vec{k}_3=\vec{k}_1-\vec{k}_2)$ due to the pump electromagnetic wave fields. The expression for $\vec{f}_{NL}$ is given (see Appendix A) by

$$\vec{f}_{NL}=\left(\frac{-ie^2E_1E_2^*}{2m_e\omega_1\omega_2}\right)\left\{\left(\hat{e}_1\cdot\vec{\vec{K}}_2\cdot\hat{e}_2^*\right)\vec{k}_1-\left(\hat{e}_2^*\cdot\vec{\vec{K}}_1\cdot\hat{e}_1\right)\vec{k}_2\right.$$

$$\left.+\left(\vec{k}_1\cdot\vec{\vec{K}}_2\cdot\hat{e}_2^*\right)\left(\vec{\vec{K}}_1-\vec{\vec{I}}\right)\cdot\hat{e}_1-\left(\vec{k}_2\cdot\vec{\vec{K}}_1\cdot\hat{e}_1\right)\left(\vec{\vec{K}}_2^*-\vec{\vec{I}}\right)\cdot\hat{e}_2^*\right\}, \qquad (2.22)$$

where we have written the electric field vectors of the pump electromagnetic waves in terms of their unit polarization vectors $\hat{\vec{e}}_j$ as

$$\vec{E}_j = E_j \hat{\vec{e}}_j = E_j g_j \left(\hat{\vec{e}}_x + \alpha_j \hat{\vec{e}}_y + \beta_j \hat{\vec{e}}_z \right), \tag{2.23}$$

where $\hat{\vec{e}}_x$, $\hat{\vec{e}}_y$ and $\hat{\vec{e}}_z$ are the unit vectors along the x, y and z axes respectively and α_j and β_j (j=1, 2) are given by

$$\alpha_j = -\left(\frac{i\omega_p^2 \Omega_e \omega_j}{\omega_j^2 \left(\omega_j^2 - \Omega_e^2 \right) - \omega_p^2 \omega_j^2 - c^2 k_j^2 \left(\omega_j^2 - \Omega_e^2 \right)} \right), \tag{2.24}$$

$$\beta_j = -\left(\frac{c^2 k_j^2 \cos\theta_j \sin\theta_j}{\omega_j^2 - \omega_p^2 - c^2 k_j^2 \sin^2\theta_j} \right), \tag{2.25}$$

$$g_j = \left(1 + \alpha_j^* \alpha_j + \beta_j^* \beta_j \right)^{-1/2}. \tag{2.26}$$

We assume the excited beat mode is an electrostatic wave:

$$\vec{E}_3 = E_3 \hat{\vec{e}}_3, \tag{2.27}$$

where

$$\hat{\vec{e}}_3 = \frac{\vec{k}_3}{|\vec{k}_3|}. \tag{2.28}$$

From Maxwell's equations and Eqs.(2.3) and (2.21), we get

$$\vec{\vec{D}}_3 \cdot \vec{E}_3 = \left(\frac{4\pi n_0 e}{m_e}\right) \vec{\vec{K}}_3 \cdot \vec{f}_{NL}, \tag{2.29}$$

where

$$\vec{\vec{D}}_3 = -\omega_3^2 \vec{\vec{I}} + \left(\omega_p^2 + 3k_3^2 v_{th}^2\right) \vec{\vec{K}}_3. \tag{2.30}$$

The three coupled mode equations (Eqs(2.17), (2.18), (2.29)) by using the expression for $\vec{f}_{NL}$ in Eq.(2.29) can be written as follows:

$$\vec{\vec{D}}_1 \cdot \vec{E}_1 = \left(\frac{iek_3\omega_1}{2m_e\omega_2}\right)\left(\vec{\vec{K}}_2 \cdot \vec{E}_2\right) E_3, \tag{2.31}$$

$$\vec{\vec{D}}_2 \cdot \vec{E}_2 = \left(\frac{-iek_3\omega_2}{2m_e\omega_1}\right)\left(\vec{\vec{K}}_1 \cdot \vec{E}_1\right) E_3^*, \tag{2.32}$$

$$\vec{\vec{D}}_3 \cdot \vec{E}_3 = \left(\frac{-iek_3\omega_{p0}^2}{2m_e\omega_1\omega_2}\right)\left(\vec{\vec{K}}_3 \cdot \vec{f}_C\right) E_1 E_2^*, \tag{2.33}$$

where

$$\vec{f}_C = k_3^{-1}\left\{\left(\hat{\vec{e}}_1\cdot\vec{\vec{K}}_2^{*}\cdot\hat{\vec{e}}_2^{*}\right)\vec{k}_1 - \left(\hat{\vec{e}}_2^{*}\cdot\vec{\vec{K}}_1\cdot\hat{\vec{e}}_1\right)\vec{k}_2\right.$$

$$\left. + \left(\vec{k}_1\cdot\vec{\vec{K}}_2^{*}\cdot\hat{\vec{e}}_2^{*}\right)\left(\vec{\vec{K}}_1 - \vec{\vec{I}}\right)\cdot\hat{\vec{e}}_1 - \left(\vec{k}_2\cdot\vec{\vec{K}}_1\cdot\hat{\vec{e}}_1\right)\left(\vec{\vec{K}}_2^{*} - \vec{\vec{I}}\right)\cdot\hat{\vec{e}}_2^{*}\right\}. \qquad (2.34)$$

Writing the electric field amplitudes as

$$\vec{E}_j(\vec{x},t) = \vec{a}_j(\vec{x},t)\exp\left(i\int \vec{k}_j\cdot\vec{dx} - i\omega t\right), \qquad (2.35)$$

(j=1,2,3)

where $\vec{a}_j(x,t)$ are the slowly varying parts of the amplitudes $\vec{E}_j(x,t)$. Now splitting the dispersion tensors $\vec{\vec{D}}_j$ into Hermitian and anti-Hermitian components as:

$$\vec{\vec{D}}_j = \vec{\vec{D}}_j^{H} + \vec{\vec{D}}_j^{A}, \qquad (2.36)$$

then slow modulations of each complex wave amplitude satisfy

$$\vec{\vec{D}}_j \cdot \vec{E}_j = \left(\vec{\vec{D}}_j^H + i\vec{\vec{D}}_j^A \right) \cdot \vec{E}_j \equiv \left(\vec{\vec{D}}_j^H \left(\omega_j + i\frac{\partial}{\partial t}, \vec{k}_j - i\nabla \right) + i\vec{\vec{D}}_j^A \right) \cdot \vec{E}_j$$

$$= i \left(\frac{\partial \vec{\vec{D}}_j^H}{\partial \omega_j} \cdot \hat{\vec{e}} \right) \exp\left(i\int \vec{k}_j \cdot \vec{dx} - i\omega_j t \right) \left(\frac{\partial}{\partial t} + \Gamma_j + \vec{u}_j \cdot \nabla \right) a_j , \qquad (2.37)$$

where Γ_j are the linear damping coefficients of the wave modes and $\vec{u}_j$ are their respective group velocities. The expressions for Γ_j and $\vec{u}_j$ are given by

$$\Gamma_j = \left(\frac{\hat{\vec{e}}_j^* \cdot \vec{\vec{D}}_j^A \cdot \hat{\vec{e}}_j}{\hat{\vec{e}}_j^* \cdot \frac{\partial \vec{\vec{D}}_j^H}{\partial \omega_j} \cdot \hat{\vec{e}}_j} \right), \qquad (2.38)$$

and

$$\vec{u}_j = - \left(\frac{\hat{\vec{e}}_j^* \cdot \frac{\partial \vec{\vec{D}}_j^H}{\partial \vec{k}_j} \cdot \hat{\vec{e}}_j}{\hat{\vec{e}}_j^* \cdot \frac{\partial \vec{\vec{D}}_j^H}{\partial \omega_j} \cdot \hat{\vec{e}}_j} \right). \qquad (2.39)$$

Therefore from Eqs.(2.31), (2.32) and (2.33):

Eq(2.31):

$$i\left(\frac{\partial\vec{\vec{D}}_1^{H}}{\partial\omega_1}\cdot\hat{\vec{e}}_1\right)\exp\left(i\int\vec{k}_1.\vec{dx}-i\omega_1 t\right)\left(\frac{\partial}{\partial t}+\Gamma_1+\vec{u}_1\cdot\nabla\right)a_1$$

$$=\left(\frac{iek_3\omega_1}{2m_e\omega_2}\right)\left(\vec{\vec{K}}_2\cdot\hat{\vec{e}}_2\right)a_2a_3\exp\left(i\int\left(\vec{k}_2+\vec{k}_3\right)\cdot\vec{dx}-i\left(\omega_2+\omega_3\right)t\right), \qquad (2.40)$$

Eq(2.32):

$$i\left(\frac{\partial\vec{\vec{D}}_2^{H}}{\partial\omega_2}\cdot\hat{\vec{e}}_2\right)\exp\left(i\int\vec{k}_2\cdot\vec{dx}-i\omega_2 t\right)\left(\frac{\partial}{\partial t}+\Gamma_2+\vec{u}_2\cdot\nabla\right)a_2$$

$$=\left(\frac{-iek_3\omega_2}{2m_e\omega_1}\right)\left(\vec{\vec{K}}_1\cdot\hat{\vec{e}}_1\right)a_1a_3^*\exp\left(i\int\left(\vec{k}_1-\vec{k}_3\right)\cdot\vec{dx}-i\left(\omega_1-\omega_3\right)t\right), \qquad (2.41)$$

Eq(2.33):

$$i\left(\frac{\partial \vec{\vec{D}}_3^{H}}{\partial \omega_3}\cdot\hat{\vec{e}}_3\right)\exp\left(i\int \vec{k}_3\cdot\vec{dx}-i\omega_3 t\right)\left(\frac{\partial}{\partial t}+\Gamma_3+\vec{u}_3\cdot\nabla\right)a_3$$

$$=\left(\frac{-ick_3\omega_{p0}^2}{2m_e\omega_1\omega_2}\right)\left(\vec{\vec{K}}_3\cdot\vec{f}_C\right)a_1a_2^*\exp\left(i\int\left(\vec{k}_1-\vec{k}_2\right)\cdot\vec{dx}-i\left(\omega_1-\omega_2\right)t\right). \qquad (2.42)$$

Taking dot product of Eqs.(2.40), (2.41) and (2.42) from the left by $\hat{\vec{e}}_1^{\,*}$, $\hat{\vec{e}}_2^{\,*}$ and $\hat{\vec{e}}_3^{\,*}$, respectively, we obtain finally, the following coupled mode equations:

$$\left(\frac{\partial}{\partial t}+\Gamma_1+\vec{u}_1\cdot\nabla\right)a_1=-C_1a_2a_3\exp\left(i\Psi(\vec{x})\right), \qquad (2.43)$$

$$\left(\frac{\partial}{\partial t}+\Gamma_2+\vec{u}_2\cdot\nabla\right)a_2=C_2a_1a_3^*\exp\left(-i\Psi(\vec{x})\right), \qquad (2.44)$$

$$\left(\frac{\partial}{\partial t}+\Gamma_3+\vec{u}_3\cdot\nabla\right)a_3=C_3a_1a_2^*\exp\left(-i\Psi(\vec{x})\right). \qquad (2.45)$$

The coupling coefficients C_1, C_2 and C_3 are given by

$$C_1 = \left(\frac{-ek_3\omega_1}{2m_e\omega_2} \right) \left(\frac{\hat{\vec{e}}_1^{*} \cdot \vec{\vec{K}}_2 \cdot \hat{\vec{e}}_2}{\hat{\vec{e}}_1^{*} \cdot \frac{\partial \vec{\vec{D}}_1^{H}}{\partial \omega_1} \cdot \hat{\vec{e}}_1} \right), \tag{2.46}$$

$$C_2 = \left(\frac{-ek_3\omega_2}{2m_e\omega_1} \right) \left(\frac{\hat{\vec{e}}_2^{*} \cdot \vec{\vec{K}}_1 \cdot \hat{\vec{e}}_1}{\hat{\vec{e}}_2^{*} \cdot \frac{\partial \vec{\vec{D}}_2^{H}}{\partial \omega_2} \cdot \hat{\vec{e}}_2} \right), \tag{2.47}$$

$$C_3 = \left(\frac{-ek_3\omega_{p0}^2}{2m_e\omega_1\omega_2} \right) \left(\frac{\hat{\vec{e}}_3^{*} \cdot \vec{\vec{K}}_3 \cdot \vec{f}_C}{\hat{\vec{e}}_3^{*} \cdot \frac{\partial \vec{\vec{D}}_3^{H}}{\partial \omega_3} \cdot \hat{\vec{e}}_3} \right), \tag{2.48}$$

where $\vec{f}_C$ is given by Eq.(2.34) and

$$\Psi(\vec{x}) = -\int \left(\vec{k}_1 - \vec{k}_2 - \vec{k}_3 \right) \cdot d\vec{x} = -\int \Delta\vec{k} \cdot d\vec{x} = \frac{1}{2} \left(\vec{x} - \vec{x}_R \right) \cdot \vec{\vec{g}} \cdot \left(\vec{x} - \vec{x}_R \right), \tag{2.49}$$

where the spatial variation of the wave vector mismatch has been well

approximated (Reiman, 1979) by the first order term in its Taylor expansion about the exact resonance point $\vec{x}_R=(z,x)=(0,x_R)$. The wave vector mismatch tensor is given by

$$\overleftrightarrow{g}= - \nabla \left(\vec{\Delta k}\right)_{| \vec{x}=\vec{x}_R} . \qquad (2.50)$$

We shall apply Eqs (2.43)-(2.45) in a steady state 2D geometry as our model equations for beat wave current drive application in Tokamaks (Amin and Cairns, 1989,1990). A more exact treatment of the wave propagation in tokamak plasmas would include ray-tracing equations, giving the equation of $\vec{k}$ along the wave trajectory. For simplicity, we have ignored this, and also the effect of different group velocities at different parts of the beam profile. For the pump waves, which are above the cyclotron frequency, we do not expect these effects to make a large difference.

There is another point, since we have used cold plasma theory to derive the coupled mode equations, the anti-Hermitian part of tensor $\overleftrightarrow{D}_j$ is zero. But in reality, this is not the case. So we have artificially included the damping

coefficients Γ_j in the coupled mode equations. However, for the high frequency pump microwaves, $\Gamma_{1,2}$ are zero, but for the beat mode, which will be Landau or cyclotron damped, its damping Γ_3 would be calculated from the hot plasma dispersion relation for an electrostatic wave (Stix, 1962). For this case we do not expect the coupling coefficients to change very much if hot plasma theory is used.

Expression for Wave Vector Mismatch Tensor

This section describes the simplification of the expression for Ψ function (Eq.(2.49)) in the exponential factors of the coupled mode equations (2.43)-(2.45) due to the wave vector mismatch of the three wave resonance process. The components of $\vec{\vec{g}}$ in 2D geometry are as follows:

$$g_{zz} = -\left(\frac{\partial}{\partial z}\Delta k_z\right)_{|\vec{x}=\vec{x}_R}, \tag{2.51a}$$

$$g_{zx} = -\left(\frac{\partial}{\partial z}\Delta k_x\right)_{|\vec{x}=\vec{x}_R}, \tag{2.51b}$$

$$g_{xz} = -\left(\frac{\partial}{\partial x}\Delta k_z\right)_{|\vec{x}=\vec{x}_R}, \qquad (2.51c)$$

$$g_{xx} = -\left(\frac{\partial}{\partial x}\Delta k_x\right)_{|\vec{x}=\vec{x}_R}, \qquad (2.51d)$$

where $\vec{x}_R$ is the exact resonance point. The components of $\vec{\Delta k}$ are as follows:

$$(\Delta k)_z \equiv \Delta k_z = k_1\cos\theta_1 - k_2\cos\theta_2 - k_3\cos\theta_3, \qquad (2.52a)$$

$$(\Delta k)_x \equiv \Delta k_x = k_1\sin\theta_1 - k_2\sin\theta_2 - k_3\sin\theta_3. \qquad (2.52b)$$

In Eqs. (2.52a) and (2.52b), θ_1, θ_2 and θ_3 are respectively the angles made by the wavevectors $\vec{k}_1$, $\vec{k}_2$ and $\vec{k}_3$ with the positive z-axis ($\hat{\vec{B}}_0 \| \hat{\vec{e}}_z$). By using equations (2.52a) and (2.52b), the expressions for the components of $\vec{\vec{g}}$ become

$$g_{zz} = -\left(\frac{\partial k_1}{\partial z}\right)_{\vec{x}_R}\cos\theta_1 + \left(\frac{\partial k_2}{\partial z}\right)_{\vec{x}_R}\cos\theta_2 + \left(\frac{\partial k_3}{\partial z}\right)_{\vec{x}_R}\cos\theta_3, \qquad (2.53a)$$

$$g_{zx} = -\left(\frac{\partial k_1}{\partial z}\right)_{\vec{x}_R} \sin\theta_1 + \left(\frac{\partial k_2}{\partial z}\right)_{\vec{x}_R} \sin\theta_2 + \left(\frac{\partial k_3}{\partial z}\right)_{\vec{x}_R} \sin\theta_3 , \qquad (2.53b)$$

$$g_{xz} = -\left(\frac{\partial k_1}{\partial x}\right)_{\vec{x}_R} \cos\theta_1 + \left(\frac{\partial k_2}{\partial x}\right)_{\vec{x}_R} \cos\theta_2 + \left(\frac{\partial k_3}{\partial x}\right)_{\vec{x}_R} \cos\theta_3 , \qquad (2.53c)$$

$$g_{xx} = -\left(\frac{\partial k_1}{\partial x}\right)_{\vec{x}_R} \sin\theta_1 + \left(\frac{\partial k_2}{\partial x}\right)_{\vec{x}_R} \sin\theta_2 + \left(\frac{\partial k_3}{\partial x}\right)_{\vec{x}_R} \sin\theta_3 , \qquad (2.53d)$$

where we have assumed that the angle of propagation of the wave modes does not change during the interaction. We now need to evaluate the z and x derivatives of the wave vectors at the exact resonant point $\vec{x}_R$. Setting the determinant of the Hermitian part of the dispersion tensor $\vec{\vec{D}}_j$ of the electromagnetic waves to zero:

$$\| \vec{\vec{D}}_j^{H} \| = 0 , \qquad (2.54)$$

gives the dispersion relation. The simplified form of the dispersion relation (2.54) of the pump electromagnetic waves is the Appleton-Hartree dispersion relation:

$$c^2k_j^2 = \omega_j^2 - \omega_p^2\left(1-\frac{\omega_p^2}{\omega_j^2}\right)\left\{1-\frac{\omega_p^2}{\omega_j^2}-\frac{\Omega_e^2\sin^2\theta_j}{\omega_j^2}\right.$$

$$\left.\pm\left[\frac{\Omega_e^4\sin^4\theta_j}{4\omega_j^2}+\left(1-\frac{\omega_p^2}{\omega_j^2}\right)^2\frac{\Omega_e^2\cos^2\theta_j}{\omega_j^2}\right]^{1/2}\right\}^{-1}. \qquad (2.55)$$

Let us define

$$P_j = \left(1-\frac{\omega_p^2}{\omega_j^2}\right), \qquad (2.56a)$$

$$Q_j = 1-\frac{\omega_p^2}{\omega_j^2}-\frac{\Omega_e^2\sin^2\theta_j}{\omega_j^2}\pm\left[\frac{\Omega_e^4\sin^4\theta_j}{4\omega_j^4}+\left(1-\frac{\omega_p^2}{\omega_j^2}\right)^2\frac{\Omega_e^2\cos^2\theta_j}{\omega_j^2}\right]^{1/2}. \qquad (2.56b)$$

The dispersion relation (Eq.(2.55)) now becomes

$$c^2k_j^2 = \omega_j^2\left(1-\frac{\omega_p^2}{\omega_j^2}\frac{P_j}{Q_j}\right). \tag{2.57}$$

Differentiating Eq.(2.57) with respect to X, we obtain

$$\frac{\partial k_j}{\partial X}=\left(\frac{-\omega_p^2 P_j}{2c^2k_jQ_j}\right)\left[\frac{2}{\omega_p}\frac{\partial\omega_p}{\partial X}+\frac{1}{P_j}\frac{\partial P_j}{\partial X}-\frac{1}{Q_j}\frac{\partial Q_j}{\partial X}\right], \tag{2.58}$$

where X=z,x and j=1,2 for the electromagnetic pump waves. By differentiating P_j and Q_j with respect to X:

$$\frac{\partial P_j}{\partial X}=-\frac{2\omega_p}{\omega_j^2}\frac{\partial\omega_p}{\partial X}, \tag{2.59a}$$

$$\frac{\partial Q_j}{\partial X} = -\left(\frac{2\omega_p}{\omega_j^2}\right)\frac{\partial \omega_p}{\partial X} - \left(\frac{2\Omega_e \sin^2\theta_j}{\omega_j^2}\right)\frac{\partial \Omega_e}{\partial X}$$

$$\pm\left\{\left[\frac{\Omega_e \sin^2\theta_j}{2\omega_j^2} + \left(1-\frac{\omega_p^2}{\omega_j^2}\right)^2 \frac{\Omega_e \cos^2\theta_j}{\omega_j^2}\right]\frac{\partial \Omega_e}{\partial X} - \left(1-\frac{\omega_p^2}{\omega_j^2}\right)\frac{2\omega_p \Omega_e^2 \cos^2\theta_j}{\omega_j^4}\frac{\partial \omega_p}{\partial X}\right\}$$

$$\times\left\{\frac{\Omega_e^4 \sin^4\theta_j}{4\omega_j^4} + \left(1-\frac{\omega_p^2}{\omega_j^2}\right)^2 \frac{\Omega_e^2 \cos^2\theta_j}{\omega_j^2}\right\}^{-1/2} . \qquad (2.59b)$$

The cold plasma dispersion relation for the excited electrostatic upper-hybrid beat wave can be written as follows:

$$\hat{e}_3^* \cdot \vec{\vec{D}}_3 \cdot \hat{e}_3 = 0 , \qquad (2.60a)$$

which eventually reduces to

$$\omega_3^2\left(\omega_3^2 - \Omega_e^2\right) = \left(\omega_p^2 + 3k_3^2 v_{th}^2\right)\left(\omega_3^2 - \Omega_e^2 \cos^2\theta_3\right). \qquad (2.60b)$$

Differentiating Eq.(2.60b) with respect to X, we get

$$\frac{\partial k_3}{\partial X}=\left(\frac{1}{3k_3v_{th}^2}\right)\left\{-\omega_p\frac{\partial \omega_p}{\partial X}+\frac{\Omega_e\left[\left(\omega_p^2+3k_3^2v_{th}^2\right)\cos^2\theta_3-\omega_3^2\right]}{\omega_3^2-\Omega_e^2\cos^2\theta_3}\frac{\partial \Omega_e}{\partial X}\right\}. \quad (2.61)$$

We assume the toroidal electron density and magnetic field profiles vary as:

$$\omega_p^2=\omega_{p0}^2\left\{1-\frac{\left(R-R_0\right)^2}{a_0^2}\right\}, \quad (2.62)$$

$$\Omega_e=\Omega_{e0}\left(\frac{R_0}{R}\right), \quad (2.63)$$

where Ω_{e0} is the electron cyclotron frequency along the axis of the tokamak, R_0 and a_0 are respectively the major and minor radius of the tokamak, and

$$\omega_{p0}^2=\left(\frac{4\pi n_0e^2}{m_e}\right), \quad (2.64)$$

$$R^2=\left(x_0-x\right)^2+z^2, \quad (2.65a)$$

$$x_0 = R_0 + a_0 . \tag{2.65b}$$

The geometry is shown in Fig. 2.1.

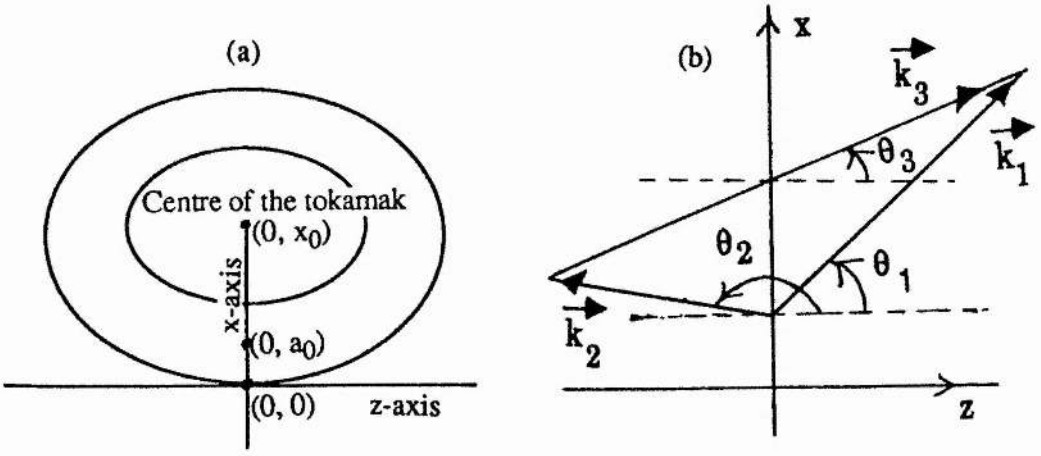

Figure 2.1: (a) Geometry showing the relation between R_0, a_0 and x_0; (b) geometry showing the propagation directions of the wave modes.

Differentiating Eqs(2.62) and (2.63) with respect to X:

$$\frac{\partial \omega_p}{\partial X} = -\left\{ \frac{\omega_{p0}^2 \left(R - R_0 \right)}{\omega_p a_0^2} \right\} \frac{\partial R}{\partial X}, \tag{2.66}$$

$$\frac{\partial \Omega_e}{\partial X} = -\left(\frac{\Omega_{e0} R_0}{R^2} \right) \frac{\partial R}{\partial X} . \tag{2.67}$$

Differentiating Eq.(2.65a) with respect to z and x:

$$\frac{\partial R}{\partial z} = -\left(\frac{x_0 - x}{R}\right), \tag{2.68a}$$

$$\frac{\partial R}{\partial x} = \left(\frac{z}{R}\right). \tag{2.68b}$$

From figure 2.1, we assume the exact resonant point is

$$\vec{x}_R \equiv (z, x) \equiv (0, x_R). \tag{2.69}$$

It can be shown that the x-coordinate of the exact resonant point $\vec{x}_R$ satisfies the equation

$$\left(\frac{\omega_3^2 a_0^2}{\omega_{p0}^2}\right)\left\{\left[1 - \left(\frac{\Omega_{e0}}{\omega_3}\right)^2\right] R_0^2 + 2R_0 f + f^2\right\}$$

$$= \left[\left(1 + \frac{3k_B^2 v_{th}^2}{\omega_{p0}^2}\right) a_0^2 - f^2\right]\left\{\left[1 - \left(\frac{\Omega_{e0}}{\omega_3}\right)^2 \cos^2\theta_3\right] R_0^2 + 2R_0 f + f^2\right\}, \tag{2.70a}$$

where

$$f = a_0 - x_R, \tag{2.70b}$$

and $\vec{k}_B = \vec{k}_1 - \vec{k}_2$ is the driving wavevector due to the pump microwaves whereas $\vec{k}_3$, used in the earlier equations, is the wavevector of the propagating beat wave, and is obtained from the dispersion relation, Eq.(2.60b), $\vec{k}_B \approx \vec{k}_3$.

For a moment if we neglect the spatial dependence of the toroidal magnetic field to calculate the exact resonant point $(0, x_R)$, then we get for an obliquely propagating upper-hybrid beat wave

$$x_R = a_0 \left[1 - \left\{ 1 - \frac{\omega_3^2 \left(\omega_3^2 - \Omega_e^2 \right)}{\omega_{p0}^2 \left(\omega_3^2 - \Omega_e^2 \cos^2\theta_3 \right)} + \frac{3 k_B^2 v_{th}^2}{\omega_{p0}^2} \right\}^{1/2} \right], \tag{2.71a}$$

whereas for a simple Langmuir type beat wave, substituting $\theta_3 \approx 0$, in Eq.(2.71a), we obtain

$$x_R = a_0 \left[1 - \left\{ 1 - \frac{\omega_3^2}{\omega_{p0}^2} + \frac{3 k_B^2 v_{th}^2}{\omega_{p0}^2} \right\}^{1/2} \right]. \tag{2.71b}$$

Now it is easy to calculate different quantities at the exact resonant point $(0,x_R)$:

$$(R)_{\vec{x}_R} = x_0 - x_R, \tag{2.72a}$$

$$\left(\frac{\partial R}{\partial z}\right)_{\vec{x}_R} = 0, \tag{2.72b}$$

$$\left(\frac{\partial R}{\partial x}\right)_{\vec{x}_R} = -1. \tag{2.72c}$$

Substituting (2.72a)-(2.72c) into Eqs.(2.66) and (2.67), we obtain

$$\left(\frac{\partial \omega_p}{\partial z}\right)_{\vec{x}_R} = 0, \tag{2.73a}$$

$$\left(\frac{\partial \omega_p}{\partial x}\right)_{\vec{x}_R} = \left\{\frac{\omega_{p0}^2 \left(a_0 - x_R\right)}{\left(\omega_p\right)_{\vec{x}_R} a_0^2}\right\}, \tag{2.73b}$$

$$\left(\frac{\partial \Omega_e}{\partial z}\right)_{\vec{x}_R} = 0, \tag{2.73c}$$

$$\left(\frac{\partial \Omega_e}{\partial x}\right)_{\vec{x}_R} = \left\{\frac{\Omega_{e0} R_0}{(x_0 - x_R)^2}\right\}. \tag{2.73d}$$

Using the expressions (2.73a)-(2.73d) and calculating the other parameters in Eqs(2.58) and (2.61) at the exact resonance point $\vec{x}_R$, we can evaluate the z and x derivatives of the wave vectors at the exact resonance point. Substitution of these in Eqs(2.53a)-(2.53d) will give the different components of the wave vector mismatch tensor $\vec{\vec{g}}$. The following simplified expression for the detuning parameter due to the wave vector mismatch can then be easily calculated:

$$\Psi \equiv \Psi(z, x) = \frac{1}{2}\left[z^2 g_{zz} + z(x - x_R)(g_{zx} + g_{xz}) + (x - x_R)^2 g_{xx}\right]. \tag{2.74}$$

chapter 3

EXPRESSION FOR CURRENT DRIVE EFFICIENCY FOR A LANGMUIR BEAT WAVE

Let us define two quantities

$$\rho = \left(\frac{J_2^{in}}{J_1^{in}} \right), \tag{3.1}$$

known as the input ratio, and

$$R_a = \left(\frac{\Delta J}{J_1^{in}} \right), \tag{3.2}$$

known as the relative action transfer (Cohen et al, 1988). Where $J_1{}^{in}$ and $J_2{}^{in}$ are the input action flux densities of the pump microwaves and ΔJ is the transfer of action flux density from the higher frequency pump to both the lower frequency pump and the excited beat wave due to the nonlinear three-wave interaction. The action flux density $\vec{J}$ of an electromagnetic wave has been defined in Eq.(1.25) in the previous chapter 1. The fraction of power delivered to the beat wave is given by

$$\left(\frac{\omega_3 \Delta J}{\omega_1 J_1^{in} + \omega_2 J_2^{in}}\right) = \left(\frac{\omega_3 R_a}{\omega_1(1+\omega_2\rho/\omega_1)}\right) = q_e R_a, \tag{3.3}$$

where

$$q_e = \left(\frac{\omega_3}{\omega_1(1+\omega_2\rho/\omega_1)}\right) \tag{3.4}$$

is known as the quantum efficiency (Cohen et al, 1988). If $\vec{J}_1$ is the action flux remaining in the higher frequency pump $(\omega_1, \vec{k}_1)$ after interaction, and assuming that its direction of propagation remains the same as before the interaction, which is appropriate for well underdense plasma, then the transfer of action flux density from the higher frequency pump to the lower frequency pump is

$$\vec{\Delta J} = \vec{J}_1^{in} - \vec{J}_1 = \Delta J\left(\cos\theta_1 \hat{\vec{e}}_z + \sin\theta_1 \hat{\vec{e}}_x\right), \tag{3.5}$$

where

$$\Delta J = J_1^{in} - J_1 . \tag{3.6}$$

The momentum flux density deposited in the beat wave, which we assume is propagating almost parallel to the toroidal magnetic field ($\vec{B}_0 \| \hat{\vec{e}}_z$) is

$$\left(\overrightarrow{\Delta J}\right)\vec{k}_3 = \left(k_3 \Delta J\right)\left(\cos\theta_1\cos\theta_3\,\hat{\vec{e}}_z\hat{\vec{e}}_z + \cos\theta_1\sin\theta_3\,\hat{\vec{e}}_z\hat{\vec{e}}_x + \sin\theta_1\cos\theta_3\,\hat{\vec{e}}_x\hat{\vec{e}}_z + \sin\theta_1\sin\theta_3\,\hat{\vec{e}}_x\hat{\vec{e}}_x\right). \quad (3.7)$$

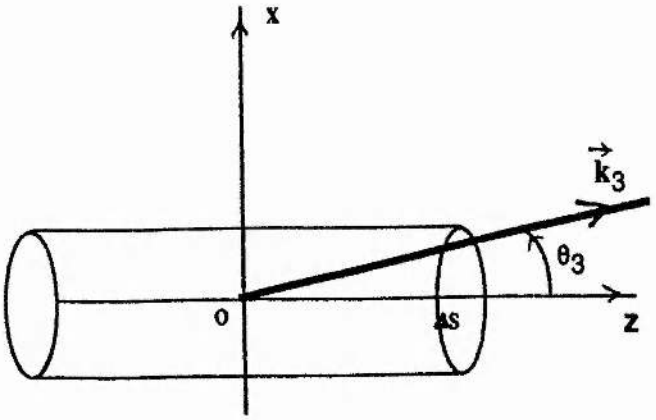

Figure 3.1: Calculation of the momentum flux density deposited in the beat wave.

Let us consider a cross-sectional area Δs [Fig. 3.1], perpendicular to the z-axis, so that its direction is along $\hat{\vec{e}}_z$. Then the rate of momentum density flow of the beat wave ($\omega_3, \vec{k}_3$) across area Δs is

$$= \left(\left(\overrightarrow{\Delta J}\right)\vec{k}_3 \cdot (\Delta s)\,\hat{\vec{e}}_z\right). \quad (3.8)$$

The z-component of the rate of momentum density flow across area Δs is then

$$= \left(\hat{\vec{e}}_z \cdot \left[\left(\vec{\Delta J} \right) \vec{k}_3 \right] \cdot (\Delta s) \hat{\vec{e}}_z \right). \tag{3.9}$$

Therefore, the z-component of the current density flow introduced on each toroidal transit of the electrons due to the beat wave is

$$\Delta j_{e\|} = \left(\frac{-e}{m_e v_\|} \right) \left(\hat{\vec{e}}_z \cdot \left[\left(\vec{\Delta J} \right) \vec{k}_3 \right] \cdot \hat{\vec{e}}_z \right). \tag{3.10}$$

Using Eq. (3.7), we can write Eq. (3.10) as

$$\Delta j_{e\|} = \left(\frac{-e}{m_e v_\|} \right) \left(k_3 (\Delta J) \cos\theta_1 \cos\theta_3 \right). \tag{3.11}$$

A simple rate equation describing the buildup of toroidal current j_t, when electron-ion collisions are the dominant loss mechanism can easily be deduced (Cohen et al, 1988) and which is

$$\frac{d}{dt} j_t = \left(\frac{\Delta j_{e\|}}{\tau} \right) - \nu_r j_t^r - \nu_b j_t^b + \left(\frac{e^2 n_e}{m_e} \right) E_t, \tag{3.12}$$

in the non-relativistic limit, where E_t is the toroidal induction current field, and

$$j_t = j_t^r + j_t^b \tag{3.13}$$

is the sum of fast resonant and bulk current contributions, ν_r is the collisional slowing down rate of a fast electron and ν_b is the slowing down rate of a bulk electron ($\nu_b \gg \nu_r$), τ (= $2\pi R_0/ v_{||}$) is the toroidal transit time, $v_{||} = \omega_3/k_3 \cos\theta_3$ is the resonant electron velocity and R_0 is the major radius of the tokamak. The expression of $\Delta j_{el||}$ assumes that the beat wave is completely damped by the resonant electrons over a toroidal transit. At steady state

$$\frac{d}{dt} j_t = E_t = j_t^b = 0, \tag{3.14}$$

and Eq.(3.12) gives the toroidal current

$$j_t = \left(\frac{\Delta j_{el||}}{\nu_r \tau} \right). \tag{3.15}$$

Using Eq.(3.11) in Eq.(3.15) and substituting the expression for τ, we obtain

$$j_t = -\left(\frac{ek_3(\Delta J)\cos\theta_1\cos\theta_3}{2\pi R_0 m_e \nu_r}\right). \tag{3.16}$$

The total input power

$$\omega_1 J_1^{in} + \omega_2 J_2^{in} = \omega_1 J_1^{in}\left(1+\omega_2\rho/\omega_1\right) = \left(\frac{\omega_3}{q_e}\right) J_1^{in}. \tag{3.17}$$

The efficiency of current drive can now be defined as

$$\eta_{bw} = \left|\frac{\text{toroidal electron current}}{\text{total input power}}\right|. \tag{3.18}$$

Using Eqs. (3.16) and (3.17) in Eq. (3.18), we obtain finally, the expression of beat wave current drive efficiency for a Langmuir beat wave as

$$\eta_{bw} = \left(\frac{q_e R_a e\cos\theta_1}{2\pi R_0 v_{\parallel} m_e \nu_r}\right). \tag{3.19}$$

The expression for ν_r is given by (Cohen et al, 1988)

$$\nu_r = 3.9\times 10^{-6}\, s^{-1}\, \varepsilon_e(eV)^{-3/2} Z_i^2 n_i \ln\Lambda\,, \qquad (3.20)$$

where n_i is the ion density, Z_i is the charge state of the ions and $\ln\Lambda$ is the Coulomb logarithm. We assume $n_i=n_e$(the electron density) and $Z_i=1$. $\varepsilon_e=m_e(v_{\parallel}^2+v_{\perp}^2)/2$, is the energy of the resonant electrons with $v_{\parallel}>>v_{\perp}$, and can be approximated as $\varepsilon_e=m_e(v_{ph}^2+v_{th}^2)/2$, where v_{ph} is the phase velocity of the beat wave and v_{th} is the thermal velocity of the electrons. The validity of Eq.(3.19) depends on the beat wave being completely damped by the resonant electrons. We see from Eq.(3.19) that the efficiency of beat wave current drive depends on the nonlinear wave interactions through two quantities q_e, the quantum efficiency, and R_a, the relative action transfer. From the definition of q_e, given by Eq.(3.4), we see that for low frequency pump lasers we get a comparatively large quantum efficiency. We need high power pump electromagnetic waves to excite a large-amplitude beat wave, and at the same time we seek comparatively low frequency of the pumps for good quantum efficiency.

That is why free electron lasers are important for beat wave current drive application. Similarly, the relative action transfer, R_a is also important for beat wave current drive. From the definition of R_a, given by Eq.(3.2), we see that the maximum value of the relative action transfer can not exceed unity. Thus the price of the advantages of the beat wave current drive described earlier is the use of two intense microwave sources and the reduction of the current drive efficiency by the factor $q_e R_a$ in Eq.(3.19), where $q_e < 1$, $R_a \leq 1$. So, for a comparatively large value of R_a, pump depletion of the highest frequency wave is important for beat wave current drive.

chapter 4

NUMERICAL SOLUTION OF THE MODEL EQUATIONS FOR A LANGMUIR BEAT WAVE

To solve the model equations (2.43)-(2.45) numerically, we consider a 2D steady state situation ($\partial/\partial t=0$, $\nabla=(\partial/\partial z, \partial/\partial x)$). The steady state condition is appropriate for times longer than the inverse damping rate of the excited beat wave (Cohen et al, 1988). The damping coefficients Γ_1 and Γ_2 for the pump electromagnetic waves are zero, whereas we assume the damping Γ_3 of the excited beat mode as Landau damping. The 2D geometry is reasonable approximation for waves incident in the median plane of the tokamak. With these assumptions, the model equations become

$$\left(u_{1x}\frac{\partial}{\partial x}+u_{1z}\frac{\partial}{\partial z}\right)a_1=-C_1a_2a_3\exp(i\Psi), \tag{4.1}$$

$$\left(u_{2x}\frac{\partial}{\partial x}+u_{2z}\frac{\partial}{\partial z}\right)a_2=C_2a_1a_3^*\exp(-i\Psi), \tag{4.2}$$

$$\left(u_{3x}\frac{\partial}{\partial x}+u_{3z}\frac{\partial}{\partial z}+\Gamma_3\right)a_3=C_3a_1a_2^*\exp(-i\Psi). \tag{4.3}$$

In Eq.(4.3), Γ_3 is the Landau damping rate, whose expression is given by

$$\Gamma_3 = \sqrt{\frac{\pi}{8}}\left(\frac{\omega_p}{k_3^3\lambda_D^3}\right)\exp\left(-\frac{1}{2k_3^2\lambda_D^2}-\frac{3}{2}\right), \tag{4.4}$$

where λ_D is the electron Debye length. For the examples we consider in this chapter, with almost antiparallel pump waves, where $0.2< k_3\lambda_D <0.6$, Eq.(4.4) can be used to calculate Γ_3. However, for shorter wavelengths, or hotter plasmas, where $k_3\lambda_D$ can be of order 1, Eq.(4.4) then becomes inaccurate and Γ_3 must be calculated numerically from the hot plasma dispersion relation (Stix, 1962). The expressions for the coupling coefficients C_1, C_2, C_3 are simplified in the Appendix B.

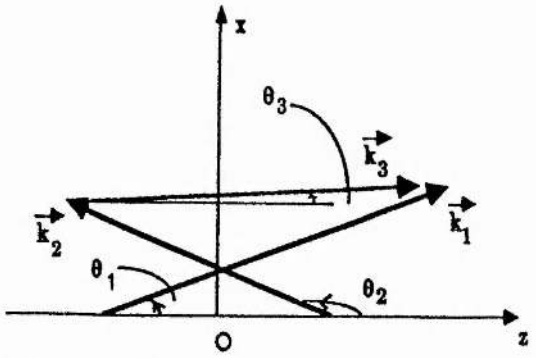

Figure 4.1: The direction of propagation of the wave modes; $\vec{k}_1$, $\vec{k}_2$, $\vec{k}_3$ are the wavevectors of the higher frequency pump, lower frequency pump and the excited beat mode respectively.

For our 2D geometry shown in Fig.4.1, where we arrange the pump wave propagation directions $\vec{k}_1$ and $\vec{k}_2$ such that $\theta_2=\pi-\theta_1$, it is found that the angle θ_3, which is the angle between $\vec{k}_3$ and +z-axis, is very small ($0^0<\theta_3<4^0$); consequently, $\vec{k}_3$ is almost parallel to the toroidal magnetic field ($\hat{e}_z \| \vec{B}_0$), so that we can consider the excited beat mode is simply a Langmuir wave. We consider our problem as an initial boundary value problem. We solve the coupled first order 2D equations (4.1)-(4.3) for the wave amplitudes by applying an explicit finite difference scheme. The independent variable x behaves like time variable and the independent variable z behaves like position variable. We assume a 2D slab geometry (Fig.4.2) shown below.

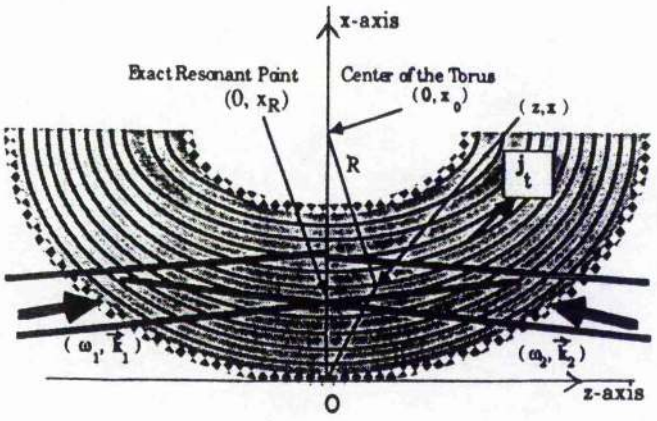

Figure 4.2: Geometry of Beat wave current drive.

x - direction ⇒ direction toward the centre of the tokamak,

z - direction ⇒ instantaneous direction of the toroidal magnetic field.

To satisfy the CFL (Courant-Friedrichs-Lewy) condition for our geometry, we take backward difference formula for $\partial_z a_1$ and $\partial_z a_3$ and forward difference formula for $\partial_z a_2$. For the x-derivatives of all the amplitudes, we take forward difference formula. The resulting nonlinear coupled difference equations for the amplitudes can then be written as follows.

$$a_1(i,j+1) = pw_1 a_1(i-1,j) + (1-pw_1)\, a_1(i,j) - \Delta x \left(\frac{C_1}{u_{1x}}\right) a_2(i,j)\, a_3(i,j) \exp\left(i\Psi(i,j)\right), \quad (4.5)$$

$$a_2(i,j+1) = -pw_2 a_2(i+1,j) + (1+pw_2)\, a_2(i,j) + \Delta x \left(\frac{C_2}{u_{2x}}\right) a_1(i,j)\, a_3^*(i,j) \exp\left(-i\Psi(i,j)\right), \quad (4.6)$$

$$a_3(i,j+1) = pw_3 a_3(i-1,j) + (1-pw_3)\, a_3(i,j) - \Delta x \left(\frac{\Gamma_3}{u_{3x}}\right) a_3(i,j)$$

$$+ \Delta x \left(\frac{C_3}{u_{3x}}\right) a_1(i,j)\, a_2^*(i,j) \exp\left(-i\Psi(i,j)\right), \quad (4.7)$$

where (i,j) is a grid point, i is along z-direction and j is along x-direction, $p=\Delta x/\Delta z$, and $w_j=u_{jz}/u_{jx}$, u_{jz} and u_{jx} are the components of the group

velocities (j=1,2,3). The mesh lengths between two consecutive grid points along x- and z-direction have been taken respectively as Δx and Δz. CFL condition requires simultaneously

$$1 - pw_1 \geq 0, \tag{4.8a}$$

$$1 + pw_2 \geq 0, \tag{4.8b}$$

$$1 - pw_3 \geq 0. \tag{4.8c}$$

We need the further condition

$$\Delta x \left(\frac{\Gamma_3}{u_{3x}} \right) \leq 1 \tag{4.9}$$

to satisfy for the geometry we have considered. However, for very small $u_3(\approx 0)$, we neglect the convective derivative term compared to the strong damping term $\Gamma_3 a_3$ in the beat wave equation (Eq.(4.3)). We consider finite spatial extent pumps, with initially Gaussian profiles:

$$a_1(z,0) = a_1^{max} \exp\left(- \frac{(z - z_1)^2 \sin^2\theta_1}{L_1^2} \right), \qquad (4.10a)$$

$$a_2(z,0) = a_2^{max} \exp\left(- \frac{(z - z_2)^2 \sin^2\theta_2}{L_2^2} \right). \qquad (4.10b)$$

We consider the identical polarization of the pump microwave fields for efficient coupling of the beat wave interaction. We take for example, two types of tokamak, one is smaller, typical of MTX at Livermore (Thomassen, 1988) and the other one is larger, such as JET. The latter provides an interesting comparison, even though there are no plans, so far as we know, to use beat wave current drive in this or any comparable machine. The typical parameters of these two types of tokamak and the microwave parameters (Thomassen, 1988) are given in Tables I and II respectively. The illuminated cross-section of the microwave beams is elliptical but we have taken the equivalent circular cross-section for our numerical calculation.

We present some graphics of the numerical solutions of our model equations in Figs.4.3 - 4.12. We see from the Figs. 4.3(a), 4.4(a), 4.7(a), 4.8(a), 4.11(a) and 4.12(a) that the pump microwave pulses approach toward each other with the higher frequency pump from the left and the lower frequency pump from the right. After the interaction the shape of the pump profiles has been changed as can be seen from the graphics. The shape of the profiles has been changed due to the nonlinear interaction. A beat wave is excited at the interaction region with frequency $\omega_3 = \omega_1 - \omega_2$ and wave vector $\vec{k}_3 = \vec{k}_1 - \vec{k}_2$. We cannot see the profile of the amplitude of the beat wave in Figs. 4.3(a), 4.4(a), 4.7(a), 4.8(a), 4.11(a) and 4.12(a) because the excited beat wave is heavily Landau damped in the interaction region. Figures 4.3(b), 4.4(b), 4.7(b), 4.8(b), 4.11(b) and 4.12(b) show the evolution of the beat wave amplitude.

Figures 4.5 and 4.9 show the variation of the relative action transfer R_a with x-coordinates for different propagation directions of the pump microwave pulses. We see from these figures that as the angle between the directions of propagation of the pump microwave pulses decreases, the relative action transfer also decreases.

Figures 4.6 and 4.10 show the variation of the relative action transfer R_a with x-coordinates for different input power ratios $r=P_2/P_1$, where P_1 and P_2 are the input powers of the pumps $(\omega_1,\vec{k}_1)$ and $(\omega_2,\vec{k}_2)$ respectively. We see from Figs 4.6 and 4.10 that the relative action transfer increases with input power ratio r. The input ratio ρ defined by Eq.(3.1) depends on the wave numbers of the pump modes (see Eqs.(1.25) and (3.1)). The wavenumbers of the pump modes depend on their polarization, therefore, for the same input power ratio $r=P_2/P_1$, the input ratio $\rho=J_2^{in}/J_1^{in}$ will be slightly different for different polarization states of the pumps.

The dependence of the fraction of energy $f_E=q_eR_a$ deposited in the beat wave and the current drive efficiency η_{bw} on the input power ratio r, the quantum efficiency q_e and the relative action transfer R_a is shown in Tables III and IV. Table V shows the dependence of the relative action transfer R_a on the input ratio ρ and the quantum efficiency q_e for small incidence angle of the pumps. In that table we consider the input ratio ρ instead of input power ratio r to compare our results with the 1D results of Cohen et al

(1988). It is noted here that the quatities ρ and r are not very different. We see from Figure 4.5 and 4.9 that the relative action transfer increases as the angle between the pump microwaves increases. Although our code can not handle exactly antiparallel pump waves, the results for incidence angle of 2^0 for LCP pumps (Table V) in MTX approach those obtained by Cohen et al (1988) for the antiparallel case. For input ratios of 0.1 and 0.01 we obtain relative action transfer of 0.756 and 0.335 respectively which compare well with the relative action transfer of 0.8 and 0.4 obtained by Cohen et al for their input ratios 0.1 and 0.01. From the Figs. 4.5(b) and 4.9(b), we can see that as the incidence angle $\theta_1(\theta_2=\pi-\theta_1)$ of the higher frequency pump increases above 2^0 the relative action transfer falls rapidly from the values obtained by Cohen et al (1988) from their exact antiparallel pump propagation case.

Due to the nonlinear interaction of the two intense microwave pulses with the plasma, an electrostatic beat wave is excited in the interaction region. This beat wave is then damped over a relatively very short distance by the resonant electrons going around the torus. On averaging over many pulses, the beat wave coupling delivers momentum to the resonant electrons, and

thus these electrons drive a current. The fraction of power delivered to the beat wave is given by the quantum efficiency q_e times the relative action transfer R_a, which depends nonlinearly on the pump wave peak intensities. The current drive efficiency depends on the peak power (to achieve a satisfactory value of R_a), and the current is proportional to the current drive efficiency times the average power. We have considered only opposed propagation of the incident pump microwaves to ensure good coupling of the beat wave interaction. We have varied the incident angles of the pumps in both cases, MTX and JET, and found good coupling and efficient action transfer, but as the angle between the pumps is decreased the coupling getting weaker and weaker (Figs 4.5 and 4.9). It has been found that the action transfer depends on the input power ratio r, the larger the input power ratio the greater the action transfer (Figs.4.6 and 4.10). However, it is important to note here that, although the relative action transfer increases with the input power ratio, the quantum efficiency decreases. As is mentioned earlier (Eq.(3.19)), the beat wave current drive efficiency is directly proportional to the product of these two quantities.

From the figures we see that as the both pump microwaves approach towards the interaction region, the right edge of the higher frequency pump and the left edge of the lower frequency pump first meet with each other, and participate in the beat wave coupling process. For strong interaction and as the interaction continues, the higher frequency pump transfers almost all of its action (pump depletion) both to the lower frequency pump (2nd pump) and to the beat wave, before traversing the complete beam cross section of the second pump. As a result, the left edge of the 2nd pump gets amplified, whereas the rest of the profile remains almost unaffected. We see this type of behaviour in MTX for small θ_1(Fig.4.3), where for a particular set of parameters we get pump depletion of the higher frequency pump. This happens because after losing the action by strongly interacting with the left edge of the 2nd pump profile, the higher frequency pump microwave has not enough action to drive the beat wave interaction process. However, for relatively weak coupling, the whole profile of the 2nd pump amplitude is being amplified, although there is a tendency of the left half of the profile to be amplified more. We see this type of behaviour in JET (Fig.4.7), where for a particular set of input parameters we get relatively weaker pump depletion.

The ray paths of the transverse pump microwaves are obliquely incident at the plasma edge as shown in Fig.1.2. So, there are two modes for any angle of propagation, the extraordinary (X) and ordinary (O) modes. For approximately antiparallel propagation of the pumps the X-mode becomes right-hand circularly polarized (RCP) mode and the O-mode becomes left-hand circularly polarized (LCP) mode. The X-mode and O-mode pumps drive distinct beat modes at the same frequency and in the same interaction region, but with different wave numbers and phase velocities. The energy of the transverse pump waves available for beat wave coupling, is shared in two independent three-wave interactions.

We have calculated the current drive efficiency for RCP and LCP pump modes in MTX and in JET. In both devices the current drive efficiency for RCP pump modes is significantly higher than that for LCP pump modes for the same input parameters. For an average power of 2 MWatts for the higher frequency pump in MTX, Table III gives 180 kAmps of beat wave current for RCP pump modes, whereas Table IV gives 64 kAmps of beat wave current for LCP pump modes. Similarly for JET, now we consider a five-fold increase in the microwave pulse rate from that in MTX, so that an

average power of 10 MWatts is provided in the first pump wave (Cohen et al, 1988) but with same peak pump power. Table III then gives 360 kAmps of beat wave current for RCP pump modes whereas Table IV gives 135 kAmps of beat wave current for LCP pump modes in JET.

TABLE I. TOKAMAK PARAMETERS

	MTX	JET
Plasma electron density, n_e(cm^{-3})	0.7-0.8 $\times 10^{14}$	0.8-1.1 $\times 10^{14}$
Electron temperature, T_e (keV)	1.5-2.0	8.5-12.0
Plasma current, I_p (MAmp)	0. 250-0.500	4.8
Toroidal magnetic field, B_0 (tesla)	3.9	3.4
Major radius, R_0 (m)	0.64	3.0
Minor radius, a_0 (m)	0.165	1.2

TABLE II. MICROWAVE PARAMETERS

Higher pump frequency	ω_1=250 - 280 GHz
Peak power of the higher frequency pump	P_1=8.0 - 24.0 GWatts
Average power of the higher frequency pump	P_{1av}=2.0 - 10.0 MWatts
Lower pump frequency	ω_2=160 - 175 GHz
Peak power of the lower frequency pump	$P_2=5.0\times10^{-3}$ - 25.0 GWatts
Average power of the lower frequency pump	$P_{2av}=1.25\times10^{-3}$-10.0 MWatts
Pulse length	t_p=50 ns
Pulse repetition rate	f_{pr}=5 - 25 kHz
Illuminated cross-section of the pumps (elliptical)	the lengths of the minor and major axes of the ellips are 3 cm and 8 cm respectively

TABLE III. DEPENDENCE OF THE CURRENT DRIVE EFFICIENCY η_{bw} ON THE INPUT POWER RATIO r, THE QUANTUM EFFICIENCY q_e AND ON THE RELATIVE ACTION TRANSFER R_a WHEN THE PUMP WAVES ARE RIGHT HAND POLARIZED MODES

	MTX: P_1=8.0 GW, ω_1=255 GHz, ω_2=170GHz, $\theta_1=5^0$, $\theta_2=175^0$, v_{ph}/v_{th}=4.6. Both pumps are RCP modes: $\eta_{bw}= 0.265\, q_e R_a \cos\theta_1$ (A/W).				JET: P_1=8.0 GW, ω_1=260 GHz, ω_2=160 GHz, $\theta_1=5^0$, $\theta_2=175^0$, v_{ph}/v_{th}=2.3. Both pumps are RCP modes: $\eta_{bw}= 0.109\, q_e R_a \cos\theta_1$(A/W).			
r	0.625	0.625×10^{-1}	0.625×10^{-2}	0.625×10^{-3}	3.125	0.625	0.625×10^{-1}	0.625×10^{-2}
q_e	0.232	0.324	0.331	0.334	0.152	0.293	0.374	0.381
R_a	1.000	0.992	0.913	0.781	1.000	0.992	0.763	0.391
f_E	0.232	0.321	0.302	0.261	0.152	0.291	0.285	0.149
η_{bw}(A/W)	0.061	0.085	0.080	0.069	0.017	0.032	0.031	0.016

TABLE IV. DEPENDENCE OF THE CURRENT DRIVE EFFICIENCY η_{bw} ON THE INPUT POWER RATIO r, THE QUANTUM EFFICIENCY q_e AND ON THE RELATIVE ACTION TRANSFER R_a WHEN THE PUMP WAVES ARE LEFT HAND POLARIZED MODES

	MTX: P_1=8.0 GW, ω_1=255 GHz, ω_2=170GHz, $\theta_1=5^0$, $\theta_2=175^0$, v_{ph}/v_{th}=3.9. Both pumps are LCP modes: η_{bw}= 0.189 $q_e R_a \cos\theta_1$ (A/W).				JET: P_1=8.0 GW, ω_1=260 GHz, ω_2=160 GHz, $\theta_1=5^0$, $\theta_2=175^0$, v_{ph}/v_{th}=1.8. Both pumps are LCP modes: η_{bw}= 0.078 $q_e R_a \cos\theta_1$ (A/W).			
r	3.125	0.625	0.625×10^{-1}	0.625×10^{-2}	3.125	0.625	0.625×10^{-1}	0.625×10^{-2}
q_e	0.083	0.214	0.312	0.332	0.100	0.245	0.368	0.381
R_a	0.988	0.731	0.257	0.154	0.972	0.607	0.174	0.086
f_E	0.082	0.156	0.080	0.051	0.097	0.149	0.064	0.033
η_{bw}(A/W)	0.015	0.030	0.015	0.009	0.008	0.012	0.005	0.003

TABLE V. CURRENT DRIVE EFFICIENCY FOR LEFT HAND POLARIZED PUMP MODES WHEN THE DIRECTION OF PROPAGATION OF THE PUMPS ARE ALMOST ANTIPARALLEL

	MTX: P_1=8.0 GW, ω_1=255 GHz, ω_2=170GHz, $\theta_1=2^0$, $\theta_2=178^0$, v_{ph}/v_{th}=3.39. Both pumps are LCP modes: η_{bw}= 0.189 $q_c R_a \cos\theta_1$ (A/W).			JET: P_1=24.0 GW, ω_1=260 GHz, ω_2=160 GHz, $\theta_1=2^0$, $\theta_2=178^0$, v_{ph}/v_{th}=1.83. Both pumps are LCP modes: η_{bw}= 0.078 $q_c R_a \cos\theta_1$ (A/W).		
ρ	0.500	0.100	0.010	0.500	0.100	0.010
q_c	0.225	0.304	0.330	0.262	0.352	0.381
R_a	0.976	0.756	0.335	0.995	0.859	0.449
f_E	0.220	0.230	0.111	0.261	0.302	0.171
η_{bw}(A/W)	0.042	0.043	0.021	0.020	0.024	0.013

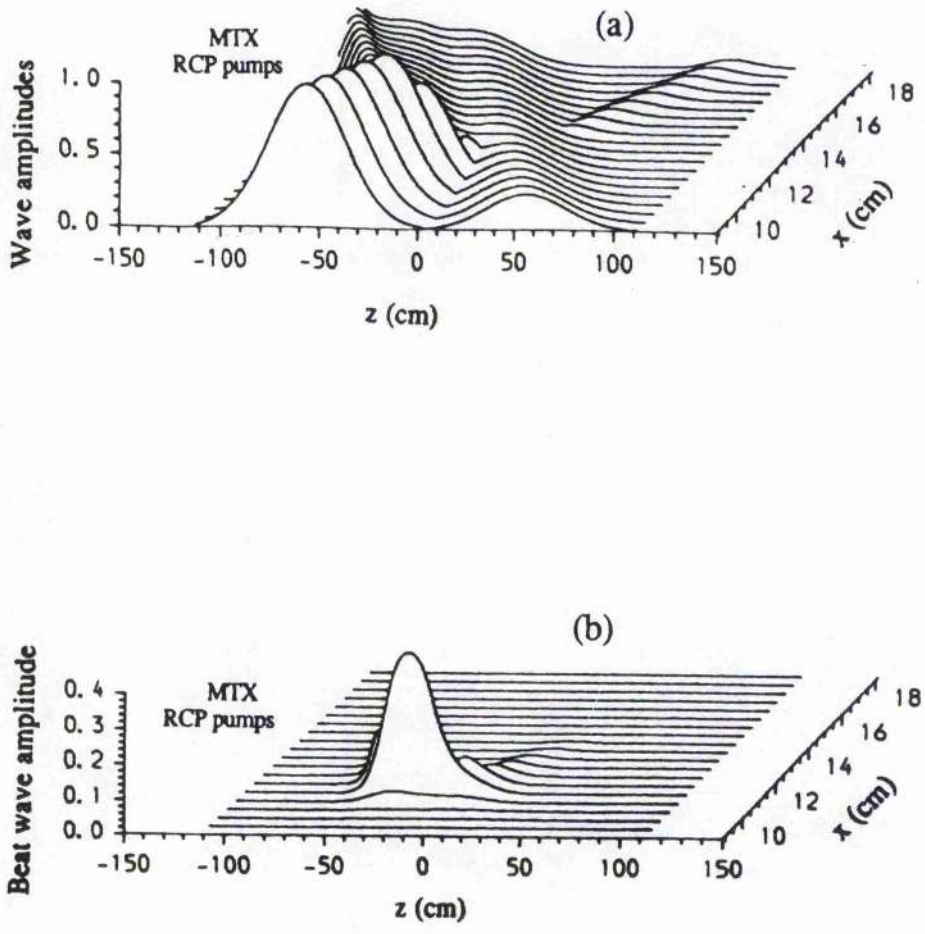

Figure 4.3: MTX parameters: (a) Evolution of the wave amplitudes. (b) Evolution of the beat wave amplitude. Both pumps are RCP modes: ω_1=255 GHz, ω_2=170 GHz, P_1=8.0 GW, P_2=0.5 GW ($r \approx 0.625 \times 10^{-1}$), $\theta_1=5^0$, $\theta_2=175^0$, $n_{e0}=0.8 \times 10^{14}$ (cm^{-3}), T_e=1.5 keV, B_0=3.9 T. The amplitudes are normalized by the initial peak amplitude of the higher frequency pump.

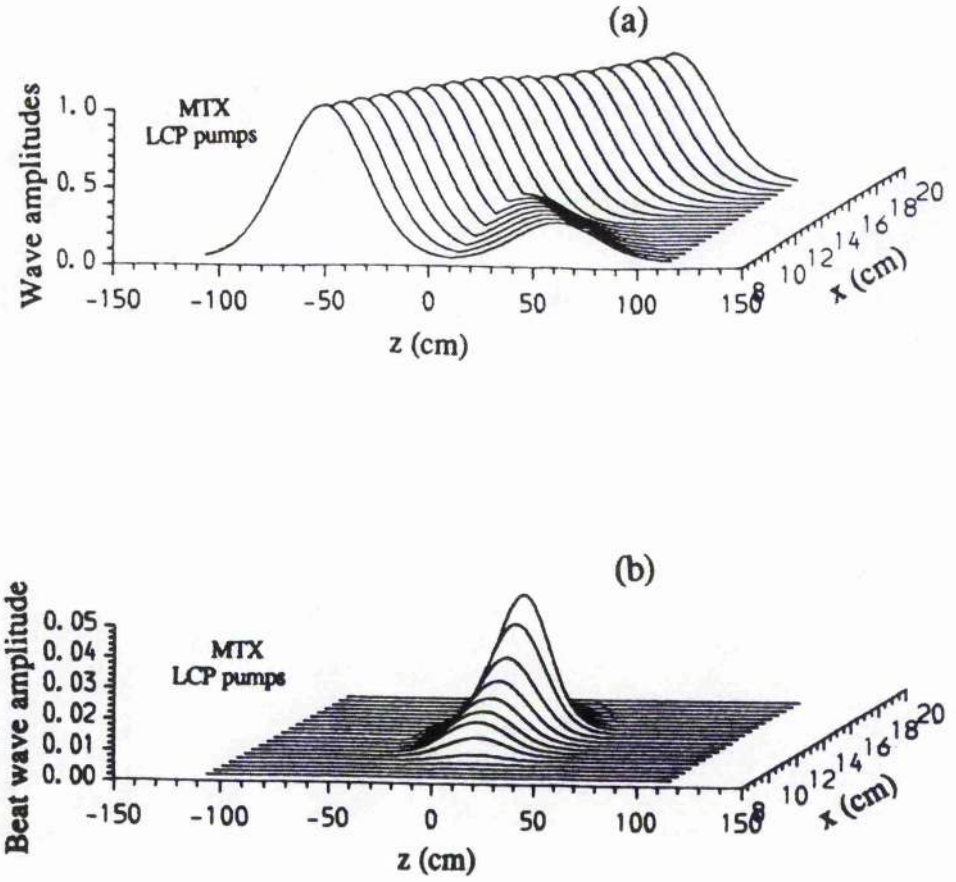

Figure 4.4: MTX parameters: (a) Evolution of the wave amplitudes. (b) Evolution of the beat wave amplitude. Both pumps are LCP modes. The parameters are same as in Fig.4.3. The amplitudes are normalized by the initial peak amplitude of the higher frequency pump.

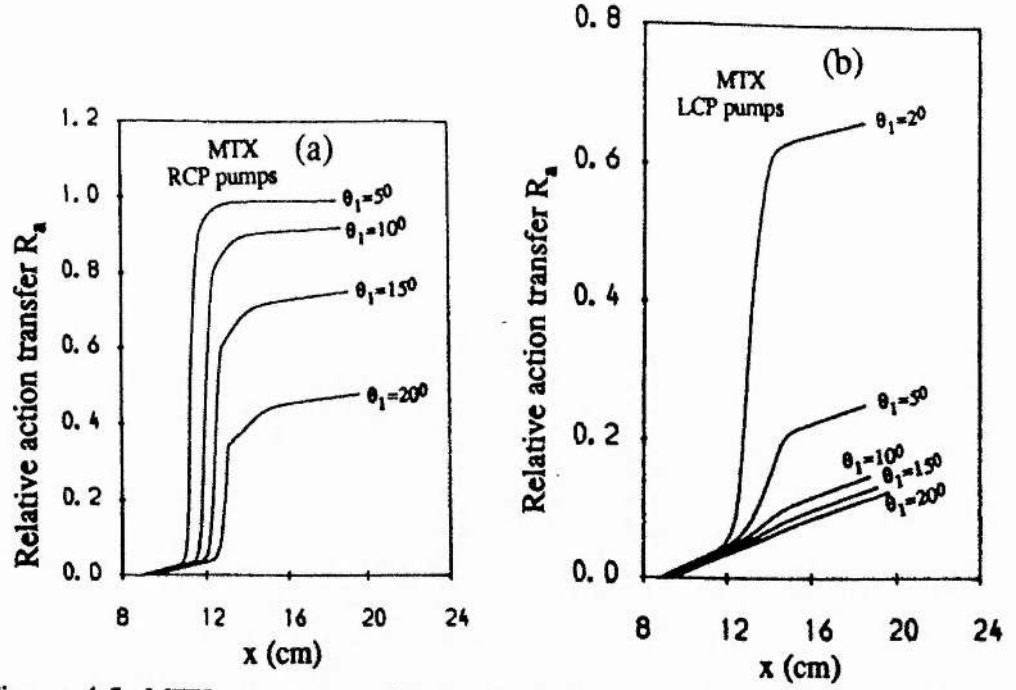

Figure 4.5: MTX parameters: the relative action transfer R_a vs. x-coordinates for different incidence angle of the pumps: (a) for RCP pump modes; (b) for LCP pump modes. The other parameters are same as in Fig. 4.3.

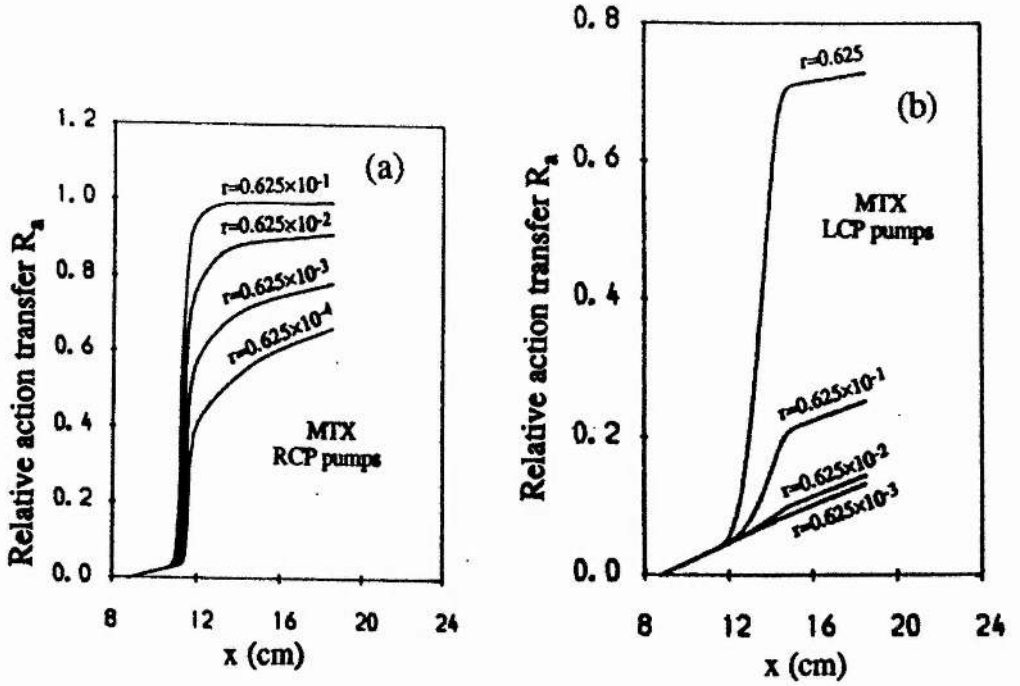

Figure 4.6: MTX parameters: the relative action transfer R_a vs. x-coordinates for different input power ratio r: (a) for RCP pump modes; (b) for LCP pump modes. The other parameters are same as in Fig. 4.3.

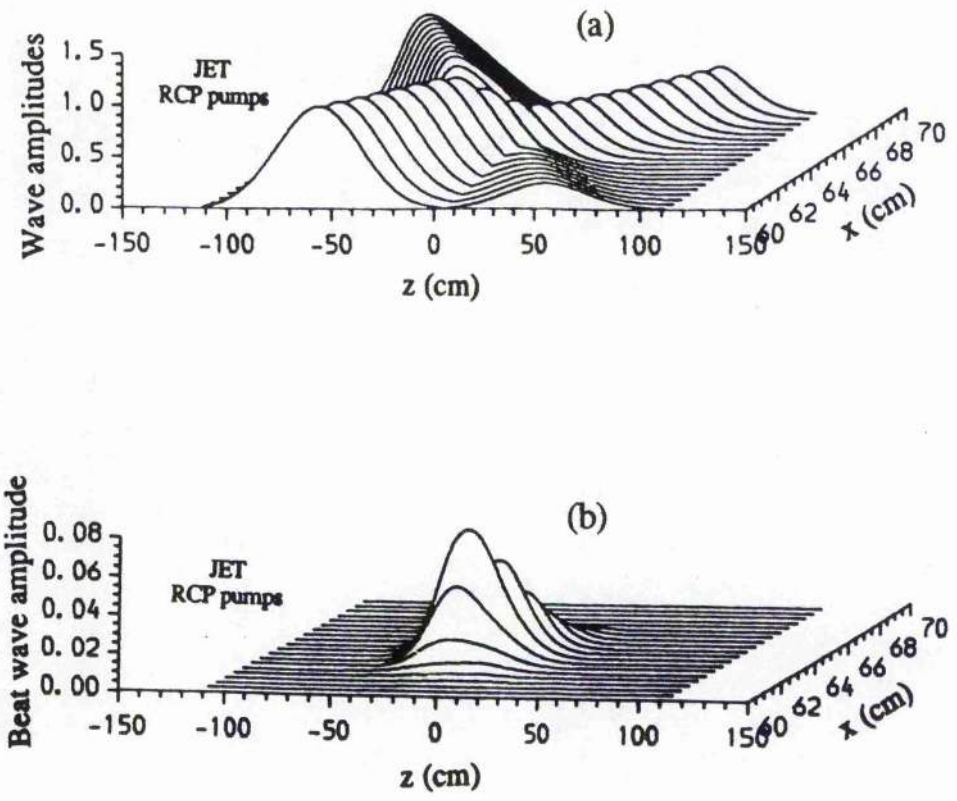

Figure 4.7: JET parameters: (a) Evolution of the wave amplitudes. (b) Evolution of the beat wave amplitude. Both pumps are RCP modes: ω_1=260 GHz, ω_2=160 GHz, P_1=8.0 GW, P_2=0.5 GW ($r \approx 0.625 \times 10^{-1}$), $\theta_1=5^0$, $\theta_2=175^0$, $n_{e0}=1.0 \times 10^{14}$ (cm^{-3}), T_e=10.0 keV, B_0=3.4 T. The amplitudes are normalized by the initial peak amplitude of the higher frequency pump.

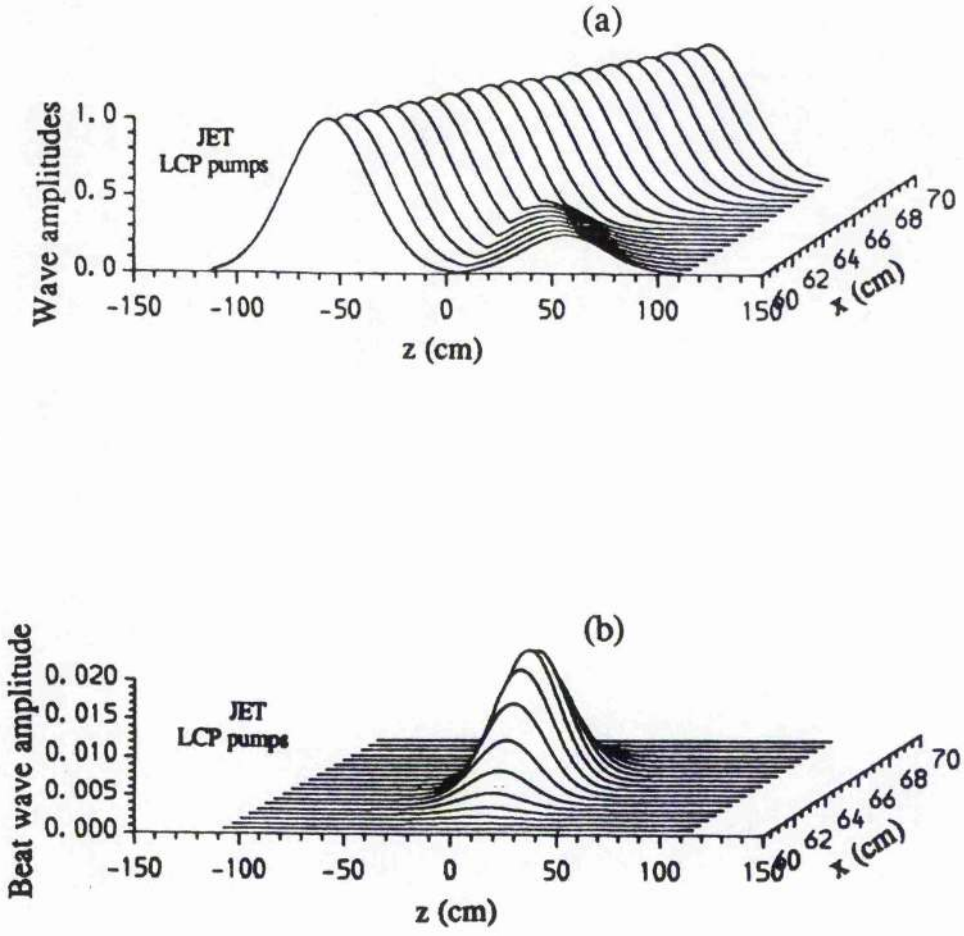

Figure 4.8: JET parameters: (a) Evolution of the wave amplitudes. (b) Evolution of the beat wave amplitude. Both pumps are LCP modes. The parameters are same as in Fig. 4.7. The amplitudes are normalized by the initial peak amplitude of the higher frequency pump.

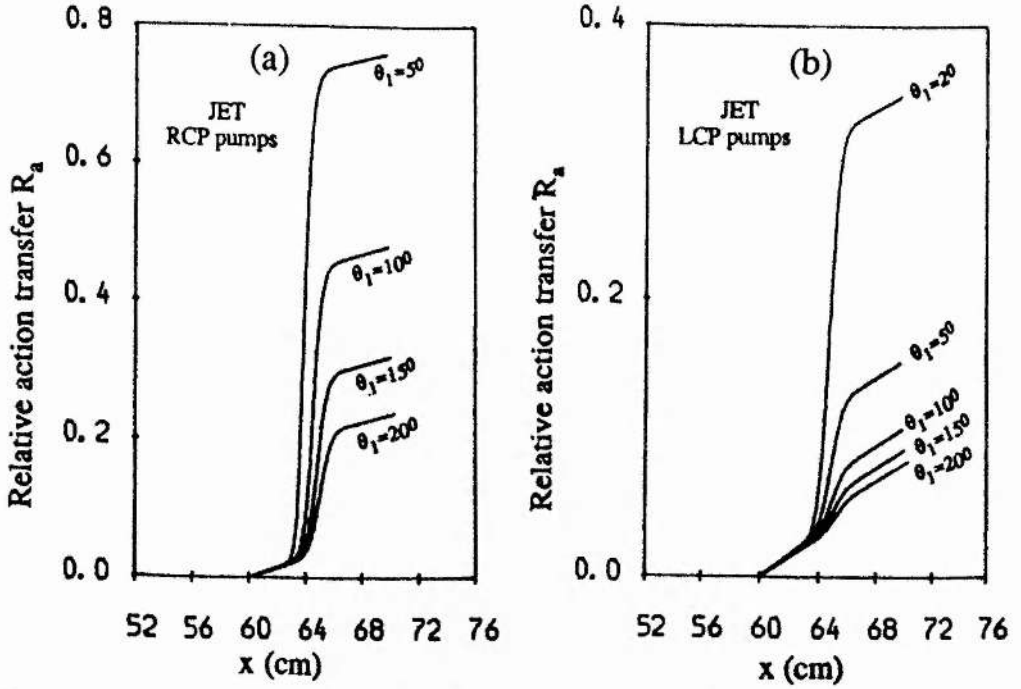

Figure 4.9: JET parameters: the relative action transfer R_a vs. x-coordinates for different incidence angle of the pumps: (a) for RCP pump modes; (b) for LCP pump modes. The other parameters are same as in Fig. 4.7.

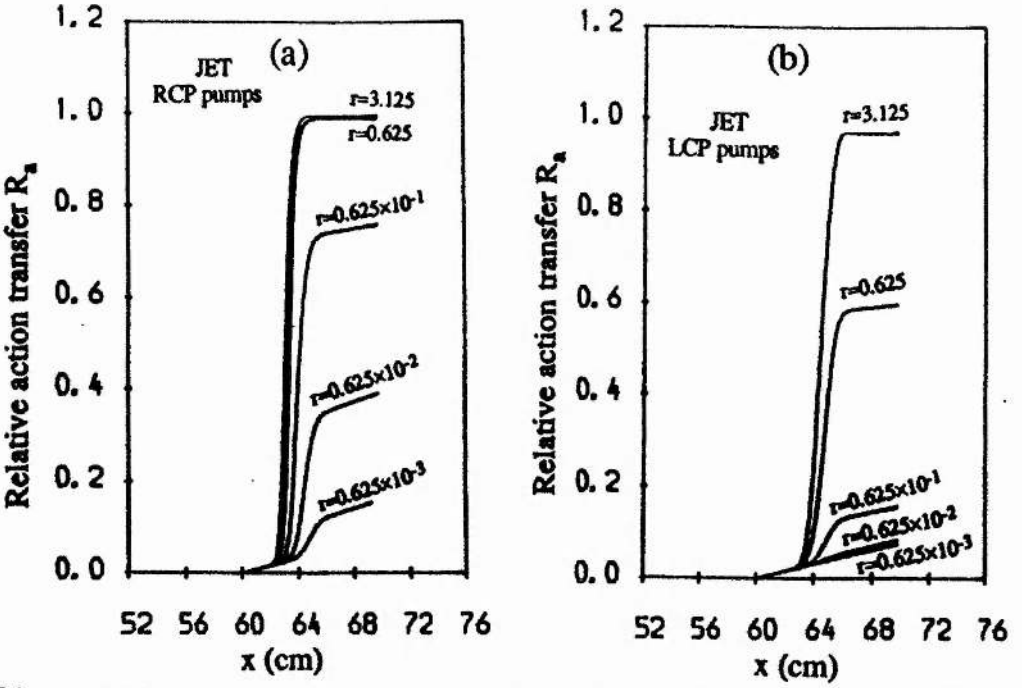

Figure 4.10: JET parameters: the relative action transfer R_a vs. x-coordinates for different input power ratio r: (a) for RCP pump modes; (b) for LCP pump modes. The other parameters are same as in Fig. 4.7.

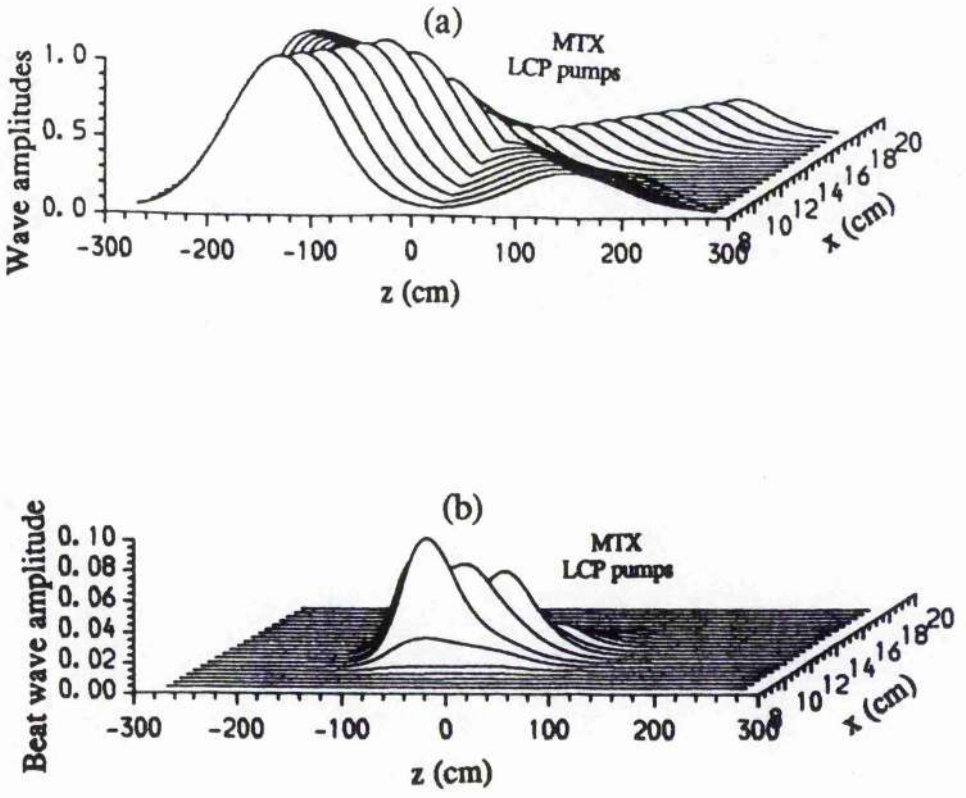

Figure 4.11: MTX parameters: (a) Evolution of the wave amplitudes. (b) Evolution of the beat wave amplitude. Both pumps are LCP modes: ω_1=255 GHz, ω_2=170 GHz, P_1=24.0 GW, P_2=1.5 GW ($r \approx 0.625 \times 10^{-1}$), $\theta_1 = 2^0$, $\theta_2 = 178^0$, $n_{e0} = 0.8 \times 10^{14}$ (cm^{-3}), T_e=1.5 keV, B_0=3.9 T. The amplitudes are normalized by the initial peak amplitude of the higher frequency pump.

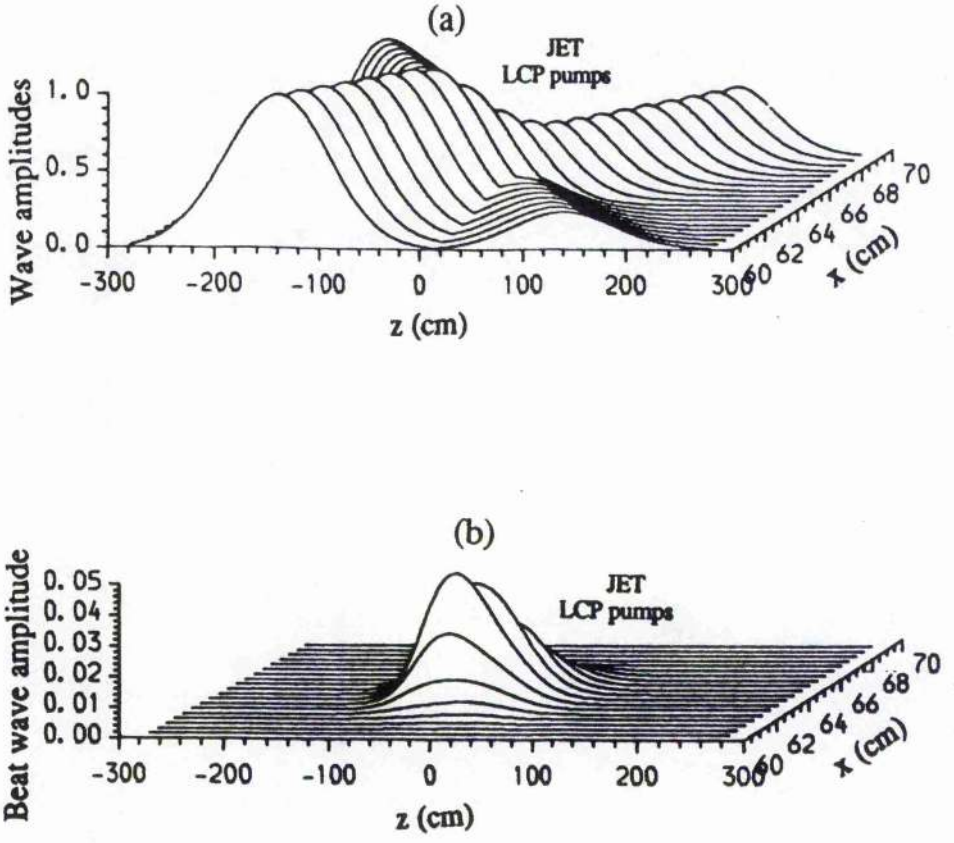

Figure 4.12: JET parameters: (a) Evolution of the wave amplitudes. (b) Evolution of the beat wave amplitude. Both pumps are LCP modes: ω_1=260 GHz, ω_2=160 GHz, P_1=24.0 GW, P_2=1.5 GW ($r \approx 0.625 \times 10^{-1}$), $\theta_1 = 2^0$, $\theta_2 = 178^0$, $n_{e0} = 1.0 \times 10^{14}$ (cm^{-3}), T_e=10.0 keV, B_o=3.4 T. The amplitudes are normalized by the initial peak amplitude of the higher frequency pump.

chapter 5

NUMERICAL SOLUTION OF THE MODEL EQUATIONS FOR AN OBLIQUELY PROPAGATING UPPER HYBRID CYCLOTRON BEAT WAVE

We now consider coupling to an obliquely propagating upper-hybrid beat wave. The calculation is similar to that for the Langmuir beat wave in chapter 4, with the same 2D geometry and Γ_1 and Γ_2 equal to zero. The system of equations (2.43)-(2.45) becomes

$$\vec{u}_1 \cdot \nabla a_1 = -C_1 a_2 a_3 \exp(i\Psi), \tag{5.1}$$

$$\vec{u}_2 \cdot \nabla a_2 = C_2 a_1 a_3^* \exp(-i\Psi), \tag{5.2}$$

$$\left(\Gamma_3 + \vec{u}_3 \cdot \nabla\right) a_3 = C_3 a_1 a_2^* \exp(-i\Psi). \tag{5.3}$$

For a cyclotron beat wave, it can be shown that the first term (the damping term) in the left hand side of Eq.(5.3) is much larger than the second term (the group velocity term). In this situation, we can reduce the set of equations (5.1)-(5.3) to two simple equations. The resulting equations then

describe the nonlinear induced scattering whereby the actions (quanta) are transferred from the linearly undamped higher frequency pump electromagnetic mode to the linearly undamped lower frequency pump electromagnetic mode through the coupling with the heavily damped cyclotron beat mode, with a net energy loss to the medium (Kaufman and Cohen, 1973; Nishikawa and Liu, 1976).

Setting

$$a_3 = a_3' \exp(-i\Psi), \tag{5.4}$$

Eq.(5.3) then can be reduced to

$$\left(\Gamma_3 - i\vec{u}_3\cdot(\nabla\Psi) + \vec{u}_3\cdot\nabla\right)a_3' = C_3 a_1 a_2^*. \tag{5.5}$$

Now we can neglect the third term in the left hand side of Eq.(5.5) compared to the other two terms to obtain

$$a_3' = \left(\frac{C_3}{\Gamma_3 - i\vec{u}_3\cdot\nabla\Psi}\right)a_1 a_2^*, \tag{5.6a}$$

which can be written by using Eq.(5.4) as

$$a_3 = \left(\frac{C_3}{\Gamma_3}\right) f_D a_1 a_2^* \exp(-i\Psi), \tag{5.6b}$$

where

$$f_D = \left[1 + i\left(\frac{\vec{u}_3 \cdot \nabla\Psi}{\Gamma_3}\right)\right]\left\{1 + \left(\frac{\vec{u}_3 \cdot \nabla\Psi}{\Gamma_3}\right)^2\right\}^{-1} \tag{5.7}$$

is the detuning factor due to the inhomogeneity of the toroidal plasma. Substituting (5.6b) into Eqs(5.1) and (5.2), the coupled mode equations become

$$\left(u_{1x}\frac{\partial}{\partial x} + u_{1z}\frac{\partial}{\partial z}\right)a_1 = -\left(\frac{C_1 C_3}{\Gamma_3}\right) f_D |a_2|^2 a_1, \tag{5.8}$$

$$\left(u_{2x}\frac{\partial}{\partial x} + u_{2z}\frac{\partial}{\partial z}\right)a_2 = \left(\frac{C_2 C_3^*}{\Gamma_3}\right) f_D^* |a_1|^2 a_2, \tag{5.9}$$

$$a_3 = \left(\frac{C_3}{\Gamma_3}\right) f_D a_1 a_2^* \exp(-i\Psi). \tag{5.10}$$

The expressions for the coupling coefficients C_1, C_2, C_3 for a cyclotron type beat wave are simplified in the Appendix B. By using the expression for Ψ from Eq.(2.74), the complex function f_D can be written as follows:

$$f_D = \left(1 + i g_f\right)\left(1 + g_f^2\right)^{-1}, \tag{5.11}$$

where

$$g_f = \left(\frac{u_3}{2\Gamma_3}\right)\left\{\left[2 z g_{zz} + (x - x_R)(g_{zx} + g_{xz})\right]\cos\theta_3 + \left[z(g_{zx} + g_{xz}) + 2(x - x_R) g_{xx}\right]\sin\theta_3\right\}, \tag{5.12}$$

where θ_3 is the angle between $\vec{k}_3$ and the +z-axis (see Fig.2.1). The damping Γ_3 of the electrostatic cyclotron beat mode can be obtained from

$$\Gamma_3 = \left(\frac{\mathrm{Im}(D)}{\frac{\partial}{\partial\omega_3}\mathrm{Re}(D)}\right), \tag{5.13}$$

where

$$D = k_{3x}^2 + k_{3z}^2 + \sum_{n=-\infty}^{\infty} \left(\frac{\omega_p^2}{v_{th}^2} \right) e^{-\lambda} I_n(\lambda) \left\{ 1 + \alpha_0 Z(\alpha_n) \right\} \cong 0 \qquad (5.14)$$

is the hot plasma dispersion relation of an obliquely propagating electrostatic beat mode (Stix, 1964). In Eq.(5.14), k_{3x} and k_{3z} are approximately the components of the wavevector of the beat mode; I_n is the modified Bessel's function, Z is the plasma dispersion function and the arguments of I_n and Z are respectively as

$$\lambda = \left(\frac{k_{3x}^2 v_{th}^2}{\Omega_e^2} \right), \qquad (5.15a)$$

and

$$\alpha_n = \left(\frac{\omega_3 - n\Omega_e}{\sqrt{2} k_{3z} v_{th}} \right). \qquad (5.15b)$$

Similar to the case of an excited Langmuir beat mode considered in chapter 4, here we also consider the problem as an initial boundary value problem. The variable x behaves like time and the variable z behaves like position; x

direction is toward the centre of the tokamak and z is the instantaneous direction of the toroidal magnetic field B_0. After finite differencing the set of Eqs. (5.8)-(5.10), the resulting nonlinear coupled difference equations for the complex wave amplitudes become

$$a_1(i,j+1) = pw_1 a_1(i-1,j) + (1-pw_1)\, a_1(i,j) - \Delta x \left(\frac{C_1 C_3}{\Gamma_3 u_{1x}} \right) f_D(i,j)\, a_2(i,j)\, a_2^*(i,j)\, a_1(i,j)\,, \tag{5.16}$$

$$a_2(i,j+1) = -pw_2 a_2(i+1,j) + (1+pw_2)\, a_2(i,j) + \Delta x \left(\frac{C_2 C_3^*}{\Gamma_3 u_{2x}} \right) f_D^*(i,j)\, a_1(i,j)\, a_1^*(i,j)\, a_2(i,j)\,, \tag{5.17}$$

$$a_3(i,j+1) = \left(\frac{C_3}{\Gamma_3} \right) f_D(i,j+1)\, a_1(i,j+1)\, a_2^*(i,j+1) \exp\left(-i\Psi(i,j+1) \right), \tag{5.18}$$

where (i,j) is a grid point of a rectangular mesh, i is along z-direction and j is along x-direction, $p=\Delta x/\Delta z$ and $w_j=u_{jz}/u_{jx}$, u_{jz} and u_{jx} are the components of the group velocities of the wave modes (j=1,2,3). The mesh lengths between two consecutive grid points along x- and z- direction have

been taken respectively as Δx and Δz.

We consider finite spatial extent pump microwaves, with Gaussian profiles, given by Eqs.(4.10a) and (4.10b) in the previous chapter 4 and with identical polarization of the pump microwave fields for efficient coupling of the beat wave interaction process. We take for example, MTX at Livermore (Thomassen, 1988). The typical parameters of MTX and the microwave sources are given in Tables I and II respectively.

We present some graphics of the numerical solutions of the model equations in Figs.(5.1)-(5.5). Figures 5.1(a) and 5.2(a) show the nonlinear interaction of the two pump microwaves and the evolution of the wave amplitudes. It can be seen from these figures that the pump microwave pulses approach toward each other with the higher frequency pump from the left and the lower frequency pump from the right making an angle with each other. After the interaction the pump microwave pulses are propagating with different shape of the profiles in the case of right-hand polarized (RHP) pump modes as can be seen from the Fig. 5.1(a), whereas for the case of left-hand polarized (LHP) pump modes, the shape of the pump profiles are

almost unchanged as can be seen from the Fig. 5.2(a).

Figures 5.1(b) and 5.2(b) show the evolution of the excited beat mode, Fig.5.1(b) for RHP pump modes and Fig. 5.2(b) for LHP pump modes.

Figure 5.3 shows the variation of the relative action transfer R_a with x-coordinates for different propagation direction of two RHP-pump microwave pulses. It can be seen from this figure that as the angle between the directions of propagation of the pumps decreases, the relative action transfer also decreases. It has been found that the coupling is negligible and constant over a certain angle.

Figure 5.4 shows the variation of the relative action transfer R_a with x-coordinates for different input power ratios $r=P_2/P_1$ of two RHP pump modes. It is seen that the relative action transfer increases with input power ratio r. The dependence of the fraction of energy $f_E=q_eR_a$ deposited in the excited beat wave on the input power ratio r, the quantum efficiency q_e and

the relative action transfer R_a is shown in Tables VI and VII. It is seen that although the relative action transfer increases with input power ratio, the quantum efficiency decreases. We notice again that the product of these two quantities gives the fraction of power deposited to the beat wave. Table VI is shown for P_1=8.0 GW, the peak power of the higher frequency pump whereas Table VII is for P_1=24.0 GW. We see from both Tables VI and VII that the fraction of energy deposited f_E in the beat wave for left hand polarized pump waves is always very small.

Figures 5.5(a) and 5.5(b) are shown for higher peak power of the pump microwaves compared to the earlier case. We notice that the coupling between two left hand pump modes is negligible compared to the coupling of two right hand pump modes for the same input parameters. However, in the left hand pump case, there is still excitation of cyclotron beat wave but the transfer of action to it from the higher frequency pump microwave is very small as can be seen from Tables VI and VII, and inefficient for plasma heating and current drive.

TABLE VI. DEPENDENCE OF THE FRACTION OF POWER DELIVERED TO THE BEAT WAVE f_E AND THE RELATIVE ACTION TRANSFER R_a ON THE INPUT POWER RATIO r, THE QUANTUM EFFICIENCY q_e FOR 8.0 GW PEAK POWER OF THE HIGHER FREQUENCY PUMP

MTX: P_1=8.0 GW, ω_1=280 GHz, ω_2=160 GHz, $\theta_1=30^0$, $\theta_2=150^0$

	RHP pump modes			LHP pump modes		
	v_{ph}/v_{th}=6.0			v_{ph}/v_{th}=7.0		
r	3.125	0.625	0.0625	3.125	0.625	0.0625
q_e	0.103	0.260	0.384	0.160	0.320	0.410
R_a	0.983	0.770	0.232	0.110	0.110	0.110
f_E	0.101	0.200	0.089	0.018	0.035	0.045

TABLE VII. DEPENDENCE OF THE FRACTION OF POWER DELIVERED TO THE BEAT WAVE f_E AND THE RELATIVE ACTION TRANSFER R_a ON THE INPUT POWER RATIO r, THE QUANTUM EFFICIENCY q_e FOR 24.0 GW PEAK POWER OF THE HIGHER FREQUENCY PUMP

MTX: P_1=24.0 GW, ω_1=280 GHz, ω_2=160 GHz, $\theta_1=30^0$, $\theta_2=150^0$

	RHP pump modes v_{ph}/v_{th}=6.0				LHP pump modes v_{ph}/v_{th}=7.0			
r	0.625	0.333	0.0625	0.00625	0.625	0.333	0.0625	0.00625
q_e	0.260	0.310	0.384	0.404	0.320	0.360	0.410	0.420
R_a	0.980	0.920	0.520	0.170	0.110	0.110	0.110	0.110
f_E	0.255	0.285	0.200	0.069	0.035	0.040	0.045	0.062

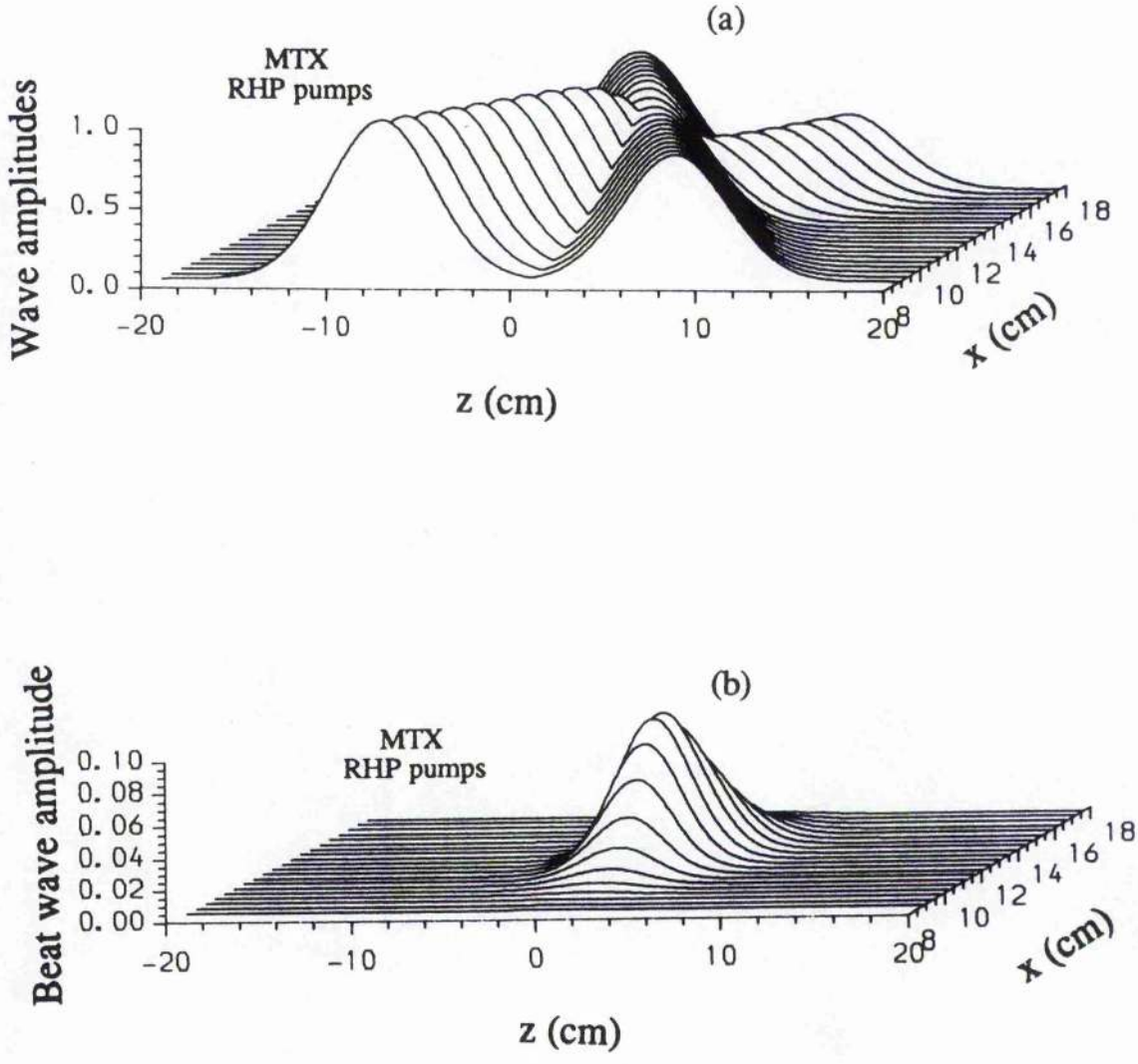

Figure 5.1: MTX parameters: (a) Evolution of the wave amplitudes. (b) Evolution of the beat wave amplitude. Both pumps are RHP modes: ω_1=280 GHz, ω_2=160 GHz, P_1=8.0 GW, P_2=5.0 GW ($r \approx 0.625$), $\theta_1=30^0$, $\theta_2=150^0$, $n_{e0}=0.8\times10^{14}$ (cm^{-3}), T_e=1.5 keV, B_0=3.9 T. The amplitudes are normalized by the initial peak amplitude of the higher frequency pump.

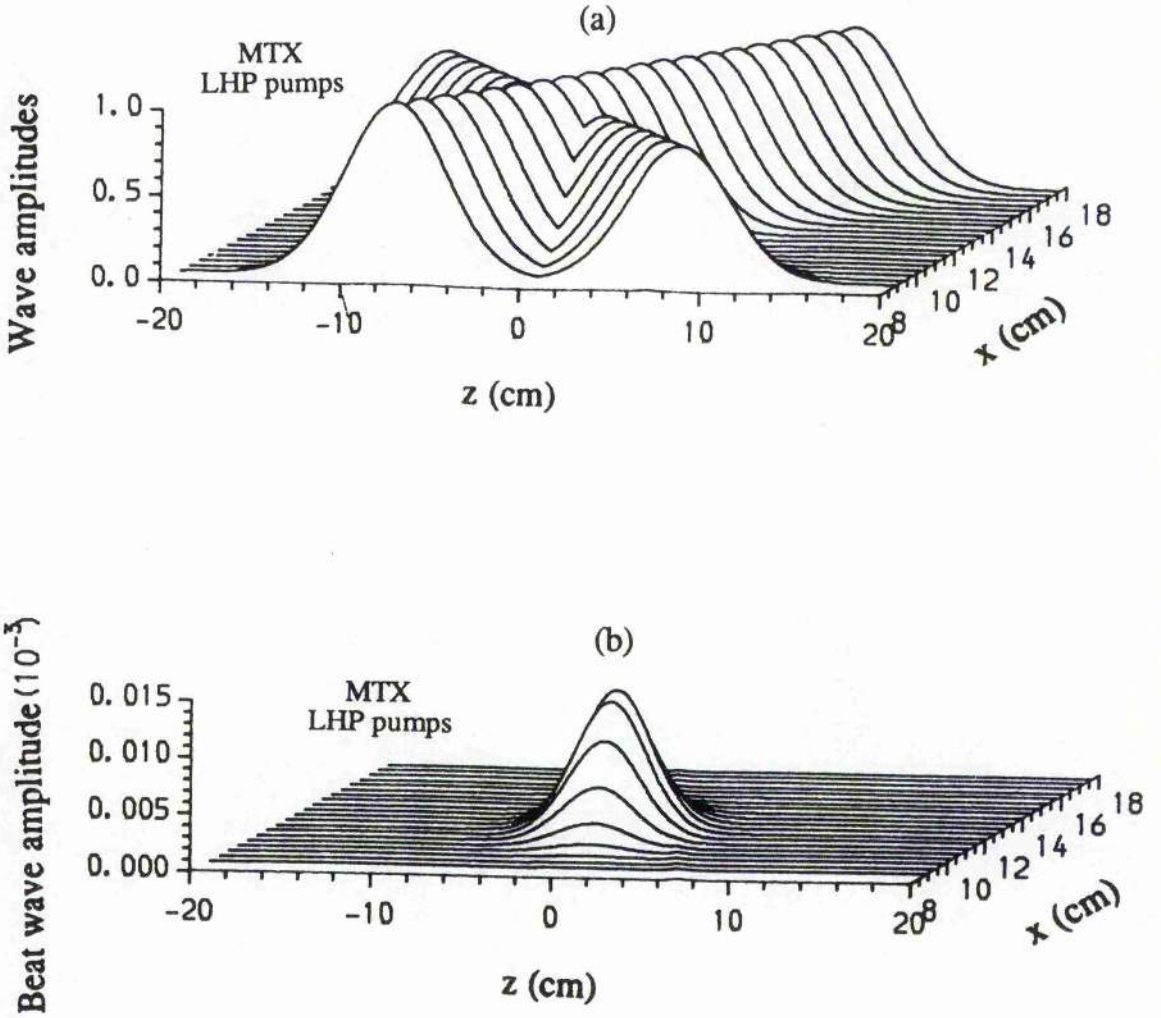

Figure 5.2: MTX parameters: (a) Evolution of the wave amplitudes. (b) Evolution of the beat wave amplitude. Both pumps are LHP modes. The parameters are same as in Fig.5.1. The amplitudes are normalized by the initial peak amplitude of the higher frequency pump.

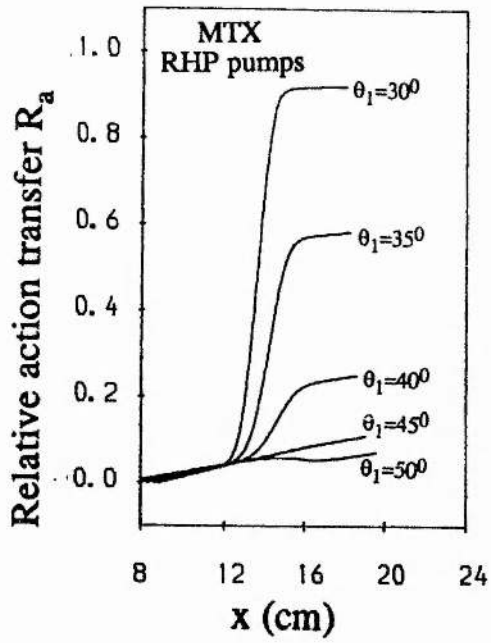

Figure 5.3: MTX parameters: the relative action transfer R_a vs. x-coordinates for different incidence angle of the pumps. The pumps are RHP: P_1=24.0 GW, P_2=8.0 GW (r≈0.333). The other parameters are same as in Fig.5.1.

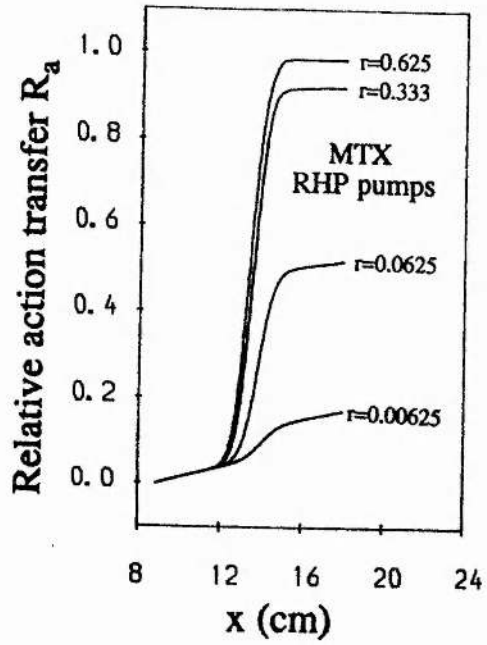

Figure 5.4: MTX parameters: the relative action transfer R_a vs. x-coordinates for different input power ratio r. The pumps are RHP: P_1=24.0 GW, P_2=8.0 GW (r≈0.333). The other parameters are same as in Fig.5.1.

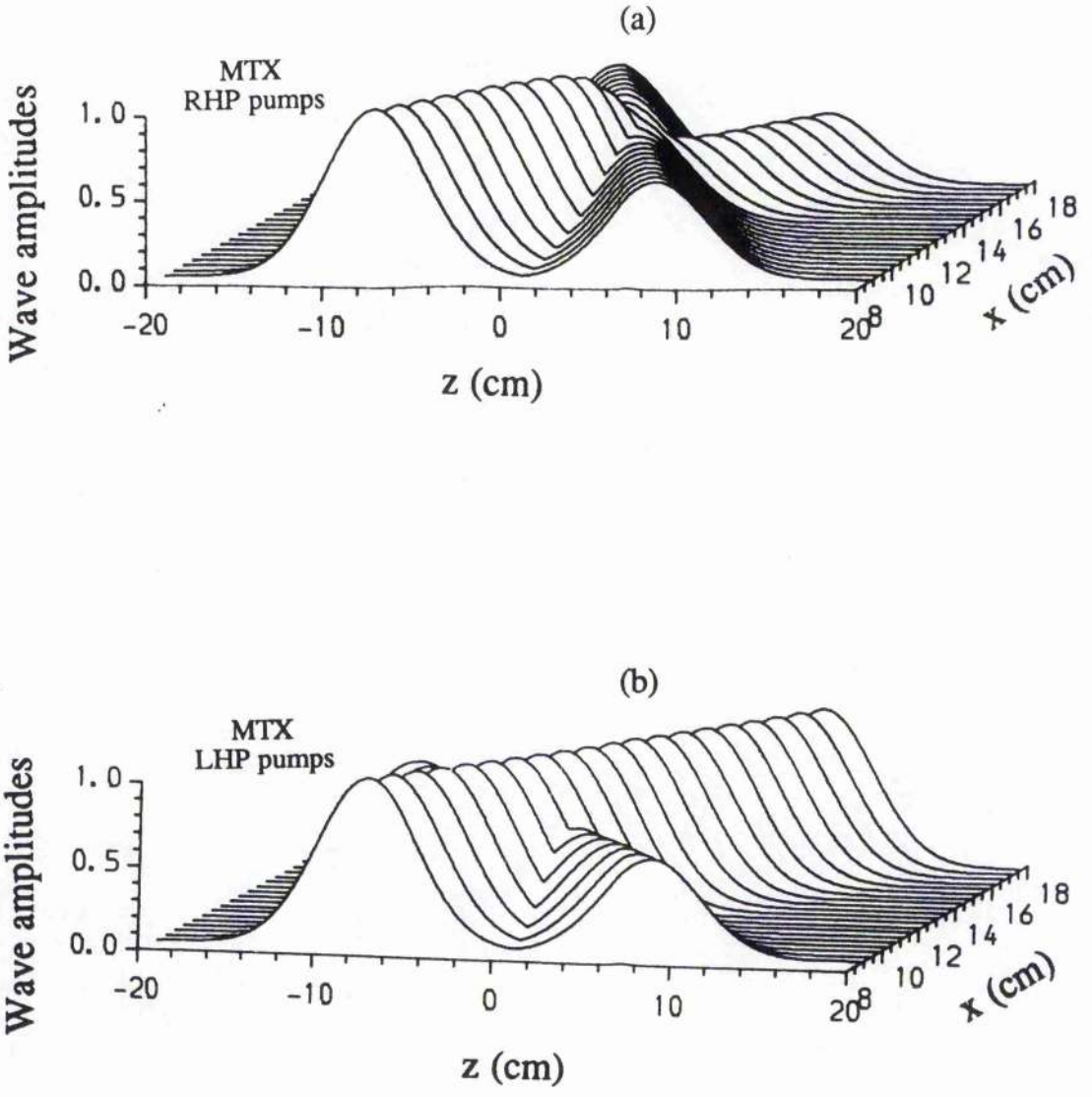

Figure 5.5: MTX parameters: (a) Evolution of the wave amplitudes for RHP pumps. (b) Evolution of the wave amplitudes for LHP pumps. P_1=24.0 GW, P_2=8.0 GW (r≈0.333). The other parameters are same as in Fig.5.1.The amplitudes are normalized by the initial peak amplitude of the higher frequency pump.

chapter 6

DISCUSSION

In this part of the thesis, the possibility of beat wave current drive by two intense free-electron laser pulses have been considered in 2D geometry. The 2D geometry is expected to be a reasonable approximation for waves incident on the median plane of the tokamak. We have considered two types of excited electrostatic beat mode in this analysis: (1) a simple Langmuir type beat mode propagating almost parallel to the toroidal magnetic field and (2) an obliquely propagating upper-hybrid beat mode. The damping of the Langmuir beat mode is simple Landau damping and the damping of the obliquely propagating beat mode is cyclotron damping. We have considered opposite propagation (90^0<angle between the pumps$\leq 180^0$) in the case of Langmuir type beat mode. For the case of a cyclotron beat wave, it is found that the damping of the mode is so strong that we can consider the three wave scattering process as a nonlinear induced scattering whereby the actions (quanta) are transferred from the linearly undamped higher frequency pump electromagnetic mode to the linearly undamped lower frequency pump electromagnetic mode through the coupling with the heavily damped cyclotron beat mode, with a net energy loss to the medium.

In both the cases, we have considered the problem as an initial-boundary value problem. The coupled mode equations have been solved numerically by applying an explicit finite difference scheme in two independent variables x and z.

The ray paths of the transverse pump microwaves are obliquely incident at the plasma edge as shown in Fig.1.2. So, there are two modes for any angle of propagation, the extraordinary (X) and ordinary (O) modes. For approximately antiparallel propagation of the pumps the X-mode becomes RCP mode and the O-mode becomes LCP mode. This is the situation for a Langmuir type beat mode. The X-mode and O-mode pumps drive distinct beat modes at the same frequency and in the same interaction region, but with different wave numbers and phase velocities.

It has been found that the Langmuir type beat wave (for almost antiparallel pump waves) is more efficient for beat wave current drive compared to the cyclotron beat mode. The most important result we have found is that the action transfer for RHP pump waves is much higher than LHP pump waves. For the case of a cyclotron beat mode due to two LHP pump waves, the beat

wave coupling is negligibly small and constant over input power of the pump microwaves. For the case of a Langmuir beat mode there is some action transfer but still small compared to the case of RHP pumps. Although the RHP pumps give the better action transfer and so current drive efficiency compared to LHP pumps for the same input parameters for a Langmuir type beat mode, there is some possibility for cyclotron absorption of the lower frequency RHP pump for the input pump frequencies considered in this analysis, where $\omega_1/\Omega_{e0}=2.4$, $\omega_2/\Omega_{e0}=1.6$ for MTX and $\omega_1/\Omega_{e0}=2.7$, $\omega_2/\Omega_{e0}=1.7$ for JET. As stated already by Cohen et al (1988), absorption of RHP-modes can be minimized by raising the wave frequency to a higher cyclotron harmonic number and arranging the cyclotron resonance to fall outside the plasma or at its edge. However, in this case, the relative action transfer will be reduced compared to the case we have considred. This will happen because raising the wave frequency of the pumps will eventually reduce the coupling of the three wave interaction process. For LHP modes, the cyclotron harmonic absorption by the electrons is much reduced and refraction is insignificant (Cohen et al, 1988).

Unlike the collinear case, the cascading (Karttunen et al, 1987) for opposed propagating pumps is not a problem. The 4th wave involved in the process is generated by the beating of the highest frequency pump wave with the excited beat wave giving $\vec{k}_4=\vec{k}_1+\vec{k}_3$, $\omega_4=\omega_1+\omega_3$. This wave is so far off resonance (Fig. 6.1) and it will not grow (it is not a resonant mode of the system). Subsequently this mode $(\omega_4,\vec{k}_4)$ cannot effectively couple with either pump $(\omega_2,\vec{k}_2)$ or beat mode $(\omega_3,\vec{k}_3)$ to provide modes at $\vec{k}_5$, $\vec{k}_6$ etc. Therefore for the opposed propagation case, only 3 modes take part in the interaction process.

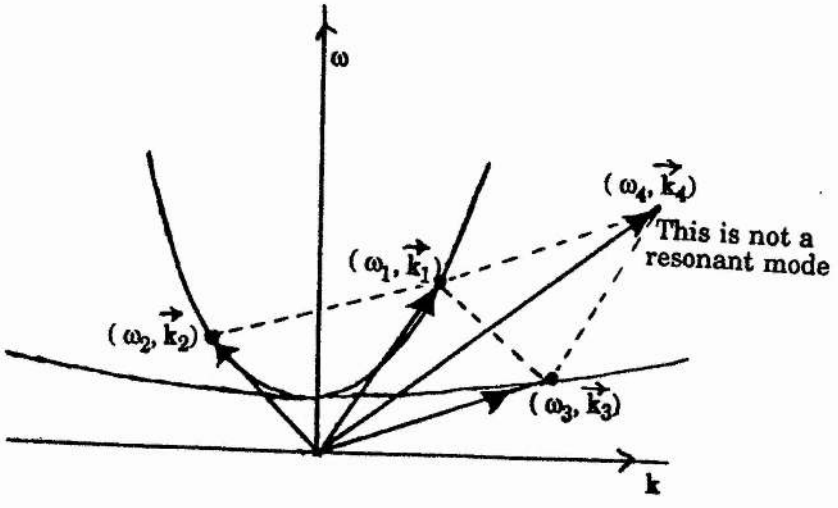

Figure 6.1: Off resonance in the cascading in counter-propagating pump waves.

There is some possibility of parasitic effects of parametric instabilities of the intense pump microwaves and also for the large amplitude beat plasmon generated by the beat wave process in beat wave current drive (Cohen et al, 1988). The effects of these parametric instabilities have been studied thoroughly by Cohen et al by performing particle simulations. Their simulations give evidence of these instabilities both for parallel as well as anti-parallel pump orientation case. For parallel pump orientation, their simulation predicts the parasitic effects of induced backscattering by resonant electrons for the higher frequency pump wave, and of scattering by resonant ions for the lower frequency pump wave and the beat wave in many cases. In this pump orientation case, the authors conclude that these parasitic effects, i.e., the induced backscattering by electrons and ions, may be significant for the amplitudes required for good beat wave action transfer. However, for anti-parallel directed pump waves, induced scattering by resonant ions and stimulated forward Raman scattering are the possible parasitic processes. In this pump orientation case, the particle simulations (Cohen et al, 1988) reveal that the parasitic effects of induced scattering are not significant. Moreover, their simulation predicts that for anti-parallel pumps, coupling of the pump waves to the beat wave supported

by the electrons was dominant over other processes and that ion effects were relatively weak for the cases in which $1.5 \leq v_{ph}/v_{th} \leq 7.5$.

In conclusion, we have considered the possibility of beat wave current drive in tokamak plasmas from the same point of view as Cohen et al (1988), but with 2D geometry. We have considered steady state condition in our analysis, which is appropriate for times longer than the inverse damping rate of the excited beat wave (Cohen et al, 1988). The same problem has been considered by including in our analysis the 2D toroidal effect and the effect of finite spatial width of the pump microwave pulses on the beat wave excitation for current drive application. Moreover, we have considered the possibility of beat wave current drive by a cyclotron beat wave. In this investigation two types of tokamak have been considered; it is found that the overall fraction of energy deposited f_E in the beat wave, and ultimately going to the electrons can be as high as 32% in MTX and 29% in JET for RHP pump modes for a Langmuir type beat wave with P_1=8.0 GW. For an obliquely propagating upper-hybrid cyclotron beat wave with P_1=8.0 GW, f_E turns out to be 20% in MTX for RHP pump microwaves. However,

increasing P_1 from 8.0 GW to 24.0 GW, f_E increases to 24% for RHP pumps. It has been found that the current drive efficiency for RHP pumps is significantly higher than that for LHP pumps with the same input parameters. It is also found that the current drive efficiency for JET is significantly reduced from the values obtained for MTX. The reduction in current drive efficiency for the larger machine is a feature of all current drive schemes (current drive efficiency depends inversely on the radius of the tokamak). It can be partially compensated by improved absorption and a resultant increase in the action transfer. In a hot reactor plasma, the high temperature would enable more energy to be put into the tail of the distribution, also helping to improve efficiency. A better current drive efficiency could be attained at higher peak pump wave powers so that R_a could be improved to a value very closer to unity (Cohen et al, 1988).

PART 2

Excitation of a Large Amplitude Plasma Wave by a Single Ultra-Short Laser Pulse for Particle Accelerators

chapter 7

INTRODUCTION

Laser and Particle Acceleration

Particular interest to accelerator physicists is the design of linear e^+-e^- colliders above 1 TeV ($1T=10^{12}$). Present radio-frequency techniques have gradients of order 0.01 - 0.1 GeV/m. TeV colliders, therefore, would be longer than 10 km. Ever since the invention of the laser it has been a source of the most intense electric fields available in free space (E=377W, where E is in V/cm and W is in Watt/cm^2). A laser power of $10^{16}\mathrm{Wcm}^{-2}$ corresponds to $E=2 \times 10^9\ \mathrm{Vcm}^{-1}$, and if this could be utilised for acceleration then the 1TeV accelerator would be only 10m long. The problem of course is that electromagnetic waves in vacuo are transverse and do not impart energy to particles moving along at close to the phase velocity of the wave. There is a transient acceleration due to the ponderomotive force, and an electron initially at rest and overtaken by a light pulse, first acquires a velocity, but is reduced to rest again as it is left behind the pulse. The acceleration is describable as the gradient of a ponderomotive potential and in a similar manner to DC particle accelerators it is not posible to cascade multiple stages.

The requirements to accelerate particles have been studied by Lawson (1982) and in some form require a material medium to change the free space dispersion relations. Four essentially different mechanisms exist: 1) The Laser Excited Cavity (Palmer, 1985); 2) The Inverse Free-Electron Laser (Pellegrini, 1982); 3) The Inverse Cerenkov Accelerator (Fontana and Pantell, 1983); and 4) Plasma Based Accelerators (Katsouleas et. al., 1985).

Plasma Based Accelerators

A plasma can support longitudinal electric fields through electrostatic waves and these can be of arbitrary phase velocity. The plasma waves can be pumped by a variety of mechanisms including two lasers whose frequencies differ by the plasma frequency, a bunch of relativistic charged particles or a single frequency ultra-short laser pulse. It is interesting to note that plasma waves can have gradients of order 100 GeV/m (Chen, 1990), leading to a possible reduction of 10^3 in the length of linear accelerators.

PLASMA BEAT WAVE ACCELERATOR (PBWA)

In plasma beat wave accelerator (PBWA), an electron plasma wave is excited by the beat between two electromagnetic waves. This excited electron plasma wave can accelerate electrons. Longitudinal fields of the order of a few GV/m can be obtained which makes the beat wave process a promising new method for particle acceleration to ultra-high energies as first shown by Tajima and Dawson (1979).

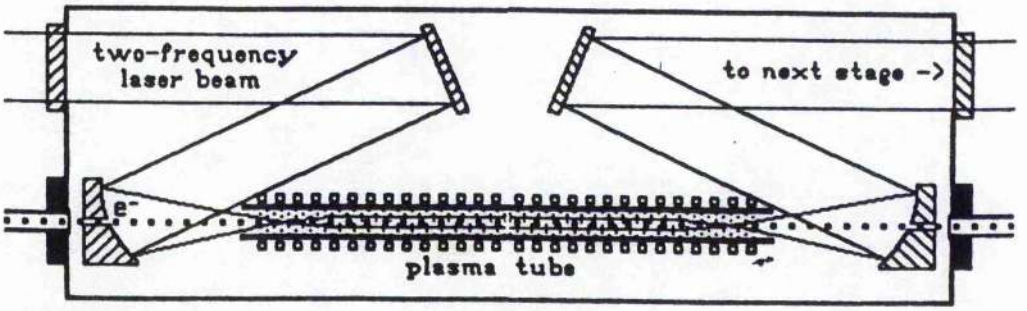

Figure 7.1: Conceptual scheme of a plasma beat wave accelerator module. After Chen (1990).

The basic idea of the PBWA is illustrated in Fig.7.1. A picosecond laser beam containing two lines of the lasing medium is brought through a window into the large chamber filled with the operating gas and is focused into the plasma tube. A fully ionized, high density plasma in the range 10^{16}-10^{18} cm^{-3} is created by one of several possible mechanisms: q- or

z-pinch, radiofrequency waves, or multiphoton ionization. If the plasma frequency is resonant with the beat frequency of the two laser lines of the picosecond driving laser, a large amplitude electron plasma wave is excited in the plasma. Bunches of electrons from an injector linac, shown coming from the left, enter the plasma chamber through a thin foil or a differential pumping tube and are injected into the plasma wave. The bunches are synchronized with the laser pulses. Those electrons trapped in the right phase in the wave will be accelerated by the wave's large longitudinal electric field. To increase the acceleration length, it may be necessary to trap the laser pulse by refracting it with an inverted density profile or by using relativistic self focusing. To achieve higher energy than can be gained in one stage, the modules can be repeated, with each module serving as the injector for the next. Successive modules can be optimized for the beam energy it is required to produce.

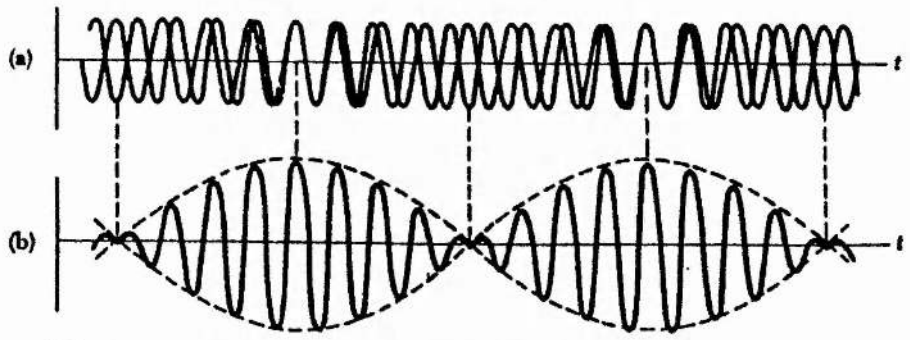

Figure 7.2: Beat pattern of two electromagnetic waves ot slightly different frequencies traveling in the same direction: (a) the individual waves; (b) the combined wave has an amplitude (broken line) that oscillates in time.

Two electromagnetic waves $(\omega_1,\vec{k}_1)$ and $(\omega_2,\vec{k}_2)$ will have a beat pattern (shown in Fig.7.2) whose ponderomotive force (Chen, 1974) can excite a lower frequency electrostatic wave $(\omega_3,\vec{k}_3)$ obeying the relations

$$\omega_1 = \omega_2 + \omega_3, \quad \vec{k}_1 = \vec{k}_2 + \vec{k}_3. \tag{7.1}$$

If $\vec{k}_1$ and $\vec{k}_2$ are oppositely directed, $|k_3|$ is large, and the phase velocity ω_3/k_3 is too small and not useful for particle acceleration to GeV energies. If $\vec{k}_1$ and $\vec{k}_2$ are co-directional, fast plasma waves are excited with

$$\omega_3 = \omega_1 - \omega_2 \equiv \Delta\omega \cong \omega_p, \tag{7.2}$$

$$k_3 = k_1 - k_2 \equiv \Delta k \cong k_p. \tag{7.3}$$

The phase velocity $v_p=\omega_3/k_3$ is seen to be equal to the group velocity of the light waves $v_g=\partial\omega/\partial k=\Delta\omega/\Delta k$ in the limit $\omega_p<<\omega_{1,2}$:

$$v_p \cong v_g = c\left(1 - \frac{n_0}{n_C}\right)^{1/2} \cong c, \tag{7.4}$$

where n_0 is the background electron plasma density and

$$\frac{n_0}{n_C} \equiv \frac{\omega_p^2}{\omega_1^2}, \qquad \omega_p^2 \equiv \frac{4\pi n_0 e^2}{m_e}, \tag{7.5}$$

e is the magnitude of the electron charge, m_e is the electron mass. It can be shown that the cold plasma wave amplitude (Chen, 1990) is

$$|E| = 0.96\,\varepsilon\sqrt{n_0}\ \text{V/cm}, \tag{7.6}$$

where ε satisfies the differential equation

$$\frac{\partial^2 \varepsilon}{\partial t^2} + \omega_p^2 \varepsilon = -\frac{1}{2} i k_p^2 c^2 \alpha_1 \alpha_2 . \tag{7.7}$$

α_1 and α_2 are given by

$$\alpha_j = \left(\frac{eE_j}{m_e \omega_j c} \right), \quad (j=1,2) \tag{(7.8)}$$

Eq.(7.7) is nonrelativistic, and this equation can be used for the initial growth rate. It is important to note here that due to the actual relativistic effect the amplitude of the beat electrostatic wave saturates at a lower value. This saturated wave amplitude is given (Chen, 1990) by

$$|E|_{sat} = 0.96\left(2\pi\alpha_1\alpha_2\right)^{1/3}\sqrt{n_0}\ . \qquad (7.9)$$

The cold plasma wave-breaking limit is obtained by setting ε=1 in Eq.(7.6). Thus, the maximum accelerating gradient is eE_{max}=1 GeV/cm at n_0=10^{18} cm^{-3}. However, atainable amplitude levels and the stability of the beat plasmon are key questions. Regarding the electron response the main saturation mechanism (Rosenbluth and Liu, 1972; Tang et. al., 1985) is the relativistic frequency shift (Akhiezer and Polovin, 1955). The collisional damping is indeed usually negligible due to high electron oscillation velocities in the laser and plasmon fields.

On a slow time scale, ion dynamics start to play an important role in the stability of the large amplitude beat plasmon. The time scale of the ion motion can be close to ω_{pi}^{-1} (ω_{pi} is the ion plasma frequency) which is fairly short (a few picoseconds) at typical densities of 10^{22}-10^{23} m^{-3}. Thus, ion effects should certainly be considered for pulses longer than 50 ps, which is the case of present day experiments (Clayton et al, 1985). Particle simulations by Forslund et al (1984) have clearly shown the

importance of ion dynamics. The build-up of ion fluctuations destroys the coherence of the beat process and sets a limit to the life time of the beat plasma wave. High intensity pump beams (lasers) may excite instabilities involving ion motion. In long homogeneous plasmas for instance, stimulated Brillouin scattering (SBS) has a large growth rate ($\leq\omega_{pi}$) (Drake et al, 1974). Besides direct reflection losses SBS excites large amplitude ion waves, which can severely disturb the beat wave generation (Darrow et al, 1986). Self focusing or filamentation of the laser light is another process which should be considered in detail in the context of the beat wave generation. The first observation (Clayton et al, 1985) of the fast beat wave was by the UCLA group. They used a CO_2 laser operating at the two wavelengths 9.6 μm and 10.6 μm and producing about 10J of energy at each wavelength in 1-2 nsec. The two wavelengths emerge together from the laser and are focussed into an arc plasma whose density can be tuned to resonance. The beat wave is diagnosed by ruby laser Thomson scattering and also by the development of Stokes and anti-Stokes sidebands on the transmitted CO_2 laser light. The value of $\delta n/n_o$ inferred from both these methods is about 0.01-0.03 and corresponds to an electric field of about 1 GeV/m in the beat wave.

A more recent experiment by the group at INRS Quebec (Ebrahim et al, 1986) has used a similar but slightly more powerful CO_2 laser. Their work differs from the UCLA experiment in two significant ways, firstly the plasma was not pre-formed but was created by breakdown of the low pressure neutral gas by the CO_2 laser focussed to 10^{14} Wcm^{-2}. Secondly the INRS group actually demonstrated electron acceleration by injecting electrons at 500 keV to 900 keV from a laser-produced plasma on a solid target. The electrons were energy selected at injection and analysed on extraction from the beat wave region. The typical exit energy was about 2.0-3.0 MeV, in an acceleration length of 1.5 mm. This gives direct evidence for a field of about 1 GeV/m, in good agreement with theory. Experiments on PBWA are in progress in other places as well; in the United Kingdom (Dangor et al, 1987, 1990), and in Japan (Kitagawa et al, 1987).

PLASMA WAKE FIELD ACCELERATOR (PWFA)

The wake of a fast particle bunch in a plasma is an electrostatic wave, which can be used for accelerating other particles to higher energies in the same manner as in the PBWA. Using a particle beam for exciting an electron plasma wave avoids problems of laser inefficiency and density tuning. The

concept, known as plasma wake field accelerator (PWFA), suggested by Chen et al (1985) and Chen (1986), is illustrated in the following figure.

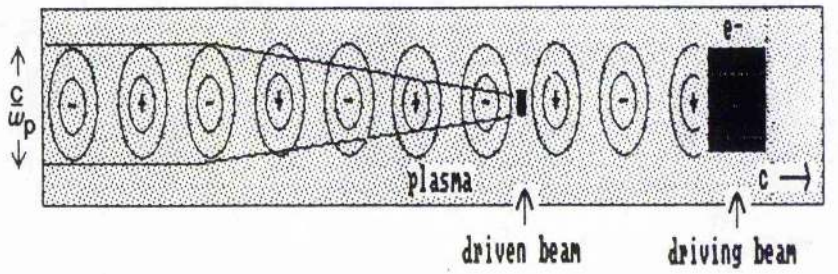

Figure 7.3: Mechanism of wake field excitation. After Chen (1990).

As shown in the above Fig. 7.3, a plasma-wave wake is excited behind an electron bunch because the cold electrons of the plasma are displaced by the first-moving electrons of the bunch. When the bunch ends, it leaves behind a large positive charge imbalance, and the plasma electrons rush into neutralize it. The electrons overshoot and oscillate at the natural frequency of the plasma, which is ω_p. Since the wave phase velocity must be the same as that of the bunch, or $\approx c$, the plasma wave has wavenumber $k=\omega_p/c$, as in the beat wave case.

The injected , accelerated bunch itself creates a wake; and if this wake is adjusted to be as large as the original wake and 180^0 out of phase with it, the wakes will cancel each other. The plasma wave energy is then completely transferred to the driven beam. The width of the wake cannot be smaller than the minimum size of a plasma wave, which is the skin depth c/ω_p. This fact allows the driven beam to be made smaller than c/ω_p without sacrificing efficient energy transfer; thus the driven particles need not sample the radial variation of field strength across the diameter of the wave.

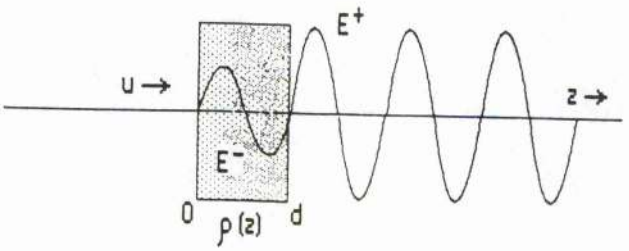

Figure 7.4: The wake fields inside and behind a finite slab of electrons moving through a plasma. After Chen (1990).

Inside the driving bunch (see Fig.7.4), electrons feel a small retarding field E^- from the wakes of the particles ahead; the bunch is shaped so that E^- is

approximately constant. The driving bunch, therefore, loses all its kinetic energy in a distance $L=(\gamma-1)m_ec^2/e|E^-|$. If the maximum wake field is E^+, the driven bunch gains energy $\Delta\gamma m_ec^2=eL|E^+|$. Thus, the driven particles have an energy gain larger than the driving energy by the ratio

$$R=\frac{|E^+|}{|E^-|}, \tag{7.10}$$

which is called the 'transformer ratio'. For unshaped bunches, it can be shown that $R \leq 2$; but for carefully shaped density profiles, R can be as high as 100. In this example, a low current, 100-GeV beam would be produced by a 1-GeV driving beam.

Since the wake must travel with the driver, the problem is time-independent in the beam frame and can easily be solved in the one-dimensional case. Figure 7.4 shows the wake of a charge sheet $\sigma\partial(z)$ which is moving to the left. In the beam frame, the cold plasma streams by with a velocity u and is set into oscillation with a velocity v and a perturbed density n_1. Setting $\partial/\partial t=0$, we may write the equations of motion, continuity, and Poisson as

$$m_e u \frac{\partial v}{\partial z} = - eE \,, \tag{7.11}$$

$$n_0 \frac{\partial v}{\partial z} + u \frac{\partial n_1}{\partial z} = 0 \,, \tag{7.12}$$

$$\frac{\partial E}{\partial z} = - 4\pi e n_1 - 4\pi\sigma\delta(z) \,. \tag{7.13}$$

Differentiating Eq.(7.13) and substituting Eqs.(7.11) and (7.12) yields

$$\left(\frac{\partial^2}{\partial z^2} + k_p^2 \right) E = - 4\pi\sigma \frac{\partial}{\partial z} \delta(z) \,, \tag{7.14}$$

where $k_p^2 = \omega_p^2/u^2 = \omega_p^2/c^2$. For shaped bunches $\rho(z)$, one integrates over this Green's function to obtain

$$E(z) = - 4\pi \int_0^z \rho(z') \cos\left(k_p (z - z') \right) dz' \,. \tag{7.15}$$

as the plasma wave wake field. If the leading bunch is to produce a wake field which is a significant fraction of the limiting field $eE = m_e c/\omega_p$ then the charge density in the leading bunch must be a significant fraction of the

background plasma density. This situation clearly gives rise to the classical two-stream instability. In the transverse direction the dominent instability is the Weibel instability (Lee and Lampe, 1973). The Weibel instability is large enough to destroy the leading bunch before it has had time to give up much of its energy. Recently (Callan et al, 1988) it has been suggested that there is a further problem with the PWFA. The transformer ratio is related to the length of the driving bunch in units of c/ω_p and if this is large then the beam is also subject to the MHD 'hose' instability. This has not been studied in great detail.

An experiment is performed on the PWFA, at the Argonne National Laboratory in Illinois (Rosenzweig et al, 1988,1990). In this experiment, a linac produces both a 6-psec, 21-MeV driving bunch with 15-20 psec full width and a 15-MeV witness beam which can be delayed by varying the time of flight so that it can be injected at various phases into the wake. The plasma of 10^{12}-10^{14} cm^{-3} density is produced by a 20-cm long hollow cathode arc in an 800 G field and a temperature T_p=2-8 eV. The result achieved was a gradient of a few MeV/m corresponding to 30% bunching.

LASER WAKE FIELD ACCELERATOR (LWFA)

A plasma wave with relativistic phase velocity may also be excited by a very short single frequency laser pulse. If the pulse duration is less than the plasma period then the ponderomotive force gives a substantial impulse to the electrons which subsequently oscilate at their natural frequency. The physical mechanism of the excitation of a large amplitude plasma wave by a single ultra-short laser pulse is shown in Fig.7.5.

In the relativistically guided laser wake field accelerator (LWFA) concept (Tajima and Dawson, 1979; Sprangle et al, 1987, 1988) the short pulse, high power laser beam provides both a radial and axial ponderomotive force on the plasma electrons. The radial ponderomotive force expels plasma electrons radially outward while the front (back) of the laser pulse exerts a forward (backward) force on the electrons. In this sense, the laser pulse acts approximately like a negative charged macro-particle propagating through the plasma (see Fig.7.5). As the plasma electrons flow around the laser pulse, large amplitude plasma waves are generated. This mechanism is similar to the plasma wake field accelerator but without the necessity to accurately tailor the axial profile of the driving beam.

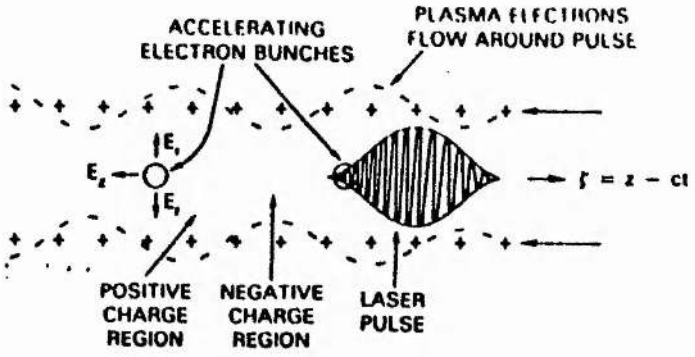

Figure 7.5: Schematic of the laser wake-field accelerator showing the ponderomotive force from an intense short pulse laser generating a plasma wave wake as it propagates through the plasma. The laser pulse acts like an intense negative charge by repelling electrons in both the radial and axial directions. After Sprangle et al (1988).

Although the PBWA has been more extensively investigated in the last few years since its birth the LWFA has been recently receiving renewed attention (Joshi et al, 1984; Gorbunov and Kirsanov, 1987; Sprangle et al, 1988; Tsytovich et al, 1989; Bulanov et al, 1989; 1990) due in part to some problems with the PBWA and the PWFA which can be solved or avoided in the LWFA. In the PBWA the resonance condition $\omega_1-\omega_2=\omega_{pe}$ for the two laser pumps raises problems such as:

i) high plasma uniformity ($\delta n/n_0 \leq 1\%$),

ii) wave saturation due to detuning ($\omega_p=\omega_{p0}/\gamma=\omega_1-\omega_2$, $\omega_{p0}^2=4\pi n_0 e^2/m_0$,

m_0 is the electron rest mass) where $\gamma=(1-v^2/c^2)^{-1/2}$ comes from the electron mass variation in the strong electromagnetic field of the pumps,

iii) fine tuning of the laser frequencies is needed as well as long pulse lengths (many plasma periods).

If the length of the packet is not much smaller than its cross-section, the one-dimensional approximation is no longer justified: 3D effects (i e the transverse ponderomotive force due to the laser beams) are not disruptive in the non-relativistic case (Fedele et al, 1986) but lead to cross-field coupling between the longitudinal and radial plasma field components in the weakly relativistic case (Miano et al, 1989) with the result that an accelerating and focusing region of useful extent can no longer be found. Other problems in the PBWA scheme are related to beam diffraction, the role of competing instabilities and ion dynamics, phase detuning and energy depletion.

In the PWFA scheme the difficulties are related to beam technology for both the driving beam and the injected beam and different kind of instabilities may occur. In the LWFA scheme, since the excitation is due to a

single pump all the problems raised by the resonance condition are absent. In particular, the plasma wave can here grow to larger amplitudes (there is no saturation due to detuning) thereby also losening the constraints on the injected beam. If a short ($\sim\omega_p^{-1}$), high power ($\geq 10^{15}$ W) laser pulse is used there could be the further advantage of avoiding diffraction due to relativistic optical guiding (Sprangle et al, 1988, Esarey et al, 1989). The penalty is that the energy put in to the excited wave must be supplied in a shorter time period and the power (but not energy) requirements on the laser are increased. The growth of sidebands from the impulsive single frequency drive has not been considered, and so no comment can be made about efficiency. From the point of view of plasma instabilities only the relativistic self focusing and modulational instability of the light waves remain as potential problems.

The purpose of the second part of the thesis is to numerically investigate the self-consistent theory of the excitation mechanism of an ultra-relativistic plasma wake field by a single ultra-short laser pulse in 1D geometry. We are particularly interested to see the effects of different shape of the laser pulse profile and of the ambient plasma density. Our plan is to first derive

the relevant self-consistent coupled equations for the spatial-temporal evolution of the scalar and vector potentials of the wave fields in 1D geometry. Although the relevant coupled equations have already been given previously by de Angelis (1990), the detailed derivation was verified and is given here. This is done in chapter 8. The coupled equations for the potentials are then solved numerically in the envelope approximation by using a numerical code. This numerical code was written originally by Mr. B. McNamara (1990). However, in the case of running it we made various modifications and improvements. Some numerical solutions of the potentials for different input parameters and a short discussion is given in chapter 9.

chapter 8

MODEL EQUATIONS FOR LASER WAKE EXCITATION IN 1D GEOMETRY

Let us consider a model (de Angelis, 1990) based on the one-fluid, 1D, cold relativistic hydrodynamics and Maxwell's equations. The plasma is unmagnetized and the ions are immobile. The equation for the electron momentum is:

$$\left(\frac{\partial}{\partial t}+v_{\parallel}\frac{\partial}{\partial z}\right)\vec{p}=-e\left(\vec{E}+\frac{1}{c}\vec{v}\times\vec{B}\right), \tag{8.1}$$

where

$$\vec{p}=m_0\gamma\vec{v}, \qquad \gamma=\left(1+\frac{p^2}{m_0^2c^2}\right)^{1/2},$$

m_0 and $\vec{v}$ being the electron rest mass and velocity. In Eq.(8.1), we have assumed that all quantities only depend on z and t, $\parallel$ signifies the z-direction which is the direction of propagation of the external pump field.

$$\vec{E}=-\frac{1}{c}\frac{\partial\vec{A}_{\perp}}{\partial t}-\hat{e}_z\frac{\partial\phi}{\partial z}; \qquad \vec{B}=\nabla\times\vec{A}; \qquad \vec{A}_{\perp}=A_x\hat{e}_x+A_y\hat{e}_y, \tag{8.2}$$

where $\hat{e}_x$, $\hat{e}_y$ and $\hat{e}_z$ are the unit vectors along x, y and z axes respectively;

$\vec{A}_\perp$ is the vector potential of the electromagnetic pulse and ϕ the ambipolar potential due to the charge separation in the plasma. We assume the high frequency part of the perpendicular component of the nonlinear terms in Eq.(8.1) is small; in that case we obtain

$$\frac{\partial \vec{p}_\perp}{\partial t} = -e\vec{E}_\perp = \frac{e}{c}\frac{\partial \vec{A}_\perp}{\partial t}, \tag{8.3a}$$

which gives

$$\frac{\vec{p}_\perp}{m_0 c} = \left(\frac{e}{m_0 c^2}\right)\vec{A}_\perp \equiv \vec{a}(z,t). \tag{8.3b}$$

We have

$$\gamma^2 = 1 + \left(\frac{p^2}{m_0^2 c^2}\right) = \left(1 + \frac{p_\perp^2}{m_0^2 c^2} + \frac{p_\parallel^2}{m_0^2 c^2}\right) = \left(1 + a^2 + \gamma^2 \frac{v_\parallel^2}{c^2}\right), \tag{8.4a}$$

from which it can be shown that

$$\gamma^2 = \left(1 + a^2\right)\left(1 - \frac{v_{\parallel}^2}{c^2}\right)^{-1}, \tag{8.4b}$$

and we write it as

$$\gamma = \gamma_a \gamma_{\parallel}, \tag{8.4c}$$

where

$$\gamma_a = \left(1 + a^2\right)^{1/2}; \qquad \gamma_{\parallel} = \left(1 - \frac{v_{\parallel}^2}{c^2}\right)^{-1/2}. \tag{8.4d}$$

From Eq.(7.4a) we can write

$$p_{\parallel} = m_0 c \gamma_a \sqrt{\gamma_{\parallel}^2 - 1}\,; \quad v_{\parallel} = c\left(\frac{\sqrt{\gamma_{\parallel}^2 - 1}}{\gamma_{\parallel}}\right). \tag{8.5a}$$

We have

$$E_{\parallel} = -\frac{\partial \phi}{\partial z}, \tag{8.5b}$$

$$\left(\vec{v} \times \vec{B}\right)_{\parallel} = \left(\vec{v} \times \left(\nabla \times \vec{A}_{\perp}\right)\right)_{\parallel} = \left(\frac{1}{m_0 \gamma}\vec{p} \times \left[\hat{\vec{e}}_z \frac{\partial}{\partial z}\right] \times \left[\hat{\vec{e}}_x A_{\perp x} + \hat{\vec{e}}_y A_{\perp y}\right]\right)_{\parallel}, \tag{8.5c}$$

from which

$$\left(\vec{v}\times\vec{B}\right)_{\parallel}=\left(\frac{1}{m_0\gamma}\right)\left(p_{\perp x}\frac{\partial A_{\perp x}}{\partial z}+p_{\perp y}\frac{\partial A_{\perp y}}{\partial z}\right). \tag{8.5d}$$

From relation (8.3b), we have

$$p_{\perp x}=\frac{e}{c}A_{\perp x}=m_0 c a_x;\quad p_{\perp y}=\frac{e}{c}A_{\perp y}=m_0 c a_y. \tag{8.5e}$$

Applying the relations (8.5e) and

$$\gamma_a^2=1+a^2$$

into Eq.(8.5d) we finally obtain

$$\left(\vec{v}\times\vec{B}\right)_{\parallel}=\left(\frac{m_0 c^3}{e\gamma_{\parallel}}\right)\frac{\partial\gamma_a}{\partial z}. \tag{8.6}$$

Therefore the parallel component of the momentum balance equation (Eq.(8.1)) can be written as

$$\frac{1}{c}\frac{\partial}{\partial t}\left(\gamma_a\sqrt{\gamma_{\parallel}^2-1}\right)+\frac{\partial}{\partial z}\left(\gamma_a\gamma_{\parallel}\right)=\frac{\partial\Phi}{\partial z}, \tag{8.7}$$

where

$$\Phi=\left(\frac{e}{m_0 c^2}\right)\phi \tag{8.8}$$

is the dimensionless potential. From the continuity equation

$$\frac{\partial n}{\partial t}+\nabla\cdot\left(n\vec{v}\right)=0, \tag{8.9}$$

we have

$$\frac{1}{c}\frac{\partial n}{\partial t}+\frac{\partial}{\partial z}\left(\frac{n\sqrt{\gamma_{\|}^{2}-1}}{\gamma_{\|}}\right)=0. \tag{8.10}$$

The Poisson's equation

$$\nabla\cdot\vec{E}=-4\pi e\left(n-n_{0}\right) \tag{8.11}$$

gives

$$\frac{\partial^{2}\Phi}{\partial z^{2}}=\frac{\omega_{p0}^{2}}{c^{2}}\left(\frac{n}{n_{0}}-1\right). \tag{8.12}$$

where $\omega_{p0}^{2}=4\pi n_{0}e^{2}/m_{0}$, $n=n_{0}+\delta n$, n_{0} is the background ambient electron plasma density and δn is the density fluctuation. The Maxwell's equation

$$\nabla\times\vec{B}=\frac{4\pi}{c}\vec{j}+\frac{1}{c}\frac{\partial\vec{E}}{\partial t}, \tag{8.13}$$

gives

$$\left(c^2\frac{\partial^2}{\partial z^2}-\frac{\partial^2}{\partial t^2}\right)\vec{a}=\left(\frac{\omega_{p0}^2 n}{n_0\gamma_a\gamma_{\parallel}}\right)\vec{a}. \qquad (8.14)$$

In this Eq.(8.14) we have used the relations (8.2) and $\vec{J}=-en\vec{v}$. Equations (8.7), (8.10), (8.12) and (8.14) form the basic set of the formulation. We assume a driving pulse of the form:

$$\vec{a}(z,t)=\frac{1}{2}\vec{a}_0\exp(-i\theta)+\text{compl. conj.}=\frac{1}{2}\vec{a}_0(\xi,\tau)\exp(-i\theta)+\text{compl. conj.}, \qquad (8.15)$$

where $\theta=\omega_0 t-k_0 z$, ω_0 and k_0 being the central frequency and wavenumber, and $\xi=z-v_g t$, where $\partial\omega_0/\partial k_0$ is the group velocity and τ is a slow time-scale:

$$\frac{1}{a_0}\left(\frac{\partial^2 a_0}{\partial\tau^2}\right)<<\omega_0^2 \qquad (8.16)$$

accounting for changes in the pump due to the plasma reaction. We use the following operators

$$\frac{\partial}{\partial z}\equiv\frac{\partial}{\partial\xi}\ , \qquad \frac{\partial}{\partial t}\equiv\frac{\partial}{\partial\tau}+\frac{\partial\xi}{\partial t}\frac{\partial}{\partial\xi}\ , \qquad (8.17)$$

to obtain the wave equation in envelope approximation. We have

$$\frac{\partial a_0}{\partial z} \cong \frac{\partial a_0}{\partial \xi}, \qquad \frac{\partial^2 a_0}{\partial z^2} \cong \frac{\partial^2 a_0}{\partial \xi^2}, \tag{8.18a}$$

and

$$\frac{\partial a_0}{\partial t} \cong \frac{\partial a_0}{\partial \tau} - v_g \frac{\partial a_0}{\partial \xi}, \qquad \frac{\partial^2 a_0}{\partial t^2} \cong -2v_g \frac{\partial^2 a_0}{\partial \tau \partial \xi} + v_g^2 \frac{\partial^2 a_0}{\partial \xi^2}. \tag{8.18b}$$

The wave equation (8.14) now reduces to

$$\left\{ 2\frac{\partial}{\partial \tau}\left(i\omega_0 \vec{a}_0 + v_g \frac{\partial \vec{a}_0}{\partial \xi} \right) + c^2 \left(1 - \frac{v_g^2}{c^2} \right) \frac{\partial^2 \vec{a}_0}{\partial \xi^2} + 2i\omega_0 \left(\frac{c^2 k_0}{\omega_0} - v_g \right) \frac{\partial \vec{a}_0}{\partial \xi} \right\} \exp(-i\theta)$$

$$+ \text{compl. conj.} = \left(c^2 k_0^2 - \omega_0^2 + \omega_{p0}^2 \frac{n}{n_0} \frac{1}{\gamma_a \gamma_\parallel} \right) \vec{a}_0 \exp(-i\theta) + \text{compl. conj.} \tag{8.19}$$

From Eqs.(8.7) and (8.10) in the quasistatic approximation (Sprangle et al, 1990) the following two first integrals can easily be obtained (de Angelis, 1990):

$$\gamma_a \left(\gamma_\parallel - \beta_0 \sqrt{\gamma_\parallel^2 - 1} \right) - \Phi = 1, \tag{8.20}$$

$$n\left(\beta_0 \gamma_\parallel - \sqrt{\gamma_\parallel^2 - 1} \right) = n_0 \beta_0 \gamma_\parallel, \tag{8.21}$$

where $\beta_0=v_g/c$ and we have approximated $\partial/\partial z\equiv\partial/\partial\xi$ and $\partial/\partial t\equiv-v_g(\partial/\partial\xi)$. The constants of integration have been chosen in such a way that:

$$n=n_0,\quad \gamma_{\|}=1,\quad \Phi=0,\quad \text{for}\ \gamma_a=1,\ (\text{where}\ \left|\vec{a}_0\right|^2=0). \tag{8.22}$$

The general system [Eqs.(8.7), (8.10), (8.12), (8.14)] is then reduced to equations (8.12) and (8.14) only which can be written, using Eqs.(8.20) and (8.21), as:

$$\frac{\partial^2\Phi}{\partial\xi^2}=\left(\frac{\omega_{p0}^2}{c^2}\right)\left[\frac{\sqrt{\gamma_{\|}^2-1}}{\beta_0\gamma_{\|}-\sqrt{\gamma_{\|}^2-1}}\right], \tag{8.23}$$

$$2\frac{\partial}{\partial\tau}\left(i\omega_0\vec{a}_0+c\beta_0\frac{\partial\vec{a}_0}{\partial\xi}\right)+\left(\frac{c^2\omega_{p0}^2}{\omega_0^2}\right)\frac{\partial^2\vec{a}_0}{\partial\xi^2}$$

$$=-\omega_{p0}^2\left[1-\frac{\beta_0}{\gamma_a\left(\beta_0\gamma_{\|}-\sqrt{\gamma_{\|}^2-1}\right)}\right]\vec{a}_0. \tag{8.24}$$

For the limiting case $\beta_0=1$ the set of equations (Eqs(8.23) and (8.24)) simplifies to

$$\frac{\partial^2 \Phi}{\partial \xi^2} = \left(\frac{\omega_{p0}^2}{2c^2} \right) \left[\frac{\gamma_a^2}{(1+\Phi)^2} - 1 \right], \tag{8.25}$$

$$2\frac{\partial}{\partial \tau}\left(i\omega_0 \vec{a}_0 + c\frac{\partial \vec{a}_0}{\partial \xi} \right) + \left(\frac{c^2 \omega_{p0}^2}{\omega_0^2} \right) \frac{\partial^2 \vec{a}_0}{\partial \xi^2} = -\omega_{p0}^2 \left[\frac{\Phi}{1+\Phi} \right] \vec{a}_0 . \tag{8.26}$$

Eq.(8.25) has been solved by Tsintsadze (1990) for the case of a given pump; the coupled system (8.25)+(8.26) has been considered by Bulanov et al (1990), whereas we are now going to consider the general system of equations (8.23) and (8.24) as our model equations for the numerical evaluation of the excitation of a relativistic nonlinear large amplitude plasma wave.

chapter 9

NUMERICAL SOLUTION OF THE MODEL EQUATIONS FOR WAKE-FIELD EXCITATION, RESULTS AND DISCUSSION

The 1D formulation for the excitation of a relativistic plasma wake-field by a single ultra-short laser pulse has been described in chapter 8. The result ends up with a set of two coupled equations (Eqs (8.23) and (8.24)) for the self consistent evolution of the laser pulse vector potential envelope a_0 and the scalar potential Φ of the excited wake-field. For convenience we write this set of coupled equations again as follows:

$$\frac{\partial^2 \Phi}{\partial \xi^2} = \frac{\omega_{p0}^2}{c^2} G , \tag{9.1}$$

$$2i\omega_0 \frac{\partial a_0}{\partial t} + 2c\beta_0 \frac{\partial^2 a_0}{\partial t \, \partial \xi} + \frac{c^2 \omega_{p0}^2}{\omega_0^2} \frac{\partial^2 a_0}{\partial \xi^2} = - \omega_{p0}^2 H a_0 , \tag{9.2}$$

where t now is a slow time scale and

$$G = \frac{\sqrt{\gamma_{\|}^2 - 1}}{\beta_0 \gamma_{\|} - \sqrt{\gamma_{\|}^2 - 1}} ,$$

$$H = 1 - \frac{\beta_0}{\gamma_a\left(\beta_0\gamma_{\|} - \sqrt{\gamma_{\|}^2 - 1}\right)}.$$

This set of equations (9.1) and (9.2) to be solved numerically in the stationary frame of the pulse. Eq(9.1) is the Poisson's equation which is to be solved by integrating back from the head of the pulse, to obtain values at a series of mesh points, with initial conditions, $\Phi=0$, $\partial\Phi/\partial\xi=0$. The right hand side of the equation, the perturbed electron density, is a very spiky function of Φ. This creats some difficulties at particular mesh points in the integration. The method we use is a simple predictor-corrector. The corrector is iterated till convergence is obtained at each point. If convergence is not obtained, the interval is divided into several sub-intervals. Values of γ_a are calculated by linear interpolation among the values of a_0 on the same mesh and the integration repeated over the interval. The total computation is not large, so many mesh points are used to minimize computational difficulties. The potential equation is integrated to some arbitrary point (say, $8\lambda_p$, $\lambda_p=2\pi c/\omega_{p0}$, is the plasma wavelength), beyond the end of the pulse.

The envelope equation (9.2), which is written as two coupled equations for the real and imaginary parts of a_0, is solved implicitly. This is essential for correct treatment of the mixed derivative term. The difference scheme is of the form

$$A_j a_0^{n+1}(j+1) + B_j a_0^{n+1}(j) + C_j a_0^{n+1}(j-1) = U_j$$

$$= P_j a_0^{n}(j+1) + Q_j a_0^{n}(j) + R_j a_0^{n}(j-1). \qquad (9.3)$$

The coefficients are mostly complex. The right hand side, U, is first calculated with the known values of Φ at time step n. We solve the difference relations in standard fashion by Gaussian elimination.

The present model is based on a quasi-static approximation, in which we have obtained two integrals of motion (Eqs(8.20) and (8.21)), described in chapter 8 for slow-time scale τ, in the assumption that $\partial/\partial\tau \cong 0$. In that approximation the electron plasma density $n=n_0+\delta n$ and the quantity $\gamma_C=\gamma_a(\gamma_{\|}^2-1)^{1/2}$ are constants. The quantity γ_C has been checked frequently in the numerical calculation and it has been found that it changes slowly with time after a certain number of plasma periods. Table VIII shows for

different input parameters, the number of plasma periods after which γ_C changes by 25%.

We present some numerical graphics for the evolution of the excited plasma wake-field potential Φ, wake-electric field E_w as well as the laser pulse field vector potential $|a_0|$. In all the following figures, we have plotted the fields as normalized quantities, $\Phi=e\phi/m_0c^2$, $E_w=e|E|/m_0c\omega_{p0}$ and $a_0=eA_0/m_0c^2$, where ϕ, E and A_0 are respectively the wake scalar potential, wake electric field and pump laser vector potential. The horizontal scale is position $\xi=z-v_gt$, normalized with the plasma wavelength $\lambda_p=2\pi c/\omega_{p0}$, ω_{p0} is the ambient angular plasma frequency. Time has been counted in terms of plasma period $T_p=2\pi/\omega_{p0}$; $|a_0^{in}|$ signifies the peak amplitude of the normalized initial vector potential of the laser pulse, ω_0 is the laser frequency, σ_r and σ_f signify the Gaussian rise and fall respectively.

Figures 9.1-9.3 show the evolution of the excited wake-field scalar potential Φ and the magnitude of the laser pulse vector potential $|a_0|$ for two

different times, different values of $|a_0^{in}|$ and with different shapes of the pump pulse profiles σ_r and σ_f. It is seen that, the larger the value of $|a_0^{in}|$, the higher the excited wake-field Φ. It is also seen that, for symmetrical Gaussian pulse, or pulse with slow Gaussian rise and steep Gaussian back, for lower value of $|a_0^{in}|$, the shape of the laser pulse almost unchanged up to a time of about $40T_p$. However, for a Gaussian pulse with steep front and slow back, there is some distortion in the pulse shape, as we see from the Fig.9.2.

Figure 9.4 shows the evolution of $|a_0|$, Φ and the real and imaginary parts of a_0. We see from these curves that there are distortions of the laser pulse at particular positions ξ where the wake-potential Φ has local minima.

Figure 9.5 shows the evolution of the density perturbation $\delta n/n_0$ for the excited laser wake field. In that figure we see the sharp peaks of the density perturbation, where the potential Φ has local minima.

Figures 9.6 and 9.7 show the evolution of $|a_0|$, Φ and wake-electric field E_w

in two different times. Figure 9.6 is for $\omega_{p0}/\omega_0=0.01$ whereas Fig 9.7 is for $\omega_{p0}/\omega_0=0.1$. As we see from the figures, distortion in the pulse shape increases with increasing the ratio ω_{p0}/ω_0.

Figure 9.8 shows the evolution of $|a_0|$, Φ and wake-electric field E_w at time $t=2T_p$ for similar parameters as considered by Tsintsadze (1990) for his fixed pump field amplitude. As we see, steep front with slow back shape of the Gaussian laser pulse is more favourable for the wake-field excitation. However as we have noticed earlier that, in this favourable case, there is some distortion in the shape of the laser pulse.

Figure 9.9 shows the evolution of $|a_0|^2/2$ and Φ for a square laser pulse. It is seen that the distortion of the pulse shape increases with the ratio ω_{p0}/ω_0.

For a numerical example, in the present 1D simulation, the energy gradient of the excited laser wake field can be of the order of 480 GeV/m. In this example (see Fig.9.6), we have considered the following input parameters: the value of the dimensionless input vector potential $|a_0^{in}|=2$, the ratio of the

ambient plasma frequency to the laser frequency ω_{p0}/ω_0=0.01, Gaussian rise σ_r=0.25λ_p, Gaussian fall σ_f=1.5λ_p; λ_p is the plasma wavelength. It is noted here that the above parameters are relevant to present-day KrF lasers.

The present study has considered different shapes of the Gaussian profile as well as a square profile for the incident laser pulse. Parameter studies suggest that an ultra-short (pulse length $l_t \leq$plasma wavelength λ_p), high intensity ($|a_0^{in}|>1$) laser pulse can excite a very large amplitude plasma wake-field. The amplitude of the excited wake-field increases with increasing the ambient plasma density but the shape of the pulse is distorted for a long pulse or a pulse with steep front with relatively long tail. An interesting feature of the behaviour of the pulse is that the distortion occurs where the wake-potential Φ has a minimum that is, $\delta n/n_0$ has a maximum. This behaviour of the laser pulse shape can be explained as follows. When a light pulse interacts with a plasma density gradient, the group velocity of the light pulse, $v_g=c(1-\omega_p^2/\omega_0^2)^{1/2}$, decreases as the plasma density increases. This has the effect of slowing the light wave down as it

propagates up the density gradient and speeding it up as it propagates down the density gradient. Thus causing a pile up of photons on one side of the gradient causing a distortion of the laser pulse profile.

Besides this pulse distortion, however, a steepening of the laser pulse is seen to occur for a steep front with long tail of the pulse. Similarly, for a square pulse, the steepening of the pulse is found to occur at the leading front. This type of behaviour of the square pulse was observed earlier by Bulanov et al (1990) for their fixed pump amplitude case.

Finally, we have numerically modelled the self-consistent theory of the excitation of a relativistic large amplitude plasma wake-field by a single ultra-short laser pulse. The theory is restricted to 1D geometry but temporal behaviour has been taken into account. The electron-fluid response has been simplified in the laser pulse frame in the slow time scale by considering a quasi-static approximation for the plasma quantities n the plasma density, and $g_C=\gamma_a(\gamma_{||}^2-1)^{1/2}$. This quasi-static approximation states that, if the laser pulse is sufficiently short, the fields a_0 and Φ which drive the plasma are expected to change little during a transit time of the plasma

through the laser pulse (Sprangle et al, 1990). This quasi-static approximation breaks down after a certain time, which of course depends on different input parameters, namely, ambient plasma density and amplitude of the pump field. The 2D effects on the evolution of the laser pulse profile as well as the excited plasma wake-field might be important for wake-field excitation and this should be investigated thoroughly in a self-consistent (r,z,t) model.

TABLE VIII. VALIDITY OF THE MODEL

	$\lvert a_0^{in}\rvert$	ω_{p0}/ω_0	Time t in terms of plasma period $T_p=2\pi/\omega_{p0}$
$\sigma_r=0.25\lambda_p$ $\sigma_f=0.25\lambda_p$	1	0.05	40
	2	0.01	250
		0.05	30
		0.10	15
	3	0.05	25
$\sigma_r=0.25\lambda_p$ $\sigma_f=1.50\lambda_p$	1	0.05	30
	2	0.01	200
		0.05	25
		0.10	10
	3	0.05	20
$\sigma_r=1.50\lambda_p$ $\sigma_f=0.25\lambda_p$	1	0.05	50
	2	0.01	250
		0.05	50
		0.10	20
	3	0.05	50
Square pulse width $l_p=1.0\lambda_p$	2	0.01	250
		0.05	40
		0.10	6

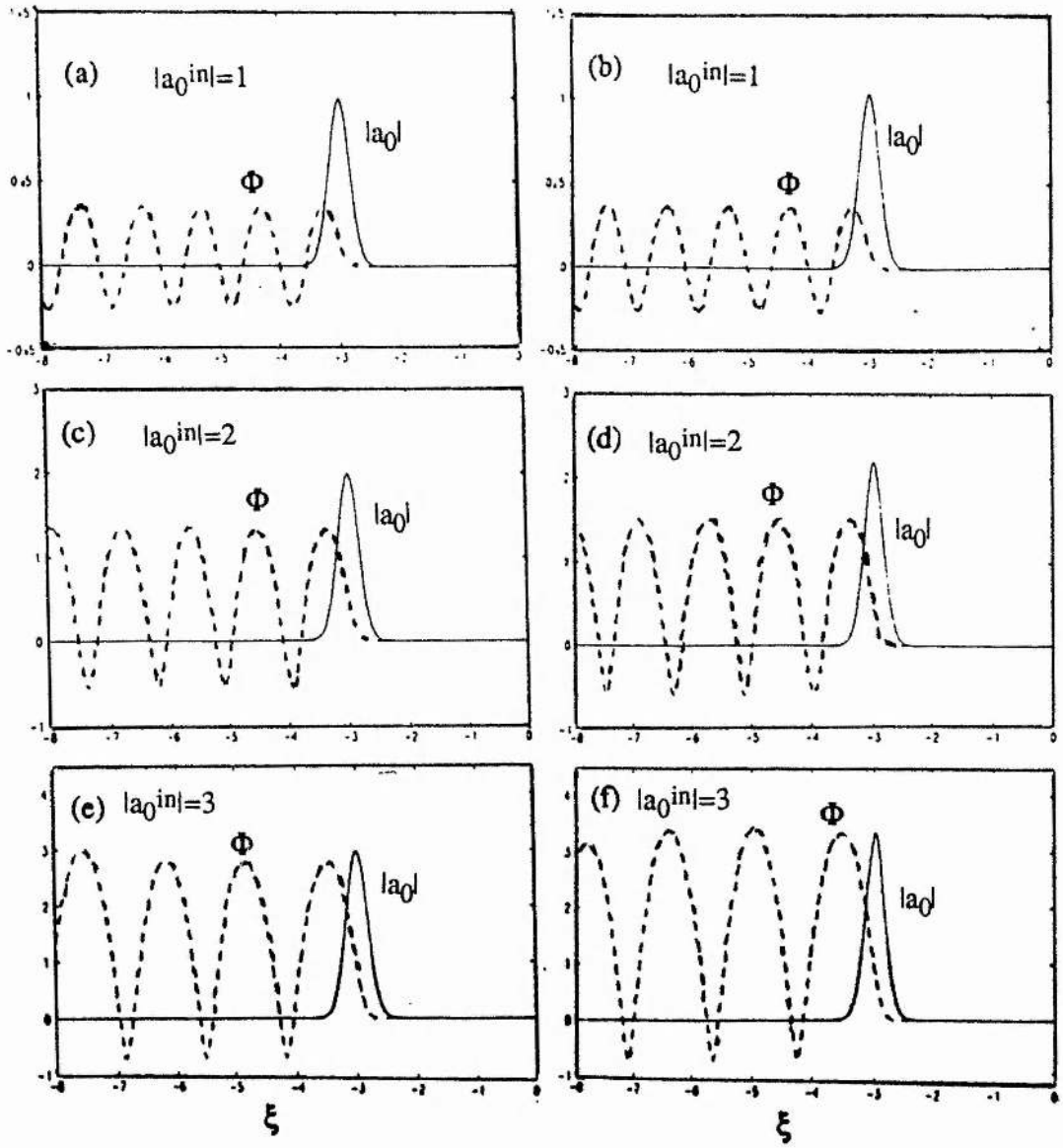

Figure 9.1: The values of the magnitude of normalised vector potential $|a_0|$ (solid curves) and scalar potential Φ (dashed curves) with position $\xi=z-v_g t$. Gaussian rise $\sigma_r=0.25\lambda_p$, Gaussian fall $\sigma_f=0.25\lambda_p$, $\omega_{p0}/\omega_0=0.05$. Curves (a) and (b) are for $|a_0^{in}|=1$; (c) and (d) are for $|a_0^{in}|=2$; (e) and (f) are for $|a_0^{in}|=3$. Curves (a), (c) and (e) are at time $t=0.4T_p$ whereas curves (b), (d) and (f) are at $t=40T_p$. $T_p=2\pi/\omega_{p0}$, is the plasma period and $\lambda_p=2\pi c/\omega_{p0}$, is the plasma wavelength.

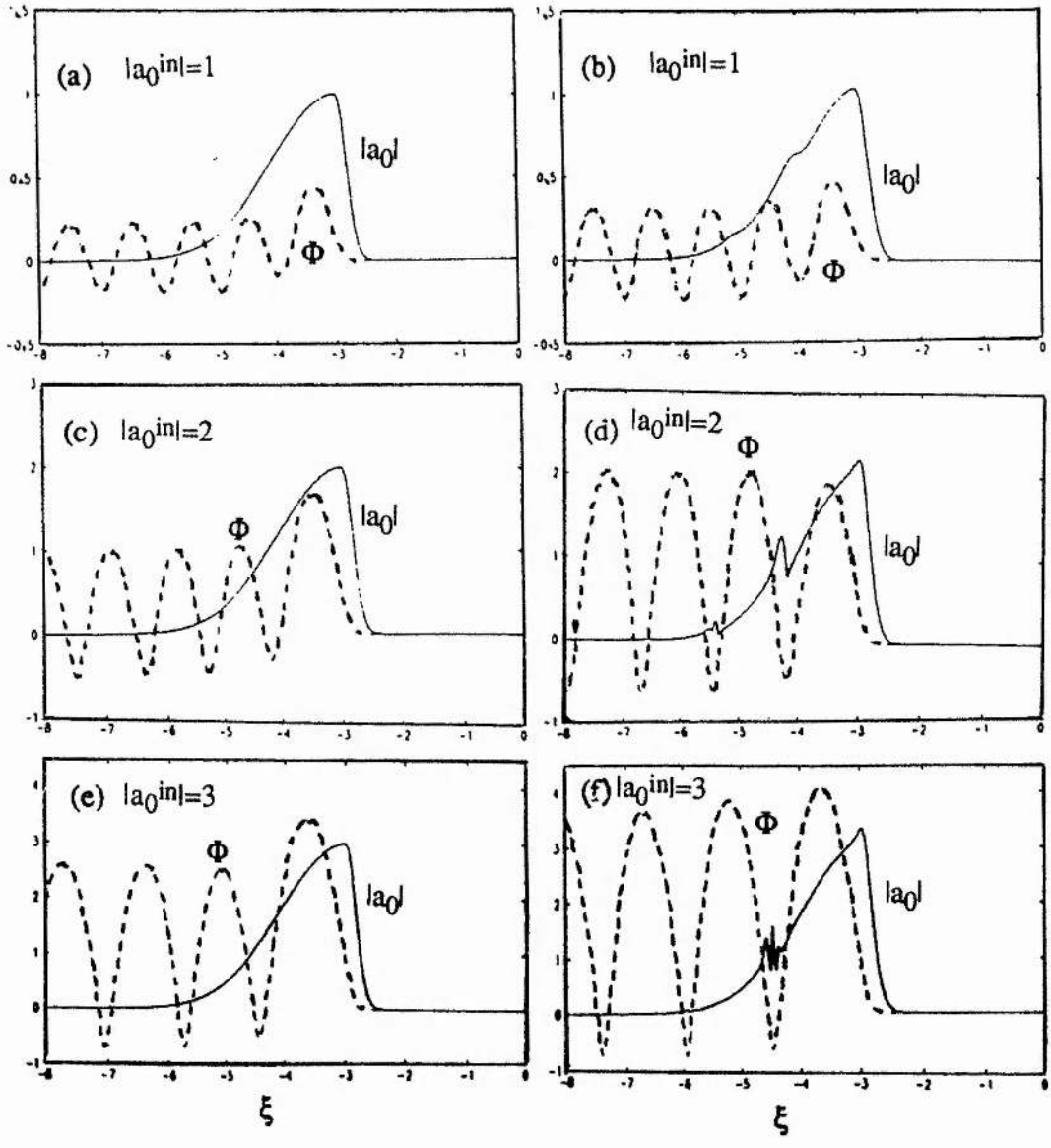

Figure 9.2: The values of the magnitude of normalised vector potential $|a_0|$ (solid curves) and scalar potential Φ (dashed curves) with position $\xi=z-v_g t$. Gaussian rise $\sigma_r=0.25\lambda_p$, Gaussian fall $\sigma_f=1.5\lambda_p$, $\omega_{p0}/\omega_0=0.05$. Curves (a) and (b) are for $|a_0^{in}|=1$; (c) and (d) are for $|a_0^{in}|=2$; (e) and (f) are for $|a_0^{in}|=3$. Curves (a), (c) and (e) are at time $t=0.4T_p$ whereas curves (b), (d) and (f) are at $t=40T_p$.

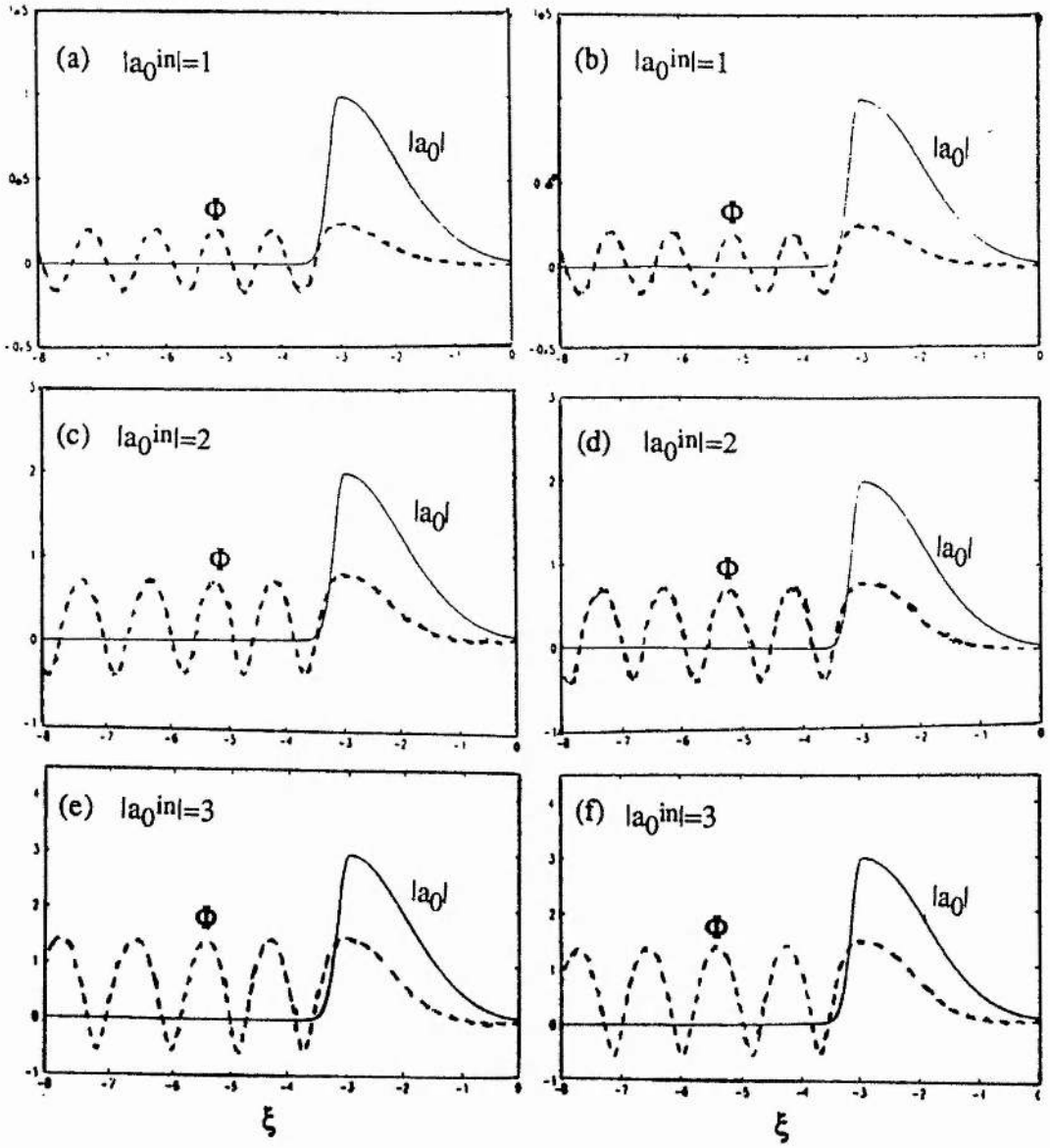

Figure 9.3: The values of the magnitude of normalised vector potential $|a_0|$ (solid curves) and scalar potential Φ (dashed curves) with position $\xi=z-v_g t$. Gaussian rise $\sigma_r=1.5\lambda_p$, Gaussian fall $\sigma_f=0.25\lambda_p$, $\omega_{p0}/\omega_0=0.05$. Curves (a) and (b) are for $|a_0^{in}|=1$; (c) and (d) are for $|a_0^{in}|=2$; (e) and (f) are for $|a_0^{in}|=3$. Curves (a), (c) and (e) are at time $t=0.4T_p$ whereas curves (b), (d) and (f) are at $t=40T_p$.

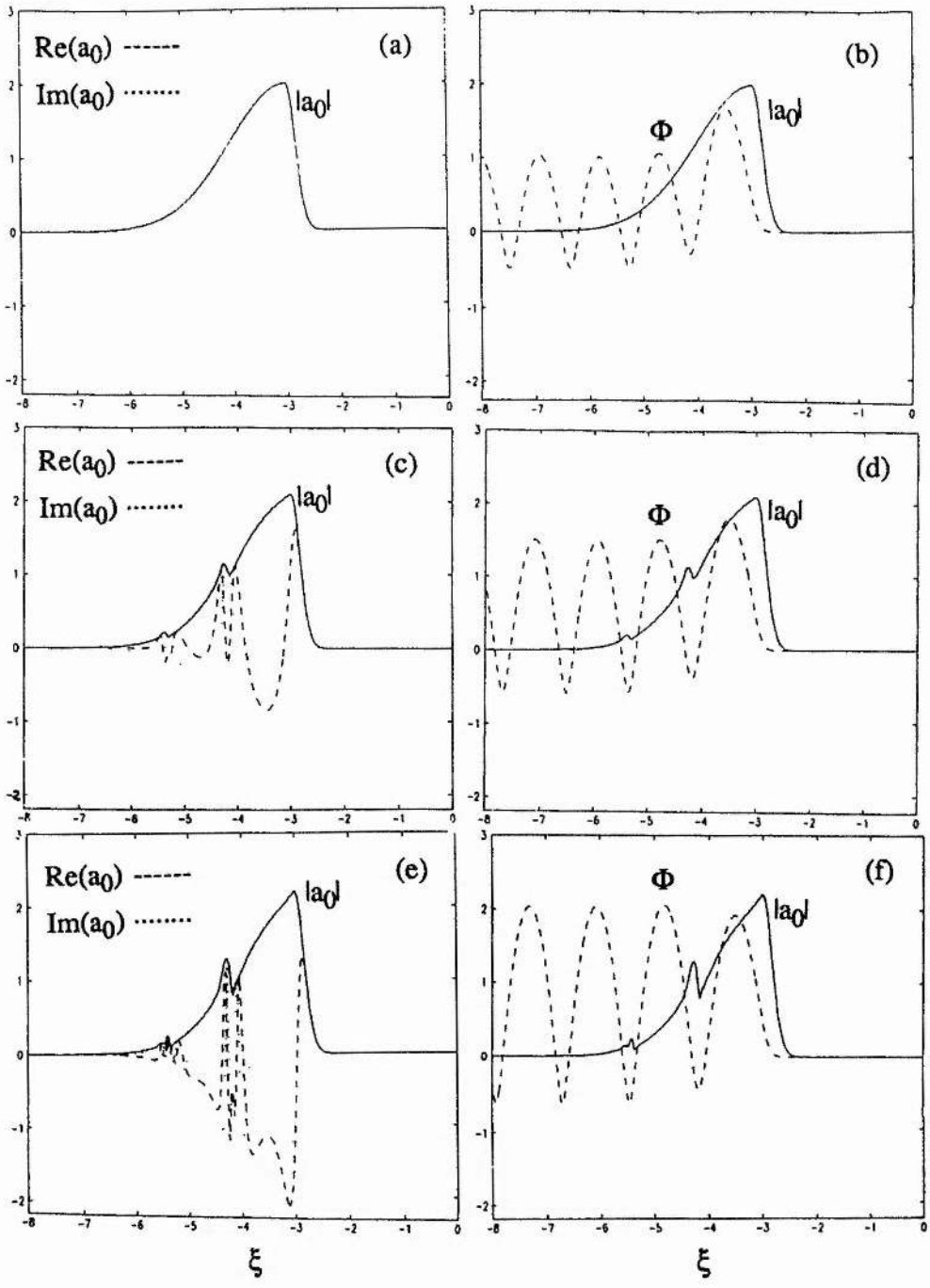

Figure 9.4: The values of the magnitude of normalised vector potential $|a_0|$ (solid curves) and the real and imaginary parts of a_0 and also Φ with position $\xi=z-v_g t$. Gaussian rise $\sigma_r=0.25\lambda_p$, Gaussian fall $\sigma_f=1.5\lambda_p$, $\omega_{p0}/\omega_0=0.05$, $|a_0^{in}|=2$. Curves (a) and (b) are for $t=0.4T_p$, (c) and (d) are for $t=20T_p$, (e) and (f) are for $t=40T_p$.

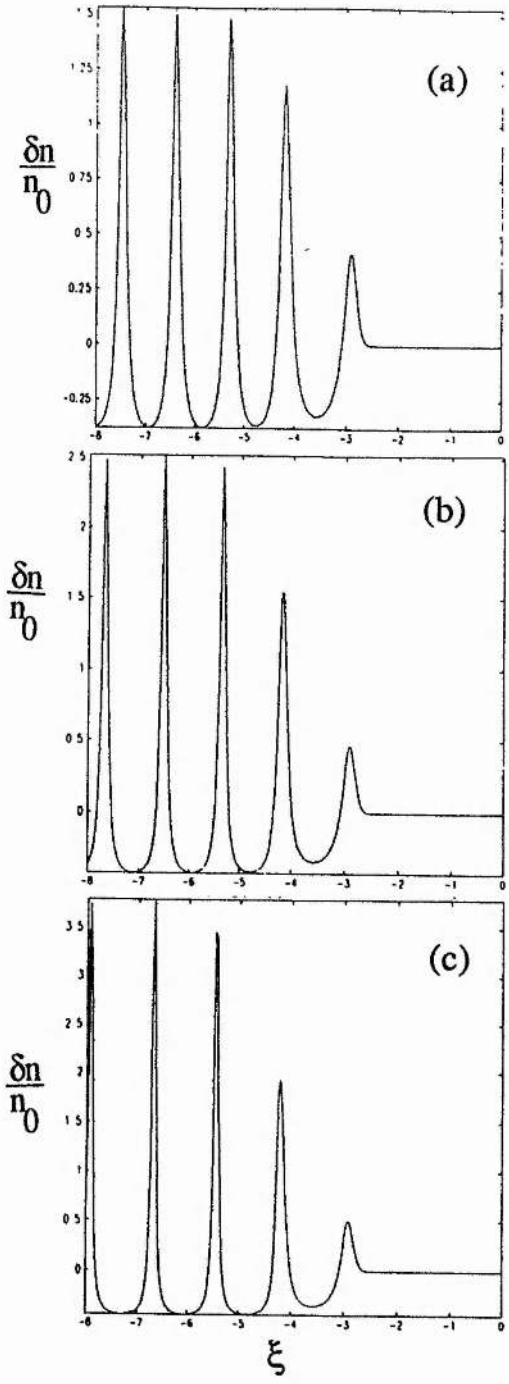

Figure 9.5: The evolution of the normalised density perturbation $\delta n/n_0$. Gaussian rise of the incident laser pulse $\sigma_r=0.25\lambda_p$, Gaussian fall $\sigma_f=1.5\lambda_p$, $\omega_{p0}/\omega_0=0.05$, $|a_0^{in}|=2$. Curves (a), (b), and (c) are for $t=0.4T_p$, $20T_p$, and $40T_p$ respectively.

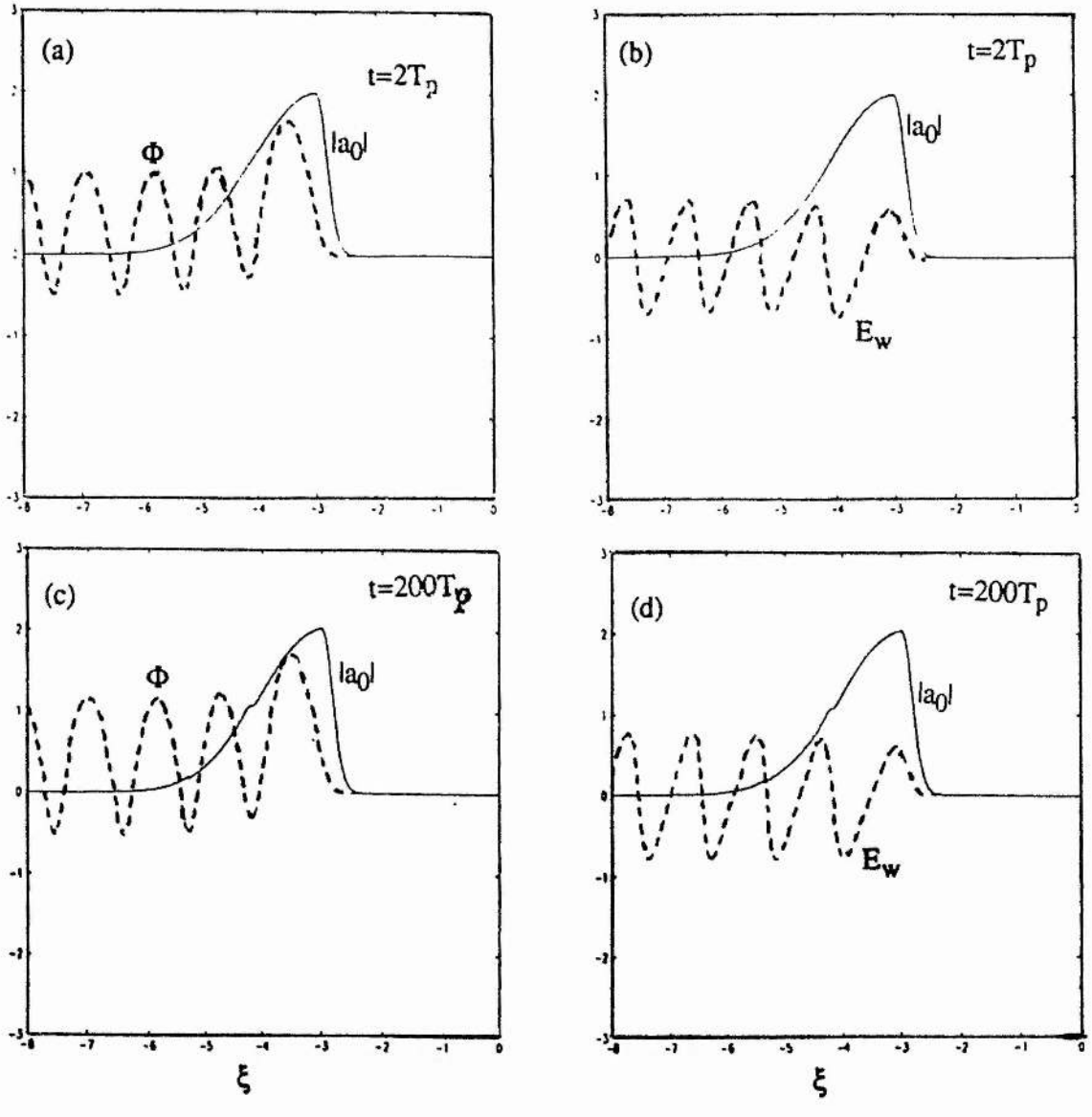

Figure 9.6: The values of the magnitude of normalised vector potential $|a_0|$ (solid curves) and scalar potential Φ and/or wake-electric field E_w (dashed curves) with position $\xi=z-v_g t$. $|a_0^{in}|=2$, $\omega_{p0}/\omega_0=0.01$. Gaussian rise $\sigma_r=0.25\lambda_p$, Gaussian fall $\sigma_f=1.5\lambda_p$, Curves (a) and (b) are at time $t=2T_p$; (c) and (d) are at $t=200T_p$.

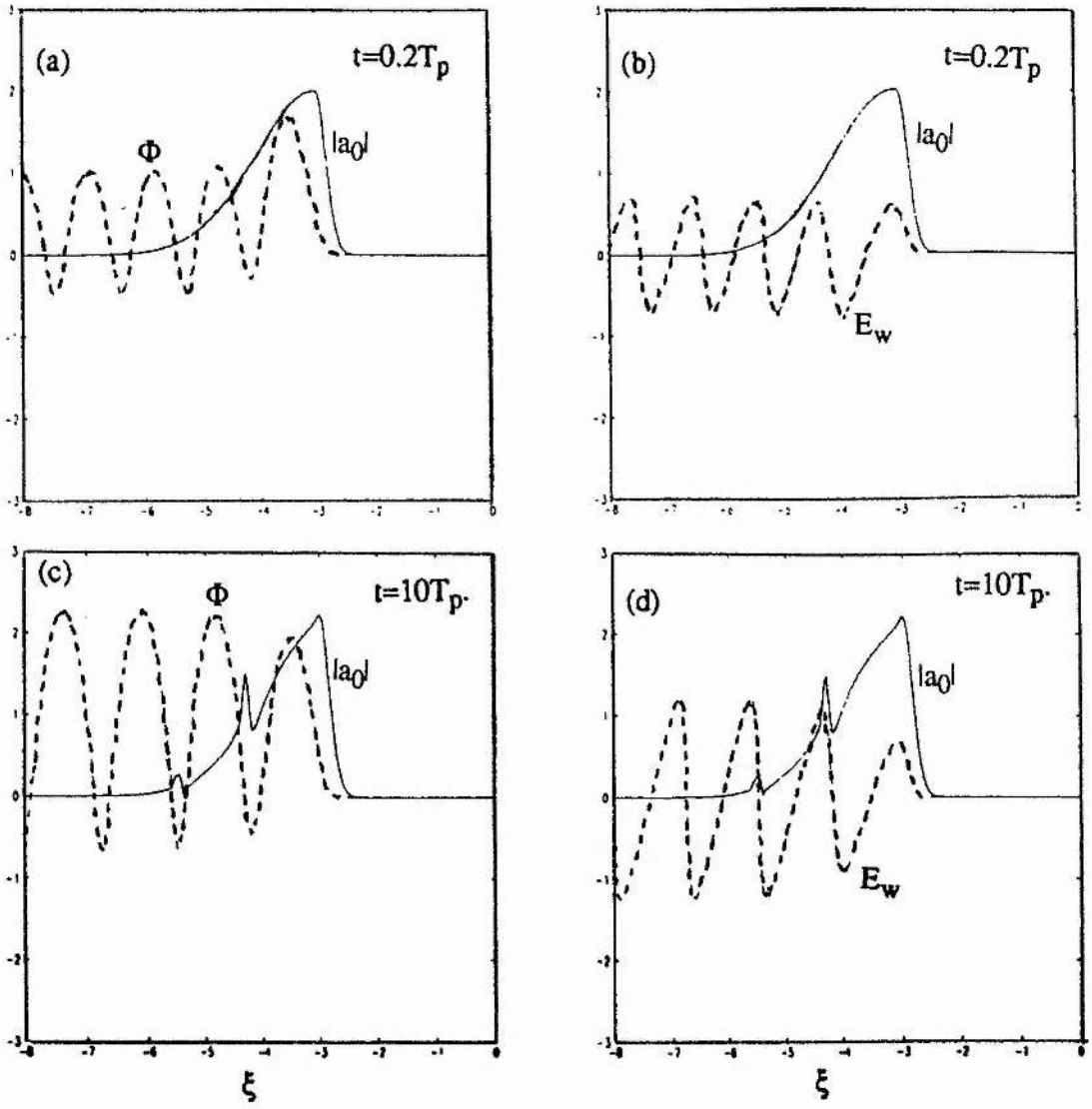

Figure 9.7: The values of the magnitude of normalised vector potential $|a_0|$ (solid curves) and scalar potential Φ and/or wake-electric field E_w (dashed curves) with position $\xi=z-v_g t$. $|a_0^{in}|=2$, $\omega_{p0}/\omega_0=0.1$. Gaussian rise $\sigma_r=0.25\lambda_p$, Gaussian fall $\sigma_f=1.5\lambda_p$, Curves (a) and (b) are at time $t=0.2T_p$; (c) and (d) are at $t=10T_p$.

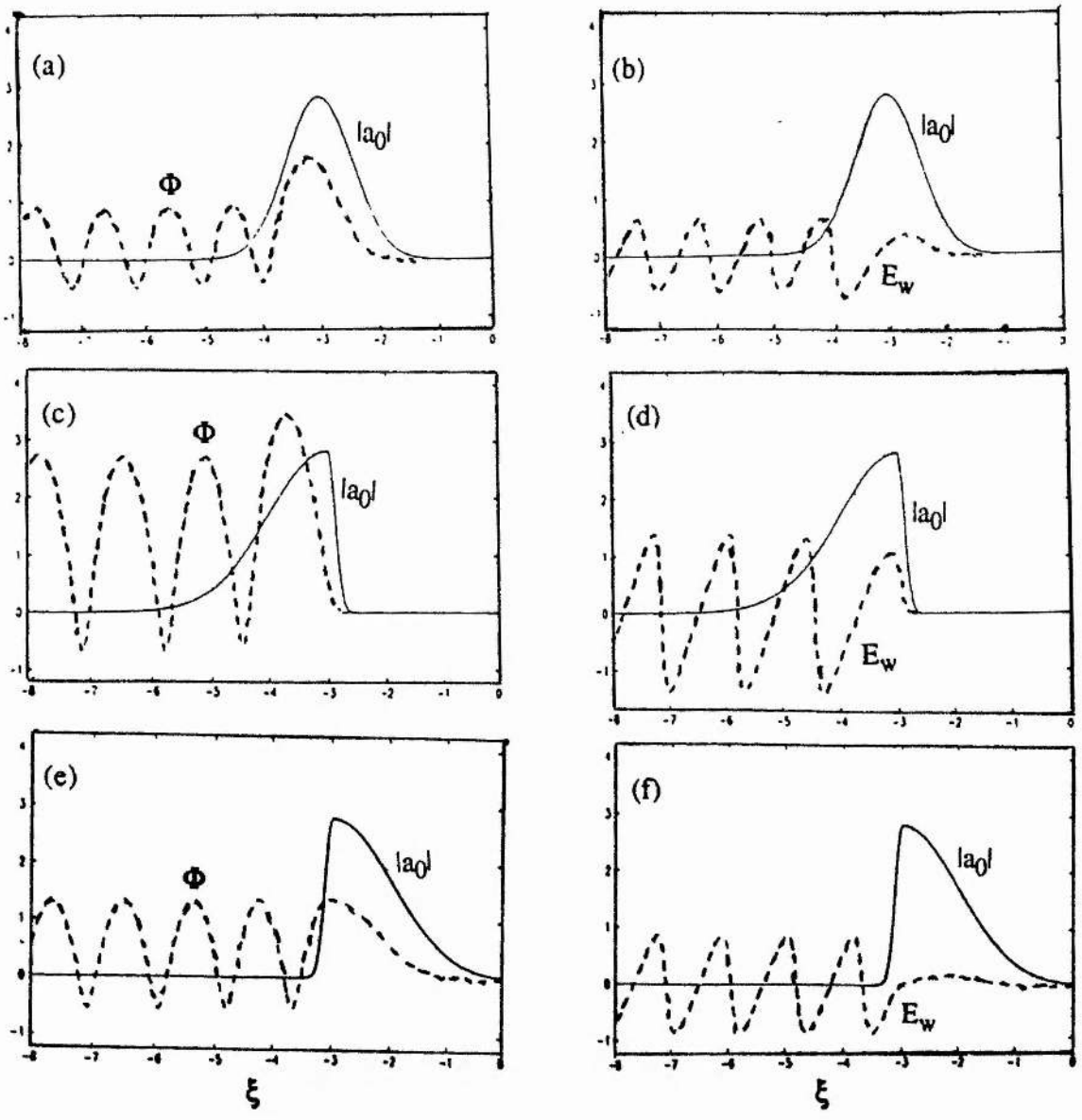

Figure 9.8: The values of the magnitude of normalised vector potential $|a_0|$ (solid curves) and scalar potential Φ and/or wake-electric field E_w (dashed curves) with position $\xi=z-v_g t$. $|a_0^{in}|=\sqrt{8}$, $\omega_{p0}/\omega_0=0.01$, $t=2T_p$. (a) and (b) Gaussian rise and fall $\sigma_r=\sigma_f=5c/\omega_{p0}=0.795\lambda_p$; (c) and (d) Gaussian rise $\sigma_r=c/\omega_{p0}=0.159\lambda_p$, Gaussian fall $\sigma_f=9c/\omega_{p0}=1.433\lambda_p$; (e) and (f) Gaussian rise $\sigma_r=9c/\omega_{p0}=1.433\lambda_p$, Gaussian fall $\sigma_f=c/\omega_{p0}=0.159\lambda_p$.

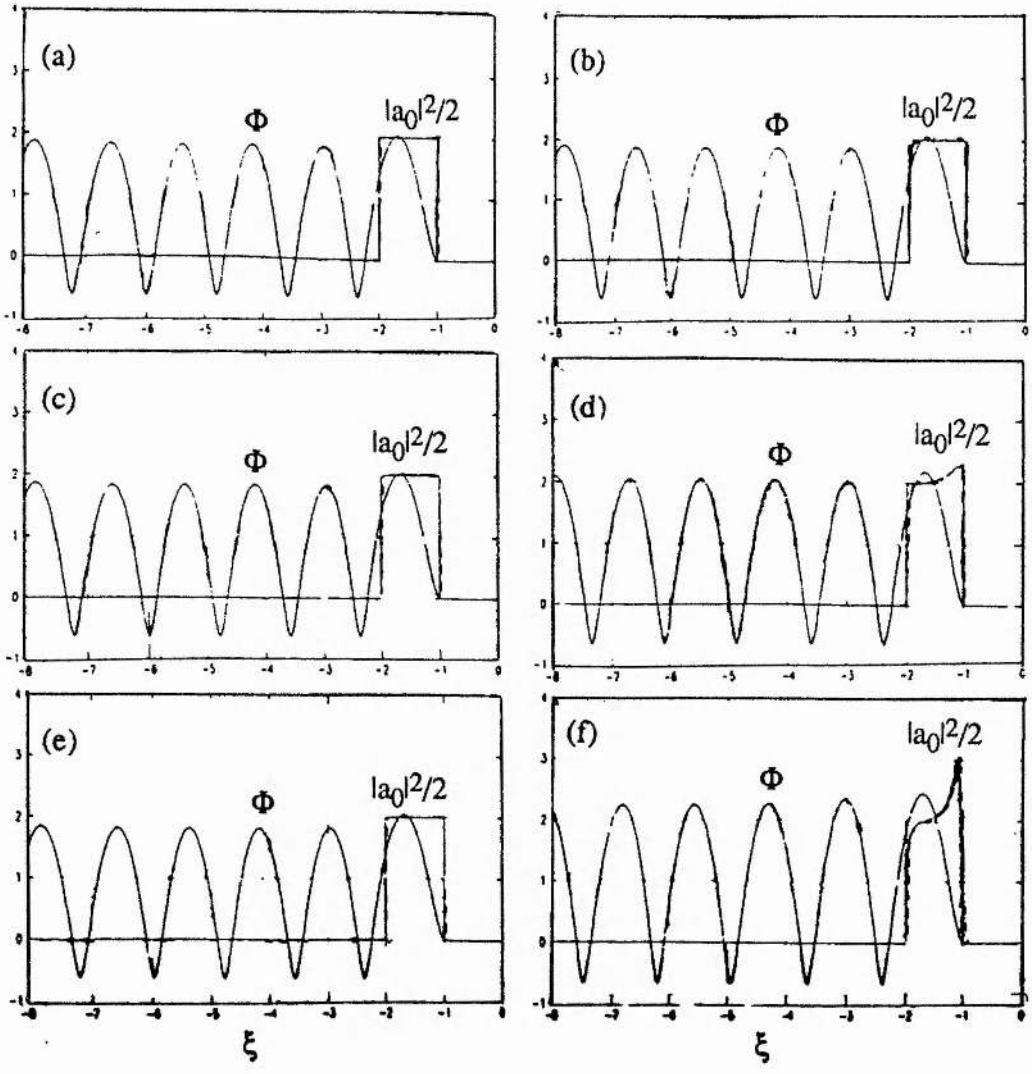

Figure 9.9: The values of $|a_0|^2/2$ (curve 1) and the potential Φ (curve 2) for square pulse-width $l_p=1.0\lambda_p$ and $|a_0^{in}|=2$. (a) and (b) are for $\omega_{p0}/\omega_0=0.01$, (c) and (d) are for $\omega_{p0}/\omega_0=0.05$, (e) and (f) are for $\omega_{p0}/\omega_0=0.1$. Curve (a) is at time $t=2T_p$, (b) is at $t=100T_p$, (c) is at $t=0.4T_p$, (d) is at $t=20T_p$, (e) is at $t=0.2T_p$ and (f) is at $t=10T_p$.

APPENDICES

Appendix A

DERIVATION OF THE EXPRESSION FOR PONDEROMOTIVE FORCE AT THE BEAT FREQUENCY OF THE PUMPS

The expression for the ponderomotive force can be written as follows:

$$\vec{f}_{NL} = -m_e\left(\vec{v}\cdot\nabla\right)\vec{v} - \frac{e}{c}\vec{v}\times\vec{B}\,. \tag{A.1}$$

The component of the nonlinear ponderomotive force oscillating at the beat frequency $\omega_3=\omega_1-\omega_2$ is given by

$$\vec{f}_{NL}(\omega_3=\omega_1-\omega_2,\ \vec{k}_3=\vec{k}_1-\vec{k}_2) = -\frac{m_e}{2}\left\{\left(\vec{v}_1\cdot\nabla\right)\vec{v}_2^{\,*} + \left(\vec{v}_2^{\,*}\cdot\nabla\right)\vec{v}_1\right\}$$

$$-\frac{e}{2c}\left(\vec{v}_1\times\vec{B}_2^{\,*} + \vec{v}_2^{\,*}\times\vec{B}_1\right)$$

$$= \vec{f}_{NL1}(\omega_3,\vec{k}_3) + \vec{f}_{NL2}(\omega_3,\vec{k}_3), \tag{A.2}$$

where

$$\vec{f}_{NL1}(\omega_3,\vec{k}_3) = -\frac{m_e}{2}\left\{\left(\vec{v}_1\cdot\nabla\right)\vec{v}_2^{\,*} + \left(\vec{v}_2^{\,*}\cdot\nabla\right)\vec{v}_1\right\}$$

$$\cong \frac{im_e}{2}\left\{\left(\vec{v}_1\cdot\vec{k}_2\right)\vec{v}_2^{\,*} - \left(\vec{v}_2^{\,*}\cdot\vec{k}_1\right)\vec{v}_1\right\},$$

and

$$\vec{f}_{NL2}(\omega_3, \vec{k}_3) = -\frac{e}{2c}\left(\vec{v}_1 \times \vec{B}_2^* + \vec{v}_2^* \times \vec{B}_1\right).$$

The electron quiver velocities $\vec{v}_j$ in the electromagnetic pump fields have been defined in Chapter 3 (see Eq.(3.6)) and is

$$\vec{v}_j = \left(\frac{-ie}{m_e \omega_j}\right)\vec{\vec{K}}_j \cdot \vec{E}_j,$$

where j=1,2; $\vec{E}_j$ are the pump electric field strengths and $\vec{\vec{K}}_j$ are related to the cold plasma mobility tensors by the relation $\vec{\vec{K}}_j = (i\omega_j/\Omega_e)\vec{\vec{M}}_j$.

Therefore, the expression for $\vec{f}_{NL1}(\omega_3, \vec{k}_3)$ can now be written as follows:

$$\vec{f}_{NL1}(\omega_3, \vec{k}_3) = \left(\frac{ie^2}{2m_e\omega_1\omega_2}\right)\left\{\left(\vec{\vec{K}}_1 \cdot \hat{\vec{e}}_1\right)\cdot \vec{k}_2 \left(\vec{\vec{K}}_2^* \cdot \hat{\vec{e}}_2^*\right)\right.$$

$$\left. - \left(\vec{\vec{K}}_2^* \cdot \hat{\vec{e}}_2^*\right)\cdot \vec{k}_1 \left(\vec{\vec{K}}_1 \cdot \hat{\vec{e}}_1\right)\right\} E_1 E_2^*. \qquad \text{(A.3)}$$

By using the relation

$$\vec{B}_j = \frac{c}{\omega_j}\vec{k}_j \times \vec{E}_j,$$

and substituting $\vec{v}_j$'s in the expression for $\vec{f}_{NL2}(\omega_3,\vec{k}_3)$, namely

$$\vec{f}_{NL2}(\omega_3,\vec{k}_3) = -\frac{e}{2c}\left(\vec{v}_1\times\vec{B}_2^{*}+\vec{v}_2^{*}\times\vec{B}_1\right),$$

we obtain

$$\vec{f}_{NL2}(\omega_3,\vec{k}_3) = \left(\frac{ie^2}{2m_e\omega_1\omega_2}\right)\left\{\left(\hat{\vec{e}}_2^{*}\cdot\vec{\vec{K}}_1\cdot\hat{\vec{e}}_1\right)\vec{k}_2-\left(\hat{\vec{e}}_1\cdot\vec{\vec{K}}_2^{*}\cdot\hat{\vec{e}}_2^{*}\right)\vec{k}_1\right.$$

$$\left.+\left(\vec{k}_1\cdot\vec{\vec{K}}_2^{*}\cdot\hat{\vec{e}}_2^{*}\right)\hat{\vec{e}}_1-\left(\vec{k}_2\cdot\vec{\vec{K}}_1\cdot\hat{\vec{e}}_1\right)\hat{\vec{e}}_2^{*}\right\}E_1E_2^{*}. \qquad (A.4)$$

Therefore, by adding (A.3) and (A.4), we finally obtain, the expression for ponderomotive force $\vec{f}_{NL}(\omega_3, k_3)$:

$$\vec{f}_{NL}(\omega_3,\vec{k}_3) = \left(\frac{-ie^2E_1E_2^{*}}{2m_e\omega_1\omega_2}\right)\left\{\left(\hat{\vec{e}}_1\cdot\vec{\vec{K}}_2^{*}\cdot\hat{\vec{e}}_2^{*}\right)\vec{k}_1-\left(\hat{\vec{e}}_2^{*}\cdot\vec{\vec{K}}_1\cdot\hat{\vec{e}}_1\right)\vec{k}_2\right.$$

$$\left.+\left(\vec{k}_1\cdot\vec{\vec{K}}_2^{*}\cdot\hat{\vec{e}}_2^{*}\right)\left(\vec{\vec{K}}_1-\vec{\vec{I}}\right)\cdot\hat{\vec{e}}_1-\left(\vec{k}_2\cdot\vec{\vec{K}}_1\cdot\hat{\vec{e}}_1\right)\left(\vec{\vec{K}}_2^{*}-\vec{\vec{I}}\right)\cdot\hat{\vec{e}}_2^{*}\right\}. \qquad (A.5)$$

Appendix B

SIMPLIFICATION OF THE EXPRESSIONS FOR THE COUPLING COEFFICIENTS

The electric field vectors of the pump electromagnetic waves can be written as follows:

$$\vec{E}_j = E_j \hat{\vec{e}}_j , \tag{B.1}$$

where

$$\hat{\vec{e}}_j = g_j\left(\hat{\vec{e}}_x + \alpha_j \hat{\vec{e}}_y + \beta_j \hat{\vec{e}}_z\right) \tag{B.2}$$

are the polarisation vectors of the pump electric fields (j=1,2).

Condition $\hat{\vec{e}}_j^{\,*} \cdot \hat{\vec{e}}_j = 1$ gives

$$g_j = \left(1 + \alpha_j^* \alpha_j + \beta_j^* \beta_j\right)^{-1/2} . \tag{B.3}$$

From Eq.(2.19) with $\vec{\vec{D}}_j = \vec{\vec{D}}_j^{H} + \vec{\vec{D}}_j^{A}$, and $\vec{\vec{D}}_j^{A} = 0$, we have

$$\vec{\vec{D}}_j = \left(c^2 k_j^2 - \omega_j^2\right)\vec{\vec{I}} - c^2 \vec{k}_j \vec{k}_j + \omega_p^2 \vec{\vec{K}}_j .$$

Appendix B

Differentiating $\vec{\vec{D}}_j$ partially with respect to ω_j, we get

$$\frac{\partial \vec{\vec{D}}_j}{\partial \omega_j} = -2\omega_j \vec{\vec{I}} + \omega_p^2 \frac{\partial \vec{\vec{K}}_j}{\partial \omega_j}. \qquad \text{(B.4)}$$

In cold plasma approximation, the components of $\vec{\vec{K}}_j$ are given by

$$K_{jxx} = K_{jyy} = \left(\frac{\omega_j^2}{\omega_j^2 - \Omega_e^2} \right),$$

$$K_{jxy} = -K_{jyx} = \left(\frac{-i\Omega_e \omega_j}{\omega_j^2 - \Omega_e^2} \right),$$

$$K_{jxz} = K_{jyz} = K_{jzx} = K_{jzy} = 0, \quad \text{and} \quad K_{jzz} = 1.$$

Now by differentiating the different components of $\vec{\vec{K}}_j$, we get

$$\frac{\partial K_{jxx}}{\partial \omega_j} = \frac{\partial K_{jyy}}{\partial \omega_j} = \left[\frac{-2\omega_j \Omega_e^2}{\left(\omega_j^2 - \Omega_e^2\right)^2} \right],$$

$$\frac{\partial K_{jxy}}{\partial \omega_j} = -\frac{\partial K_{jyx}}{\partial \omega_j} = \left[\frac{i\,\Omega_e\,(\omega_j^2 + \Omega_e^2)}{\left(\omega_j^2 - \Omega_e^2\right)^2} \right],$$

and the other derivatives are zero.

We have from Eq.(B.4)

$$\left(\frac{\partial \vec{\vec{D}}_j^H}{\partial \omega_j} \right)_{xx} = -2\,\omega_j + \omega_p^2 \left(\frac{\partial \vec{\vec{K}}_j}{\partial \omega_j} \right)_{xx} = -2\,\omega_j \left[1 + \frac{\omega_p^2\,\Omega_e^2}{\left(\omega_j^2 - \Omega_e^2\right)^2} \right],$$

$$\left(\frac{\partial \vec{\vec{D}}_j^H}{\partial \omega_j} \right)_{xy} = -\left(\frac{\partial \vec{\vec{D}}_j^H}{\partial \omega_j} \right)_{yx} = \omega_p^2 \left(\frac{\partial \vec{\vec{K}}_j}{\partial \omega_j} \right)_{xy} = \left[\frac{i\,\omega_p^2\,\Omega_e\,(\omega_j^2 + \Omega_e^2)}{\left(\omega_j^2 - \Omega_e^2\right)^2} \right],$$

$$\left(\frac{\partial \vec{\vec{D}}_j^H}{\partial \omega_j} \right)_{yy} = -2\,\omega_j + \omega_p^2 \left(\frac{\partial \vec{\vec{K}}_j}{\partial \omega_j} \right)_{yy} = -2\,\omega_j \left[1 + \frac{\omega_p^2\,\Omega_e^2}{\left(\omega_j^2 - \Omega_e^2\right)^2} \right],$$

Appendix B

$$\left(\frac{\partial \vec{\vec{D}}_j^H}{\partial \omega_j}\right)_{zz} = -2\omega_j + \omega_p^2\left(\frac{\partial \vec{\vec{K}}_j}{\partial \omega_j}\right)_{zz} = -2\omega_j ,$$

and

$$\left(\frac{\partial \vec{\vec{D}}_j^H}{\partial \omega_j}\right)_{xz} = \left(\frac{\partial \vec{\vec{D}}_j^H}{\partial \omega_j}\right)_{zx} = \left(\frac{\partial \vec{\vec{D}}_j^H}{\partial \omega_j}\right)_{yz} = \left(\frac{\partial \vec{\vec{D}}_j^H}{\partial \omega_j}\right)_{zy} = 0 .$$

We have

$$\vec{e}_j^* \cdot \frac{\partial \vec{\vec{D}}_j^H}{\partial \omega_j} \cdot \vec{e}_j = g_j\left(\vec{e}_x + \alpha_j^* \vec{e}_y + \beta_j^* \vec{e}_z\right) \cdot \frac{\partial \vec{\vec{D}}_j^H}{\partial \omega_j} \cdot g_j\left(\vec{e}_x + \alpha_j \vec{e}_y + \beta_j \vec{e}_z\right)$$

$$= g_j^2\left[\left(1+\alpha_j^*\alpha_j\right)\left(\frac{\partial \vec{\vec{D}}_j^H}{\partial \omega_j}\right)_{xx} + \left(\alpha_j - \alpha_j^*\right)\left(\frac{\partial \vec{\vec{D}}_j^H}{\partial \omega_j}\right)_{xy} + \beta_j^*\beta\left(\frac{\partial \vec{\vec{D}}_j^H}{\partial \omega_j}\right)_{zz}\right],$$

(B.5)

To calculate the coupling coefficient C_3, we use Eq.(2.30) with $\vec{\vec{D}}_3^A$=0:

$$\hat{e}_3^* \cdot \frac{\partial \vec{\vec{D}}_3^H}{\partial \omega_3} \cdot \hat{e}_3 = \left(\cos\theta_3 \hat{e}_z + \sin\theta_3 \hat{e}_x\right) \cdot \frac{\partial \vec{\vec{D}}_3^H}{\partial \omega_3} \cdot \left(\cos\theta_3 \hat{e}_z + \sin\theta_3 \hat{e}_x\right)$$

$$= \cos^2\theta_3 \left(\frac{\partial \vec{\vec{D}}_3^H}{\partial \omega_3}\right)_{zz} + \sin^2\theta_3 \left(\frac{\partial \vec{\vec{D}}_3^H}{\partial \omega_3}\right)_{xx}, \qquad \text{(B.6)}$$

$$\hat{e}_i^* \cdot \vec{\vec{K}}_j \cdot \hat{e}_j = g_i \left(\hat{e}_x + \alpha_i^* \hat{e}_y + \beta_i^* \hat{e}_z\right) \cdot \vec{\vec{K}}_j \cdot g_j \left(\hat{e}_x + \alpha_j \hat{e}_y + \beta_j \hat{e}_z\right)$$

$$= g_i g_j \left\{\left(1 + \alpha_i^* \alpha_j\right) K_{jxx} + \left(\alpha_j - \alpha_i^*\right) K_{jxy} + \beta_i^* \beta_j K_{jzz}\right\}, \qquad \text{(B.7)}$$

where, when i=1 then j=2 and when i=2 then j=1.

$$\hat{e}_1 \cdot \vec{\vec{K}}_2^* \cdot \hat{e}_2^* = g_1 \left(\hat{e}_x + \alpha_1 \hat{e}_y + \beta_1 \hat{e}_z\right) \cdot \vec{\vec{K}}_2^* \cdot g_2 \left(\hat{e}_x + \alpha_2^* \hat{e}_y + \beta_2^* \hat{e}_z\right)$$

$$= g_1 g_2 \left\{\left(1 + \alpha_2^* \alpha_1\right) K_{2xx} + \left(\alpha_1 - \alpha_2^*\right) K_{2xy} + \beta_2^* \beta_1 K_{2zz}\right\}, \qquad \text{(B.8)}$$

$$\hat{e}_3^* \cdot \vec{\vec{K}}_3 \cdot \vec{k}_1 = \left(\cos\theta_3 \hat{e}_z + \sin\theta_3 \hat{e}_x\right) \cdot \vec{\vec{K}}_3 \cdot k_1 \left(\cos\theta_1 \hat{e}_z + \sin\theta_1 \hat{e}_x\right)$$

$$= k_1 \left(K_{3zz} \cos\theta_1 \cos\theta_3 + K_{3xx} \sin\theta_1 \sin\theta_3\right). \qquad \text{(B.9)}$$

Similarly,

$$\hat{\vec{e}}_3^{*} \cdot \vec{\vec{K}}_3 \cdot \vec{k}_2 = k_2 \left(K_{3zz} \cos\theta_2 \cos\theta_3 + K_{3xx} \sin\theta_2 \sin\theta_3 \right). \tag{B.10}$$

Again

$$\vec{k}_1 \cdot \vec{\vec{K}}_2^{*} \cdot \hat{\vec{e}}_2^{*} = k_1 \left(\cos\theta_1 \hat{\vec{e}}_z + \sin\theta_1 \hat{\vec{e}}_x \right) \cdot \vec{\vec{K}}_2^{*} \cdot g_2 \left(\hat{\vec{e}}_x + \alpha_2^{*} \hat{\vec{e}}_y + \beta_2^{*} \hat{\vec{e}}_z \right)$$

$$= g_2 k_1 \left\{ \beta_2^{*} K_{2zz} \cos\theta_1 + \left(K_{2xx} - \alpha_2^{*} K_{2xy} \right) \sin\theta_1 \right\}, \tag{B.11}$$

and

$$\vec{k}_2 \cdot \vec{\vec{K}}_1 \cdot \hat{\vec{e}}_1 = k_2 \left(\cos\theta_2 \hat{\vec{e}}_z + \sin\theta_2 \hat{\vec{e}}_x \right) \cdot \vec{\vec{K}}_1 \cdot g_1 \left(\hat{\vec{e}}_x + \alpha_1 \hat{\vec{e}}_y + \beta_1 \hat{\vec{e}}_z \right)$$

$$= g_1 k_2 \left\{ \beta_1 K_{1zz} \cos\theta_2 + \left(K_{1xx} + \alpha_1 K_{1xy} \right) \sin\theta_2 \right\}, \tag{B.12}$$

Now

$$\hat{e}_3^* \cdot \vec{\vec{K}}_3 \cdot \left(\vec{\vec{K}}_1 - \vec{\vec{I}}\right) \cdot \hat{e}_1 = \left(\cos\theta_3 \hat{e}_z + \sin\theta_3 \hat{e}_x\right) \cdot \vec{\vec{K}}_3 \cdot \left(\vec{\vec{K}}_1 - \vec{\vec{I}}\right) \cdot g_1 \left(\hat{e}_x + \alpha_1 \hat{e}_y + \beta_1 \hat{e}_z\right)$$

$$= g_1 \sin\theta_3 \Big[K_{3xx} \left\{ K_{1xx} - 1 + \alpha_1 K_{1xy} \right\}$$

$$+ K_{3xy} \left\{ \alpha_1 \left(K_{1xx} - 1 \right) - K_{1xy} \right\} \Big], \qquad \text{(B.13)}$$

and similarly

$$\hat{e}_3^* \cdot \vec{\vec{K}}_3 \cdot \left(\vec{\vec{K}}_2^* - \vec{\vec{I}}\right) \cdot \hat{e}_2^* = \left(\cos\theta_3 \hat{e}_z + \sin\theta_3 \hat{e}_x\right) \cdot \vec{\vec{K}}_3 \cdot \left(\vec{\vec{K}}_2^* - \vec{\vec{I}}\right) \cdot g_2 \left(\hat{e}_x + \alpha_2^* \hat{e}_y + \beta_2^* \hat{e}_z\right)$$

$$= g_2 \sin\theta_3 \Big[K_{3xx} \left\{ K_{2xx} - 1 - \alpha_2^* K_{2xy} \right\}$$

$$+ K_{3xy} \left\{ \alpha_2^* \left(K_{2xx} - 1 \right) - K_{2xy} \right\} \Big]. \qquad \text{(B.14)}$$

By using (B.5)-(B.14) into Eqs.(2.46)-(2.48), the coupling coefficients C_1, C_2, and C_3 can easily be evaluated. The relations (B.5)-(B.14) can further be simplified for the case of a Langmuir type beat mode. In this special case, for small incidence angle of the pump waves, both pumps can be considered to be circularly polarized waves. For circularly polarized pump

electromagnetic waves

$$\alpha_{1,2} = \pm\sqrt{-1} = \pm i, \quad \beta_{1,2} = 0, \quad g_{1,2} = \frac{1}{\sqrt{2}}, \quad \cos\theta_3 \cong 1, \quad \sin\theta_3 \cong 0 .$$

Therefore, the polarization unit vectors of the pump electromagnetic waves become

$$\hat{\vec{e}}_1 = \hat{\vec{e}}_2 = \left(\frac{\hat{\vec{e}}_x \pm i\hat{\vec{e}}_y}{\sqrt{2}} \right),$$

where the upper positive sign is for right-hand polarization and the lower minus sign is for left-hand polarization respectively.

Eq.(B.5) becomes

$$\hat{\vec{e}}_j^{*} \cdot \frac{\partial \vec{\vec{D}}_j^{H}}{\partial \omega_j} \cdot \hat{\vec{e}}_j \cong \left(\frac{\partial \vec{\vec{D}}_j^{H}}{\partial \omega_j} \right)_{xx} \pm i \left(\frac{\partial \vec{\vec{D}}_j^{H}}{\partial \omega_j} \right)_{xy} = -2\omega_j ; -2\omega_j \text{ (for two polarizations).} \quad \text{(B.15)}$$

(j=1,2)

For a Langmuir beat wave propagating almost parallel to the toroidal magnetic field $\hat{\vec{e}}_3 = \hat{\vec{e}}_z$, Eq.(B.6) then becomes

$$\hat{e}_3^* \cdot \frac{\partial \vec{\vec{D}}_3^H}{\partial \omega_3} \cdot \hat{e}_3 \cong \left(\frac{\partial \vec{\vec{D}}_3^H}{\partial \omega_3} \right)_{zz} \cong -2\omega_3 . \qquad \text{(B.16)}$$

Eq.(B.7) becomes

$$\hat{e}_1^* \cdot \vec{\vec{K}}_2 \cdot \hat{e}_2 = K_{2xx} \pm iK_{2xy} \cong \left(\frac{\omega_2}{\omega_2 - \Omega_e} \right); \left(\frac{\omega_2}{\omega_2 + \Omega_e} \right) \qquad \text{(B.17)}$$

for two polarizations (RCP and LCP) respectively.

Similarly

$$\hat{e}_2^* \cdot \vec{\vec{K}}_1 \cdot \hat{e}_1 \cong \left(\frac{\omega_1}{\omega_1 - \Omega_e} \right); \left(\frac{\omega_2}{\omega_1 + \Omega_e} \right) \text{ (for two polarizations).} \qquad \text{(B.18)}$$

Eq.(B.8) becomes

$$\hat{e}_1 \cdot \vec{\vec{K}}_2^* \cdot \hat{e}_2^* \cong K_{2xx} \pm iK_{2xy} = \left(\frac{\omega_2}{\omega_2 - \Omega_e} \right); \left(\frac{\omega_2}{\omega_2 + \Omega_e} \right) \qquad \text{(B.19)}$$

for two polarizations like before.

Eqs.(B.9) and (B.10) become

$$\hat{e}_3^* \cdot \vec{\vec{K}}_3 \cdot \vec{k}_1 \cong k_1 \cos\theta_1 , \qquad \text{(B.20)}$$

and

$$\hat{\vec{e}}_3^{*} \cdot \vec{\vec{K}}_3 \cdot \vec{k}_2 \cong k_2 \cos\theta_2 \,. \tag{B.21}$$

Eq.(B.11) becomes

$$\vec{k}_1 \cdot \vec{\vec{K}}_2^{*} \cdot \hat{\vec{e}}_2^{*} \cong \left(\frac{k_1 \sin\theta_1}{\sqrt{2}} \right) \left(K_{2xx} \pm i K_{2xy} \right)$$

$$= \left(\frac{k_1 \sin\theta_1}{\sqrt{2}} \right) \left(\frac{\omega_2}{\omega_2 - \Omega_e} \right) ; \left(\frac{k_1 \sin\theta_1}{\sqrt{2}} \right) \left(\frac{\omega_2}{\omega_2 + \Omega_e} \right), \tag{B.22}$$

and similarly Eq.(B.12) reduces to

$$\vec{k}_2 \cdot \vec{\vec{K}}_1 \cdot \hat{\vec{e}}_1 \cong \left(\frac{k_2 \sin\theta_2}{\sqrt{2}} \right) \left(K_{1xx} \pm i K_{1xy} \right)$$

$$= \left(\frac{k_2 \sin\theta_2}{\sqrt{2}} \right) \left(\frac{\omega_1}{\omega_1 - \Omega_e} \right) ; \left(\frac{k_2 \sin\theta_2}{\sqrt{2}} \right) \left(\frac{\omega_1}{\omega_1 + \Omega_e} \right). \tag{B.23}$$

Eqs.(B.13) and (B.14) reduce to

$$\hat{\vec{e}}_3^{*} \cdot \vec{\vec{K}}_3 \cdot \left(\vec{\vec{K}}_1 - \vec{\vec{I}} \right) \cdot \hat{\vec{e}}_1 \cong 0, \tag{B.24}$$

and

$$\hat{\vec{e}}_3^{*} \cdot \vec{\vec{K}}_3 \cdot \left(\vec{\vec{K}}_2^{*} - \vec{\vec{I}} \right) \cdot \hat{\vec{e}}_2^{*} \cong 0. \tag{B.25}$$

Using Eqs.(B.15) and (B.17) into Eq.(2.46), we obtain

$$C_1 = \left(\frac{ek_3}{4m_e} \right) \left(\frac{1}{\omega_2 \pm \Omega_e} \right). \tag{B.26}$$

Using Eqs.(B.15) and (B.18) into Eq.(2.47), we obtain

$$C_2 = \left(\frac{ek_3}{4m_e} \right) \left(\frac{1}{\omega_1 \pm \Omega_e} \right). \tag{B.27}$$

Similarly, by using Eqs.(B.16), (B.18) - (B.25) into Eq.(2.48), we obtain

$$C_3 = \left(\frac{e\omega_{p0}^2}{4m_e\omega_1\omega_2\omega_3} \right) \left\{ k_1 \cos\theta_1 \left(\frac{\omega_2}{\omega_2 \pm \Omega_e} \right) - k_2 \cos\theta_2 \left(\frac{\omega_1}{\omega_1 \pm \Omega_e} \right) \right\}. \qquad \text{(B.28)}$$

In Eqs (B.26)-(B.28), ± signs are respectively for left and right circularly polarized pump waves.

REFERENCES

REFERENCES

Akhiezer, A. I., and Polovin, R. V. (1955), Dokl. Akad. Nauk SSSR **102**, 919.

Amin, M. R., and Cairns, R. A. (1989), 'Radio-Frequency Power in Plasmas', p.406, AIP Conference Proceedings No. **190**. publ. AIP, New York; (1990), Nucl. Fusion **30**, 327.

Bernabei, S., et al (1982), Phys. Rev. Lett. **49**, 1255.

Bickerton, R. J. (1972), Comments Plasma Phys. Controlled Fusion **1**, 95.

Bulanov, S. V., Kirsanov, V. I., and Sakharov, A. S. (1989), JETP Lett. **50,** 199; (1990), Physica Scripta **T30**, 208.

Callen, C. et al (1988), 'Advanced Accelerators', US DOE Report JSR-85-302.

Chen, F. F. (1974), 'Laser Interaction and Related Plasma Phenomena', Schwarz, H. J., and Hora, H., edt. (Plenum, New York), Vol.3A, p.291.

Chen, F. F. (1989), ICTP Report H4-SMR 393/17.

Chen, F. F. (1990), Physica Scripta **T30**, 14.

Chen, P. et al (1985), Phys. Rev. Lett. **54**, 693.

Chen, P. (1986), Particle Accelerators **20**, 171.

REFERENCES

Clark, W. H. M. et al (1980), Phys. Rev. Lett. **45**, 1101.

Clayton, C. E. et al (1985), Phys. Rev. Lett. **54**, 2343.

Cohen, B. I. (1984), Comments Plasma Phys. Controlled Fusion **8**, 197.

Cohen, B. I. et al (1988), Nucl. Fusion **28**, 1519.

Dangor, A. E. et al (1987), 'New Developments in Particle Acceleration Techniques', Proceedings, Vol. II, Turner, S., edited, CERN 87-11, ECFA 87/110, p.375.

Dangor, A. E., Dymoke-Bradshaw, A. K. L., and Dyson, A. E. (1990), Physica Scripta **T30**, 107.

Darrow, C. et al (1986), Phys. Rev. Lett. **56**, 2629.

de Angelis, U. (1990), Physica Scripta **T30**, 210.

Drake, J. F. et al (1974), Phys. Fluids **17**, 778.

Ebrahim, N. A. et al (1986), Proc. 1986 Linear Accelerator Conf. Standford Accelerator Centre, Standford, California, June 2-6.
Esarey, E. et al (1989), Comm. Plasma Phys. Controll. Fusion **12**, 191.

Fedele, R., de Angelis, U., and Katsouleas, T. (1986), Phys. Rev. A **33**, 4412.

REFERENCES

Fisch, N. J. (1978), Phys. Rev. Lett. **41**, 873.

Fisch, N. J. (1980), Proc. 2nd Joint Varenna-Grenoble Int. Symp. on Heating in Toroidal Plasmas, Como, Vol II, 1157.

Fisch, N. J., and Boozer, A. H. (1980), Phys. Rev. Lett. **45**, 720.

Fisch, N. J. (1987), Rev. Mod. Phys. **59**, 175.

Fontana, J. R., and Pantell, R. H. (1983), J. Appl. Phys. **54**, 4285.

Forslund, D. W. et al (1984), Phys. Fluids **17**, 778.

Galvao, R. M. O., Mendonca, T. J., and Tajima, T. (1984), in International Conference on Plasma Physics (Proc. Joint Conf. of 6th Int. Conf. on Plasma Theory and 6th Int. Congr. on Waves and Instabilities, Lausanne, 1984), **Vol. I**, Centre de Recherches en Physique des Plasmas, Ecole Polytechnique Federal de Lausanne, Lausanne, p.223.

Gorbunov, L., and Kirshanov, V. (1987), Sov. Phys. JETP **66**, 290.

Goree, J. et al (1985), Phys. Rev. Lett. **55**, 1669.

Hooke, H. et al (1983), in Plasma Physics and Controlled Nuclear Fusion 1982, proceedings of the Ninth International Conference on Plasma Physics and Controlled Nuclear Fusion Research, edited by the IAEA editorial staff (IAEA, Vienna), **Vol. 1**, p. 239.

REFERENCES

Jobes, F. C. et al (1984), Phys. Rev. Lett. **52**, 1005.

Joshi, C., Mori, W., and Katsouleas, T. (1984), Nature **311**, 525.

Karttunen, S. J., and Salomaa, R. R. E. (1987), IEEE Trans. Plasma Sci. **PS-15**, 134.

Katsouleas, T. et al (1985), 'Laser Acceleration of Particles', p.63, AIP Conference Proceedings No.**130**, publ. AIP, New York.

Kaufman, A. N., and Cohen, B. I. (1973), Phys. Rev. Lett. **30**, 1306.

Kitagawa, Y. et al (1987), New Developments in Particle Acceleration Techniques', Proceedings, Vol. II, Turner, S., edited, CERN 87-11, ECFA 87/110, p.375.

Lawson, J. D. (1982), 'The Challenge of Ultra High Energies', p.29, Proceedings of ECFA-RAL meeting, Oxford, publ. Rutherford Appleton Laboratory.

Lee, R., and Lampe, M. (1973), Phys. Rev. Lett. **23**, 1390.

Mayberry, M. J. et al (1985), Phys. Rev. Lett. **55**, 829.

McNamara, B. (1990), Private Communication.

McWilliam, R., and Platt, R. C. (1985), Phys. Rev. Lett. **56**, 835.

REFERENCES

Miano, A., de Angelis, U., and Bingham, R. (1989), Plasma Phys. Controll. Fusion **31**, 1381.

Nishikawa, K., and Liu, C. S. (1976), in Advances in Plasma Physics, Simon, A., and Thompson, W. B., edt. (John Wiley & Sons, New York), Vol. **6**, p. 71.

Ohkawa, T. (1970), Nucl. Fusion **10**, 185.

Orzechowski, T. J. et al (1986), Phys. Rev. Lett. **57**, 2172.

Osovets, S. M. et al (1972), in Fifth European Conference on Controlled Fusion and Plasma Physics (Grenoble, France), P. 8; (1976), Sov. Phys. Tech. Phys. **21**, 401.

Palmer, R. B., et al (1985), 'Laser Acceleration of Particles', p.234, AIP Conference Proccedings No.**130**, publ. AIP, New York.

Pellegrini, C. (1982), 'The Challenge of Ultra High Energies', p.249, Proceedings of ECFA-RAL meeting, Oxford, publ. Rutherford Appleton Laboratory.

Porkolab, M. et al (1984), Phys. Rev. Lett. **53**, 450.

Reiman, A. (1979), Rev. Mod. Phys. **51**, 311.

Rosenbluth, M. N., and Liu, C. S. (1972), Phys. Rev. Lett. **29**, 701.

REFERENCES

Rosenzweig, J. B. et al (1988), Phys. Rev. Lett. **61**, 98; (1990), Phys. Scripta **T30**, 110.

Sprangle, P., Tang, C. M., and Essarey, E. (1987), IEEE Trans. Plasma Sci. **PS-15**, 145.

Sprangle, P. et al (1988), Appl. Phys. Lett. **53**, 2146; (1990), Phys. Rev. Lett. 64, 2011.

Start, D. F. H. et al (1978), Phys. Rev. Lett. **40**, 1497; (1982), Phys. Rev. Lett. **48**, 624.

Stix, T. H. (1962), in The Theory of Plasma Waves (McGraw-Hill, New York), p. 225.

Tajima, T., and Dawson, J. M. (1979), Phys. Rev. Lett.43 , 267.

Tang, C. M., Sprangle, P., and Sudan, R. N. (1985), Phys. Fluids **28**, 1974.

Thomassen, K. I. (1988), Plasma Phys. Controll. Fusion **30**, 57.

Tsintsadze, N. L. (1990), Physica Scipta **T30**, 41.

Tsytovich, V., de Angelis, U., and Bingham, R. (1989), Comm. Plasma Phys. Controll. Fusion **12**, 249.

Wort, D. J. H. (1971), Plasma Phys. **13**, 258.